

Journal of Print and Media Technology Research

Scientific contents

Lubrication theory of ink hydrodynamics in
the flexographic printing nip

Hans Martin Sauer, Dominik Daume, Edgar Dörsam

163

Effect of coating pigment, binder type and binder
amount on planar liquid wicking on coated substrates

Eveliina Jutila, Risto Koivunen, Patrick A. C. Gané

173

Formation and photoluminescent properties of
nanophotonic elements with nanosized ZnO for
smart packaging, deposited by screen printing

Olha Sarapulova, Valentyn Sherstiuk

187

Formulation of drop on demand soy inkjet inks

*Alexandra Pekarovicova, Zahra Mashbadi Khodabakhsh,
Paul D. Fleming III*

195

Image analysis as a tool to discriminate counterfeit
from true 2D printed codes

*Nadège Reverdy-Bruas, Lionel Chagas,
Jean-Pascal Poletti, Raphaël Passas*

205

Investigating the effects of publishing approaches
using print, electronic and augmented reality media
on user experience

Elena Fedorovskaya, Lufei Yu

217



9 772223 890003

Editor-in-Chief

Gorazd Golob (Ljubljana)

Published by **iarigai**

The International Association of Research
Organizations for the Information, Media
and Graphic Arts Industries

www.iarigai.org

Journal of Print and Media Technology Research

A peer-reviewed quarterly

PUBLISHED BY

The International Association of Research Organizations
for the Information, Media and Graphic Arts Industries
Magdalenenstrasse 2, D-64288 Darmstadt, Germany
<http://www.iarigai.org> E-mail: journal@iarigai.org

EDITORIAL BOARD

EDITOR-IN-CHIEF

Gorazd Golob (Ljubljana, Slovenia)

EDITORS

Timothy C. Claypole (Swansea, UK)
Edgar Dörsam (Darmstadt, Germany)
Nils Enlund (Helsinki, Finland)
Mladen Lovreček (Zagreb, Croatia)
Renke Wilken (Munich, Germany)
Scott Williams (Rochester, USA)

ASSOCIATE EDITOR

Markéta Držková (Pardubice, Czech Republic)

SCIENTIFIC ADVISORY BOARD

Darko Agić (Zagreb, Croatia)
Anne Blayo (Grenoble, France)
Wolfgang Faigle (Stuttgart, Germany)
Elena Fedorovskaya (Rochester, USA)
Patrick Gane (Helsinki, Finland)
Diana Gregor Svetec (Ljubljana, Slovenia)
Jon Yngve Hardeberg (Gjøvik, Norway)
Ulrike Herzau Gerhardt (Leipzig, Germany)
Gunter Hübner (Stuttgart, Germany)
Marie Kaplanová (Pardubice, Czech Republic)
John Kettle (Espoo, Finland)
Helmut Kipphan (Schwetzingen, Germany)
Björn Kruse (Linköping, Sweden)
Yuri Kuznetsov (St. Petersburg, Russian Federation)
Magnus Lestelius (Karlstad, Sweden)
Patrice Mangin (Trois Rivières, Canada)
Thomas Mejtoft (Umeå, Sweden)
Erzsébet Novotny (Budapest, Hungary)
Anastasios Politis (Athens, Greece)
Anu Seisto (Espoo, Finland)
Johan Stenberg (Stockholm, Sweden)
Philipp Urban (Darmstadt, Germany)

A mission statement

To meet the need for a high quality scientific publishing in its research fields of interest, the International Association of Research Organizations for the Information, Media and Graphic Arts Industries (iarigai) publishes the peer reviewed quarterly Journal of Print and Media Technology Research.

The Journal is fostering multidisciplinary research and scholarly discussion on scientific and technical issues in the field of graphic arts and media communication, thereby advancing scientific research, knowledge creation and industry development. Its aim is to be the leading international scientific periodical in the field, offering publishing opportunities and serving as a forum for knowledge exchange between all those scientist and researchers interested in contributing to or benefiting from research in the related fields.

By regularly publishing peer-reviewed high quality research articles, position papers, survey and case studies, the Journal will consistently promote original research, networking, international collaboration and the exchange of ideas and know how. Editors will also consider for publication review articles, topical and professional communications, as well as opinions and reflections of interest to the readers. The Journal will also provide multidisciplinary discussion on research issues within the field and on the effects of new scientific and technical development on society, industry and the individual. Thus, it will serve the entire research community, as well as the global graphic arts and media industry.

The Journal will cover fundamental and applied aspects of at least, but not limited to the following fields of research:

Printing technology and related processes

- ◇ Conventional and special printing
- ◇ Packaging
- ◇ Printed fuel cells and other printed functionality
- ◇ Printing on biomaterials
- ◇ Textile and fabric printing
- ◇ Materials science
- ◇ Process control

Premedia technology and processes

- ◇ Color management and color reproduction
- ◇ Image and reproduction quality
- ◇ Image carriers (physical and virtual)
- ◇ Workflow management
- ◇ Content management

Emerging media and future trends

- ◇ Media industry developments
- ◇ Developing media communication value system
- ◇ Online and mobile media development
- ◇ Cross-media publishing

Social impacts

- ◇ Environmental issues and sustainability
- ◇ Consumer perception and media use
- ◇ Social trends and their impact on media

Submissions to the Journal

Submission details and guidelines for authors can be found on the inside back cover of this issue, as well as downloaded from <http://www.iarigai.org/publications/journal>.

Subscriptions

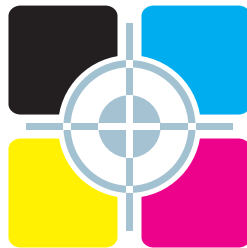
<http://www.iarigai.org/publications/journal/order>
or send your request to office@iarigai.org.

✉ Contact the Editorial office: journal@iarigai.org

Journal of Print and Media Technology Research

3-2015

September 2015



The information published in this journal is obtained from sources believed to be reliable and the sole responsibility on the contents of the published papers lies with their authors. The publishers can accept no legal liability for the contents of the papers, nor for any information contained therein, nor for conclusions drawn by any party from it.

Journal of Print and Media Technology Research is listed in:

Index Copernicus International
PiraBase and PaperBase (by Smithers Pira)
NSD – Norwegian Register for
Scientific Journals, Series and Publishers

Contents

A letter from the Editor <i>Gorazd Golob</i>	161
Scientific contributions	
Lubrication theory of ink hydrodynamics in the flexographic printing nip <i>Hans Martin Sauer, Dominik Daume, Edgar Dörsam</i>	163
Effect of coating pigment, binder type and binder amount on planar liquid wicking on coated substrates <i>Eveliina Jutila, Risto Koivunen, Patrick A. C. Gane</i>	173
Formation and photoluminescent properties of nanophotonic elements with nanosized ZnO for smart packaging, deposited by screen printing <i>Olha Sarapulova, Valentyn Sherstink</i>	187
Formulation of drop on demand soy inkjet inks <i>Alexandra Pekarovicova, Zabira Mashbadi Khodabakhsh, Paul D. Fleming III</i>	195
Image analysis as a tool to discriminate counterfeit from true 2D printed codes <i>Nadège Reverdy-Bruas, Lionel Chagas, Jean-Pascal Poletti, Raphaël Passas</i>	205
Investigating the effects of publishing approaches using print, electronic and augmented reality media on user experience <i>Elena Fedorovskaya, Lufei Yu</i>	217

Topicalities

Edited by Markéta Držková

News & more	229
Bookshelf	231
Events	237



A letter from the Editor

Gorazd Golob

Editor-in-Chief

E-mail: gorazd.golob@jpmtr.org

journal@iarigai.org

50 years of iarigai

iarigai – The International Association of Research Organizations for the Information, Media and Graphic Arts Industries – is celebrating half of the century of successful and fruitful existence. More than 30 years before formally **establishing the iarigai in 1965**, cooperation in common projects, exchanges of ideas and information, and presentation of the results of research work was supported by graphic arts research and professional institutes and organizations from Denmark, France, Netherlands, Germany, Sweden and Great Britain. Today **iarigai** is a strong international association with 44 members from 23 countries.

History of **iarigai** was as interesting as it was dynamic. First informal and formal research conferences extended to biennial management conferences and symposia on different topics. Research activities, oriented mainly into conventional printing technology, colour reproduction challenges and interactions between paper and ink, evolved in the past decades into communication and multimedia issues, printed functionality, printed electronics and all other topics, recognized as our interdisciplinary research field.

During the first conferences, the scientific book *Advances in Printing and Media Technology* (previously *Advances in Printing Science and Technology*) became the main publication for dissemination of the results of scientific and research work. In past years, the leading role of the *Advances* has been transferred to the *Journal of Print and Media Technology Research*. With this decision, the print and media research community, gathered under **iarigai**, made a great step forward to the recognition comparable with other scientific disciplines.

The 50th anniversary celebration of **iarigai** took place in Finland, where the association was founded, in the pleasant and working atmosphere at the 42nd International research conference of **iarigai**. The conference overlapped with meeting of COST Action FP1104 *New possibilities for print media and packaging – combining print with digital* (EU supported project), giving added value to the common event. All authors, who have successfully participated at the conference and COST event, are kindly invited to extend and improve their conference contributions into full scientific or research papers for publication in the *Journal*. Every manuscript will be double-blind peer reviewed and edited under well-established standard procedure.

In the present issue, six original scientific and research papers are published with interesting content from theoretical study of hydrodynamics of inks in the flexographic printing unit, following with reports of the research on functional printing, where authors respond to the challenges in medical diagnostics, pharmacy and smart packaging, continuing with solving of sustainability problems with soy based inks, following with investigation of counterfeiting at 2D codes and finally by the research of contemporary media and their impact on the end user. This selection again demonstrates the breadth of our research areas and multidisciplinary approach. I am convinced that these topics will be of great interest to you, our readers.

In the “Topicalities section”, edited by the Associate Editor Markéta Držková (marketa.drzkova@jpmtr.org), we are again bringing you an overview of new published books, three short abstracts from Doctoral theses, defended at the University of Oslo, the KTH Royal Institute of Technology Stockholm and from

the Loughborough University, and an overview on news and events that might be interesting for our readers.

We are continuously expecting news from your institutions, your partners from other academic or research institutions from other countries and from the industry, to open new paths for dissemination of our achievements and to find new opportunities for future cooperation and common international research projects. At this occasion, I would like to point out that the primary role of the Journal is, and will remain also in the future, the publishing and dissemination of the scientific, research and technical papers where most important and valuable results, comments and conclusions are presented.

At the final page you will find invitation to the Evolutions in food packaging printing, an international network meeting, organized by [iarigai](#) and [vigc](#) in Brussels in November. This kind of events are important as a meeting point for the scientists, professionals and decision makers from the academic and research institutions and from the industry, who are looking for the new way of cooperation in the future. Next important event in 2016 will be [iarigai](#) International research conference in Toronto.

Ljubljana, September 2015

JPMTR 063 | 1426
DOI 10.14622/JPMTR-1426
UDC 655 : 681.6 (532.5)

Original scientific paper
Received: 2014-07-15
Accepted: 2015-09-10

Lubrication theory of ink hydrodynamics in the flexographic printing nip

Hans Martin Sauer, Dominik Daume, Edgar Dörsam

Institute of Printing Science and Technology (IDD),
Technische Universität Darmstadt,
Magdalenenstraße 2, D-64289 Darmstadt

E-mail: sauer@idd.tu-darmstadt.de

Abstract

On the base of hydrodynamical lubrication theory, we develop a mathematical model for the ink transfer in a flexographic printing process. When using the specific parameter ranges the model may also be applicable to the offset process. Specifically, we show how our model can be applied to viscous ink flows in the printing nip in presence of elastic printing plates, and how this sets limits to the possible resolution of the printing image. We also discuss the structure of the contact zone between printing plate and the substrate which is determined by the viscous and elastic stresses within the ink layer and the printing form. We also estimate the dynamic pressure profile in the ink during the transfer process. Finally, we discuss the phenomenon of ink seam formation at the rim of a flexographic printed pattern, and viscous finger formation. Explicitly, we show that important parameters, such as the width of an ink seam, the actual nip height, the size of the contact zone, and the ink shear, scale nonlinearly with printing speed. We derive the respective scaling exponents and compare the predictions with printing experiments.

Keywords: flexography, lubrication theory, ink viscosity, ink splitting, viscous fingering

1. Introduction

We present a model for viscous ink flow phenomena between an elastic and structured printing form, and the printing substrate, as it is characteristic for the flexographic process. Our aim is to obtain quantitative predictions for the liquid flows which determine printing resolution, ink squeezing and defect formation, and to understand the role of further parameters such as printing form elasticity, ink viscosity and surface tension, and cylinder diameter. Moreover, we are interested in a more detailed understanding of hydrodynamic nip instabilities such as the famous viscous fingering phenomenon, and of the occasionally appearing ink squeeze at the rim of printed areas in flexographic printed products. The conditions of this annoying phenomenon and the relation to ink viscosity, printing plate elasticity and other printing parameters are still not fully understood, and we expect hydrodynamic theory to give at least some reasonable hint how to remove the problem.

Although printing resolution and quality is crucially depending on the wetting properties of the ink, and the surface free energies of the various materials, the importance of viscous ink flows in the transfer process and specifically at the instant of ink splitting have been emphasized by numerous researchers. Early systematic modelling of ink splitting flows is due to Hopkins (1957). Roller coating processes including defect formation regimes have been studied by Gaskell, Innes and

Savage (1998), Varela López et al. (2002), and Varela López and Rosen (2002). The problem of viscous finger formation, or ribbing, has been of continuous interest for several decades, and is usually treated as an analogy of the Saffman-Taylor instability (Saffman and Taylor, 1958). We refer here to the work of Fields and Ashby (1976), of Maher (1985), and of Gingras and Rácz (1989) who emphasized the stochastic nature of finger formation. The importance of the phenomenon for the ink splitting in a printing process has been acknowledged by Behler (1993). Ben Amar (1991) and Lindner and coauthors (Lindner et al., 1999; Lindner, Coussot and Bonn, 2000) have also considered the phenomenon under a more generalized boundary condition, namely in a wedge-shaped rather than a rectangular nip geometry, and for yield stress liquids. An overview is also given in the review of Casademunt (2004). The yield stress aspect is of particular interest for printing inks, and has also been considered by Sauer, Bornemann and Dörsam (2011). The complexity of the problem has been addressed to by the numerical studies of Bohan et al. (2003). We also refer the reader to the PhD thesis of Voss (2002) who presents a systematic collection of the hydrodynamical boundary value problems related to ink splitting. Although we are mainly referring to flexography (Figure 1) in this paper, related instabilities are known to exist also in gravure printing. In flexography, printing ink is supplied to the anilox

roler by a blading system. The anilox roller transports the ink to the protruding parts of the elastic printing plate which is mounted on the plate cylinder. From here the ink is deposited on the printing substrate. This implies lubrication flows in the printing nip, which crucially depend on e.g. the elasticity of the printing plate and on ink viscosity. Bornemann, Sauer and Dörsam (2011), and Bornemann in his PhD thesis (2013), have analyzed viscous flows in a gravure printing nip and show that, quite similar as for flexography, the formation and instability of an ink meniscus are responsible for finger formation, specifically when using printing liquids with extremely low viscosity, which are characteristic for printed electronics. Lubrication approximation of viscous flows has proven to be a fruitful tool here. We shall take this theory as our starting point as well. However, we shall enhance it by discussing the effect of structured and elastic surfaces, which can be deformed by the mechanical and hydrodynamical forces in the nip.

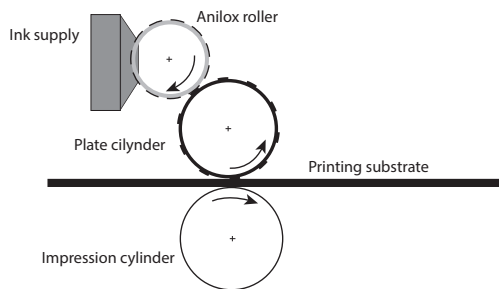


Figure 1: The principal design of a flexographic printing unit

2. Viscous flow in the gap between two parallel plates which are pressed together or are moving apart

Consider two parallel rectangular plates of width b and length L (oriented in the xy plane, where b corresponds to the x axis) as indicated in Figure 2. We assume that $L \gg b$, and we shall finally identify L with the printing width of the plate. The mutual distance $D(t)$ of the plates, where the distance vector is oriented in z -direction perpendicular to the plates, may be time-dependent, but we assume $|D(t)| \ll b$. The gap between the plates, i.e. the cuboid given by $-b/2 < x < b/2$, $-L/2 < y < L/2$, $-D(t)/2 < z < D(t)/2$ is filled with an ink of viscosity η , which we assume to be Newtonian.

Neglecting inertial versus viscous forces, the flow velocities of the ink in x -, y -, and z -direction are solutions of Stokes equation for incompressible liquids

$$\eta \nabla^2 \vec{v} = \vec{\nabla} p \quad [1]$$

where η is the dynamic viscosity, ∇ is the del operator, v is the kinematic viscosity, and p is the pressure, with the incompressibility constraint $\vec{\nabla} \cdot \vec{v} = 0$. The solutions

Introducing the model we proceed in five steps: we first discuss a viscous squeeze flow between two parallel plates which are mutually approaching. We then generalize the solution for moderately structured and elastic plates. At this state the model is already capable of describing many aspects of the ink flow between the flexo plate and the substrate, such as details of the ink squeezing at the borders of the plate. In the next step we consider the ink flow between two cylinders, at least one of which has an elastic surface. We identify the stagnation points of the ink flow in the nip. We argue that in a stationary flow the stagnation points define the positions of the ink menisci in the incoming and outgoing wedge between the cylinders. We show that hydrodynamic ink flows give rise to a pressure-driven interaction between incoming and outgoing ink meniscus. We also show how viscous fingering becomes effective here. Although we shall not discuss this point exhaustively, we shall show that our model is in good agreement with the work mentioned above.

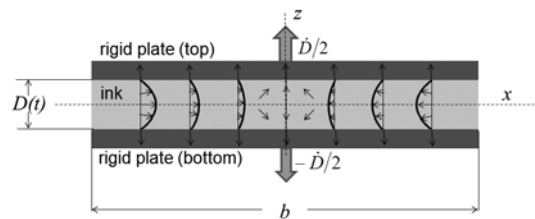


Figure 2: Geometry and flow velocity profile (indicated by the arrows and the bold-printed curves) of a viscous ink between two expanding (or approaching) parallel rigid plates

we are interested in are time-dependent due to the boundary conditions given by the moving plates. In the lubrication limit, the viscous shear stress in x - and y -direction is neglected compared to the stress in z -direction, and one obtains

$$\eta \frac{\partial^2 \vec{v}}{\partial z^2} = \vec{\nabla} p \quad [2]$$

with boundary conditions $v_x = 0$ and $v_z = \pm \dot{D}/2$ at $z = +D(t)/2$ and $z = -D(t)/2$, where $\dot{D} = \partial D / \partial t$. Note here that we do not claim the velocity component v_z and its gradients in z -direction to be negligible, in contrast to Darcy's equation which is suited for cuvette flows as e.g. employed by Saffman and Taylor (1958). This is specifically important for printing inks where elongational ink flows usually cannot be ignored.

Due to the incompressibility, the hydrostatic pressure between the plates satisfies the Laplace equation $\nabla^2 p = 0$. If L is assumed to be very large or infinite,

such that flows and pressure gradients in y -direction are negligible, one finds

$$p(x, z, t) = p_0 + \frac{6\eta \dot{D}}{D^3(t)} \left(x^2 - z^2 - \frac{b^2}{4} \right) \quad [3]$$

where p_0 is the atmospheric pressure outside of the gap, including capillary forces at the ink meniscus. The solution is entirely defined by the condition that the hydrostatic pressure difference towards p_0 should vanish at $|x| \sim b$, with $|x| \gg |z|$. By direct inspection one easily shows that the solutions v_x and v_z read as follows

$$v_x(x, z, t) = \frac{6\dot{D}x}{D^3} \left(z^2 - \frac{D^2}{4} \right) \quad [4]$$

$$v_z(x, z, t) = -\frac{6\dot{D}}{D^3} \left(\frac{z^3}{3} - \frac{D^2z}{4} \right) \quad [5]$$

and $v_y = 0$. This also satisfies the incompressibility relation $\vec{\nabla} \cdot \vec{v} = 0$. The viscous stress in the printing ink is given by two components of the viscous flow tensor: the shear rate $\gamma_{xz} = 12\dot{D}xz/D^3$, and the elongational flow rate $\gamma_{zz} = -12\dot{D}(z^2 - D^2/4)/D^3$. Comparing these components one finds that the shear component is dominant over the elongational one whenever $|x| > |z|$. In the early stage of the plate movement when the distance $D(t)$ is small compared to the plate length b , and when pressure differences are large – hydrostatic pressure p scales as $1/D^3$ – this applies to almost the entire ink volume, except for a narrow strip of width $\approx 2D$ in the very center of the nip. This ratio will be reversed in the later stages of ink splitting when printing plate has substantially lifted from substrate. Hydrostatic pressure will have dropped here. We conclude that the forces acting on the printing plate and the related elastic

deformation are a consequence of viscous shear rather than of elongational stress. The lubrication approximation used by Eq. [1] is no longer valid here, and one has to take account of viscous shear in x - and y -direction. We shall again raise this question in a later section when discussing viscous flows between cylinders (Figure 3).

These above velocity functions can be generalized to plates with a weakly deformed or corrugated instead of a flat surface. This corresponds to a gap of spatially variable width $D(x, y, t)$, with $|dD/dx| \ll 1$ and $|dD/dy| \ll 1$:

$$v_x(x, z, t) \approx \int_0^x \frac{6\dot{D}(x', t) dx'}{D(x', t)} \left(\frac{z^2}{D^2(x, t)} - \frac{1}{4} \right) \quad [6]$$

For general $D(x, y, t)$ the integration path should follow a contour in the lateral plane from the reference point 0 to position (x, y) . This result is approximate as the flow satisfies the incompressibility condition only up to terms of order of $|dD/dx| z^2/D^2$. For the velocity component v_z Eq. [5] still applies, now however with D being dependent on x, y , and t .

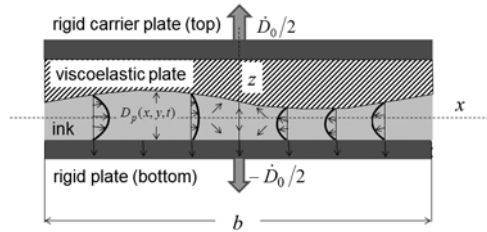


Figure 3: Geometry and ink flow profile between two expanding plates one of which is viscoelastic and deformed by the local hydrodynamic ink pressure

3. Squeeze flow between compressible plates

Our model applies to elastic plates as well. However, we must take account of an additional variability of the gap size $D(x, y, t)$ which is due to the hydrostatic ink pressure p inside the gap. This situation is shown in Figure 3. For the plates we assume a linear viscoelastic compressibility relation

$$D_p = D_0 + \kappa_p (p - p_0) - \alpha_p \int_0^t (p(t') - p_0) dt' \quad [7]$$

The time derivative reads

$$\frac{dD_p}{dt} = \dot{D}_0 + \kappa_p \frac{dp}{dt} - \alpha_p (p - p_0) \quad [8]$$

where $D_0(t)$ is the gap width in absence of any pressure, $\kappa_p = d_{s,1}/E_1 + d_{s,2}/E_2$ is the plate compressibility; $d_{s,1}$ and $d_{s,2}$ denote the thicknesses of the printing plate and the adhesive bonding tape, respectively, and E_1 and E_2

are the elastic moduli of both materials. Further, α_p describes the viscous creep of the flexo plate in terms of thickness loss per time at unit excess pressure.

Considering the hydrostatic pressure p between the elastic plates Eq. [3] is not applicable any more. The pressure gradients may be obtained from Stokes equation [1] inserting the flow velocity distribution from Eq. [5]. Differentiating this equation three times with respect to z yields the identity

$$\frac{\partial^2 p}{\partial z^2} = \eta \frac{\partial^3 v_z}{\partial z^3} = -\frac{12\eta}{D_p^3} \frac{dD_p}{dt} \quad [9]$$

with D_p being dependent on x, y, t , and p according to Eq. [8]. By ink incompressibility p is harmonic in 3D space, i.e. $\frac{\partial^2 p}{\partial z^2} = \frac{\partial^2 p}{\partial x^2} + \frac{\partial^2 p}{\partial y^2}$, and $p(x, y, z, t)$ is thus fully

determined through the projection of the function p to the x - y -plane, in addition with the viscous boundary conditions at the plates that are already implemented in Eq. [9]. We thus obtain a 2D differential equation for p in the x - y -printing plane, describing viscous ink flow between the deformable plates

$$\left(\frac{\partial^2}{\partial x^2} + \frac{\partial^2}{\partial y^2} \right) p = \frac{12 \eta \kappa_p}{D_0^3} \frac{\partial p}{\partial t} - \frac{24 \eta (\kappa_p \dot{D}_0 + \alpha_p D_0)}{D_0^4} (p - p_0) + \frac{12 \eta \dot{D}_0}{D_0^4} \quad [10]$$

We have omitted here terms which are of quadratic order in the compressibility parameter κ_p . Note that, although Eq. [10] is a 2D differential problem, it is capable of describing the full 3D pressure distribution between the plates. We do not assume here that pressure gradients in z -direction are absent. Rather, z -gradients can be reconstructed from Eq. [10] by inserting it into $\nabla^2 p = 0$. Further, the ink flow velocities v_x and v_y , (i.e. their average over the liquid layer thickness) can be calculated using Darcy's equation $\vec{v} = -(D^2 / 12\eta) \vec{\nabla} p$, see e.g. Whitacker (1986).

Squeezed ink volume. By use of Darcy's equation, and by integrating the left hand side of Eq. [10] over the printing area A in the x - y -plane, and over the time history up to the present moment, one can calculate the amount of ink squeezed at the rim ∂A of A up to time t from the beginning of plate movement

$$\begin{aligned} & \int_{-\infty}^t \frac{D^3(t')}{12\eta} \int_A \left(\frac{\partial^2}{\partial x^2} + \frac{\partial^2}{\partial y^2} \right) p \, dx \, dy \, dt' = \\ & - \int_{-\infty}^t D(t') \int_A \left(\frac{\partial v_x}{\partial x} + \frac{\partial v_y}{\partial y} \right) dx \, dy \, dt' \quad [11] \\ & = \int_{-\infty}^t \oint_{\partial A} D(t') \vec{q} \cdot \vec{v}(t') \, dl \, dt' = V_{sq}^{(A)}(t) \end{aligned}$$

Here, \vec{q} is the unit vector in the x - y -plane normal to the rim of the printing plate, and dl is a line segment of that rim. We have replaced the Laplacian of p by the flow velocity according to Darcy's law, and then applied Gauss' integral theorem. Calculating the amount of ink squeeze for an elastic printing plate is now possible according the following procedure: solve Eq. [8] for the specific plate–substrate distance and the boundaries of the printing area as being defined by the printing layout, take the Laplacian of the pressure, and obtain its integral according to Eq. [11].

Mathematically Eq. [10] corresponds to a standard 2D-heat diffusion equation, where the pressure p has the role of the temperature. We refer the reader to the textbook of Landau and Lifshitz (1970) where the

physical content of the coefficients in such equations is thoroughly discussed. From this analogy, we can define macroscopic parameters which determine the overall behavior of the system such as a constant of pressure relaxation, the ink squeeze length, and the power dissipation endowed with viscous ink shear.

For sake of simplicity we omit the creep constant a_p in the sequel but emphasize that it could easily be integrated by a simple redefinition of the coefficients in the differential equation.

Consider the case that the two plates have been approaching each other so that some hydrostatic pressure has developed in the gap. When the plate movement is interrupted at time t_0 , i.e. if $dD_0/dt = 0$ for $t > t_0$ Eq. [8] reduces to

$$\left(\frac{\partial^2}{\partial x^2} + \frac{\partial^2}{\partial y^2} \right) p = \frac{12 \eta \kappa_p}{D_0^3} \frac{\partial p}{\partial t} \quad [12]$$

from t_0 on. The pressure between the plates is now described by the strongly simplified diffusion Equation [12]. The pressure and its gradients do not disappear immediately at $t = t_0$, but pressure relaxation will take some time depending on the spatial pressure distribution between the plates and specifically at the edges. The key observation is that ink flow is characterized by some kind of diffusion constant

$$\Lambda_p = \frac{D_0^3}{12 \eta \kappa_p} \quad [13]$$

During the period of relaxation there is an ink flow along the gradient direction of the pressure. This specifically applies to the rims of the printing area of plates, where ink is squeezed out.

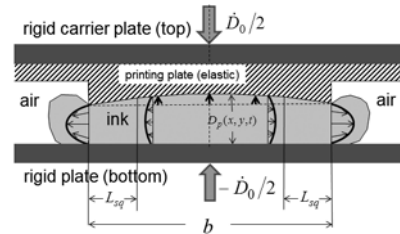


Figure 4: The squeezing of ink at the rim of a printing element of width b on the printing plate with the flow profiles; the pressure-related elastic deformation of the printing form is indicated by the bold printed arrows

When b is the length of the plate in printing direction, or of the structure element on a printing form, we can estimate the time span in which ink will still be squeezed out at the rim after t_0

$$\Delta t_{sq} \propto \frac{b^2}{\Lambda_p} = \frac{12 \eta d_s}{D_0^3 E} b^2 \quad [14]$$

The ink forms a more or less pronounced seam, or halo, at the rim as indicated in Figure 4, with printing results as shown in Figure 5.

Consider now the case that the printing plate is approaching the substrate with small but constant velocity dD_0/dt . The protruding elements on the printing plate, covered with ink, will come into contact with the printing substrate at some point. After contact the ink pressure will start to increase more or less constantly in time throughout the printing area, except for a narrow seam along the rim of the protruding element. The pressure here will cease to rise accordingly, as ink is continuously escaping sideways beyond the rim. We denote the width of the zone where this ink squeeze is substantial as the squeeze length L_{sq} . It can be determined from the coefficient of the steady-state diffusion problem, and depends on dD_0/dt as follows

$$L_{sq} = \frac{D_0^2}{\sqrt{24\eta\kappa_p\dot{D}_0}} \quad [15]$$

4. Squeeze flow between elastic rotating cylinders

Cylindrical surfaces can be approximated by parabolic ones as far as the nip region is concerned. The gap width (in absence of elastic deformation) is

$$D_0(x, y, t) \propto D_n + \frac{1}{2r_n}(x - v_p t)^2 \quad [16]$$

where D_n is the minimum distance between printing plate surface and substrate in the nip,

$\frac{1}{r_n} = \frac{1}{R_p} + \frac{1}{R_i}$ is the total surface curvature in the nip, defined by the radii R_p of the printing and R_i of the impression cylinder, and v_p is the printing velocity. By the analogous derivation as described in Eq. [10] one can again obtain an equation for the ink pressure as measured by an observer attached to the substrate who is moving through the nip with printing velocity $-v_p$:

$$\left(\frac{\partial^2}{\partial x^2} + \frac{\partial^2}{\partial y^2} \right) p = \frac{96\eta r_n^3}{(\lambda_n^2(p) + (x - v_p t)^2)^3} \times \left(\kappa_p \frac{\partial p}{\partial t} + \kappa_p v_p \frac{\partial p}{\partial x} + \frac{4\kappa_p v_p (x - v_p t)}{\lambda_n^2(p) + (x - v_p t)^2} \right) \quad [17]$$

$$\left(p - p_0 \right) - \frac{v_p (x - v_p t)}{r_n}$$

where

$$\lambda_n(p) = \sqrt{2r_n(D_n + \kappa_p(p - p_0))} \quad [18]$$

is the pressure-corrected nip length, i.e. the width of the contact zone of printing plate and substrate where a

This width essentially determines a limit for the resolution of the flexo printing process imposed by viscous ink flows. The aim of accurate printing is, of course, to keep this length small.



Figure 5: Typical seam or “halo” of a flexo printed pattern: the ink has been squeezed and has been deposited in the seam at the rim of the printed pattern; depositing ink within the intended areas has failed: only residuals of the ink have remained, and form a labyrinth-shaped structure

substantial shear flow is created. Note also that the right hand side of Eq. [17] is substantially distinct from 0 in a range of width

$$\lambda_n = \sqrt{2r_n D_n} \quad [19]$$

in the nip. In the sequel, this length will essentially have the role of b in Eqs. [3] and [12]. We call this the effective nip length. From the observation that according to Eq. [19] the effective nip length $\lambda_n \gg D_n$ is much larger than its width, and considering that elongational stress in the ink is dominant only within the small range $|x| < D_n$, we also conclude that viscous shear and not elongational stress in the ink is dominant for hydrostatic pressure formation and for printing form deformation. As the width is a function of the ink pressure, the squeeze problem now becomes essentially a nonlinear one. Nevertheless, the solutions of this equation have a number of general properties. In the case of hard surfaces ($\kappa_p = 0$), and assuming a steady-state process, the pressure equation can be integrated, yielding the time-independent solution

$$p(x) = p_0 + p_{visc} \left(\zeta(x / \lambda_n) - \frac{x}{x_m} \zeta(x_m / \lambda_n) \right) \quad [20]$$

with $p_{visc} = 12\eta v_p r_n^2 / \lambda_n^3$ and the dimensionless function $\zeta(x) = \frac{x}{1+x^2} + \arctan x \cdot$

We have assumed here that the pressure at the ink menisci on both sides of the nip (i.e. $p(x)$ at $x = -x_m$ and $x = x_m$ equals the atmospheric air pressure p_0 .

For $|x_m| > x > -|x_m|$ the solution predicts that a point on the substrate which is moving through the nip first experiences a pressure maximum well above the air pressure. The pressure then drops to a minimum situated on the outgoing half of the nip. This pressure minimum is responsible for the back flow of ink from the diverging surfaces to the nip.

Assuming parameters here as listed in Table 1, however, clearly indicates that the hard-cylinder case strongly overestimates the pressure, and that viscous ink flows in the nip cause a significant increase of the nip length $\lambda_n(p)$ by the exerted hydrostatic pressure according to Eq. [18].

Moreover, viscous forces give rise to a small but finite mechanical torque acting on the printing cylinder. This torque is directed such as to hamper the rotation of the cylinder.

In order to obtain a more realistic estimate on the length $\lambda_n(p)$ we consider its value at the pressure maximum p_{visc} and insert this into Eq. [18]. Resolving this equation for $\lambda_n(p)$, and provided that the printing velocity v_p

satisfies $|v_p| \gg v_{sq} = \frac{D_n^2}{24\pi\eta\kappa_p} \sqrt{2D_n/r_n}$, one obtains a nip length scaling with the printing velocity v_p

$$\lambda_n(p_{visc}) \propto (24r_n^3\kappa_p\eta|v_p|)^{0.2} \quad [21]$$

Velocity v_{sq} essentially is the typical squeeze flow velocity of the ink and of order of mm/s. Eq. [21] is a remarka-

ble result as it shows that the nip length does no longer depend on the initial nip height D_n , and is much larger than the value predicted from hard cylinders.

Using the parameter set assumed in Table 1, we obtain values of approximately 2 mm instead of 600 μm . The nip length is therefore determined by the equilibrium of elastic and viscous forces in the nip as created by the ink flow. Inserting this result into Eq. [18] we can conclude that there are scaling relations of further quantities as well. Pressure scales as $p - p_0 \propto v_p^{0.4}$,

the average nip height satisfies

$$D(p_{visc}) \propto \sqrt{2r_n\kappa_p p_{visc}} \propto v_p^{0.2},$$

and the squeeze time is $\Delta t_{sq} \approx \lambda_n(p_{visc}) / v_p \propto v_p^{-0.8}$.

Finally, using again Darcy's equation, we obtain the scaling law for the squeeze velocity

$$v_{sq} = \left| -(D^2(p_{visc}) / 12\eta) \bar{\nabla} p \right| \propto v_p^{0.6}.$$

We can further estimate the ink displacement

$W(v_p) \propto v_{sq} \Delta t_{sq}$ caused by the squeeze flow.

$$W(v_p) = v_{sq} \Delta t_{sq} \propto \frac{D^2(p_{visc})}{12\eta} \frac{p - p_0}{\lambda_n(p)} \Delta t_{sq} \propto \frac{(v_p^{0.2})^2 v_p^{0.4}}{v_p^{0.2}} v_p^{-0.8} = v_p^{-0.2} \quad [22]$$

Eq. [22] implies that ink squeeze is reduced with increasing printing velocity with a specific exponent of -0.2 .

Table 1: Typical orders of magnitude of the relevant parameters for a flexo printing process

Parameter	Symbol	Equation	Typical values
Ink viscosity	η	[1]	20 mPa·s
Thickness of the flexo plate & adhesive tape	d_s	[8]	2 mm
Young modulus of the flexo plate	E	[8]	20–100 MPa
Compressibility constant	κ_p	[8]	$0.2-1 \cdot 10^{-10} \text{ m}^3/\text{N}$
Pressure diffusivity	L_p	[13]	0.01–0.1 m^2/s
Squeeze time at $b = 600 \mu\text{m}$	Δt_{sq}	[14]	0.1–10 s
Squeeze length	L_{sq}	[15]	20–100 μm
Nip height	D_n	[16]	1–2 μm
Static nip length for hard cylinders ($r_n = 10 \text{ cm}$)	λ_n	[19]	600 μm
Dynamic nip length for elastic cylinders ($r_n = 10 \text{ cm}$) with self-consistent calculation	$\lambda_n(p)$	[18]	2 mm

Table 2: Overview over flexo printing parameters X and length scales which depend on the printing velocity v_p according to $X \propto v_p^k$ and the respective exponents k ; the increase or decrease of X that is predicted if v_p is doubled is indicated as well

Parameter X	Symbol	Exponent k	Expected relative change at doubled printing speed
Nip length	$\lambda_n(p_{visc})$	+0.2	+15 %
Nip pressure	p_{visc}	+0.4	+32 %
Effective nip height	$D(p_{visc})$	+0.2	+15 %
Ink squeeze time	Δt_{sq}	-0.8	-53 %
Ink squeeze velocity	v_{sq}	+0.6	+52 %
Ink shear	$\propto v_{sq} / D(p_{visc})$	+0.4	+32 %
Ink seam width	$W(v_p)$	-0.2	-13 %

Considering a specific flexo printing job this means that seam formation at the rim of printed patterns should reduce by 13 % when accelerating the printing press by a factor of 2. Further tendencies are summarized in Table 2. This prediction can be checked experimentally by examination of printed samples as we shall show now.

Figure 6 shows scans of flexo printed samples with specific defects that will be discussed using the above model. Arrays of full-area rectangles of 30×15 mm in size were printed on coated paper (IGEPA Maxisatin, 90 g/m^2) at different printing speeds between 20 and 160 m/min using a Gallus RCS 330 printing press. As printing ink, water based gravure/flexo ink type 8/110305 WD from Ruco (A. M. Ramp & Co. GmbH, Eppstein, Germany) was used and diluted with 50 vol. % of deionized water. The anilox roller (Zecher GmbH, Paderborn, Germany, standard Cr_2O_3 ceramic surface on aluminium) had a raster width of 130 lines per cm and a transfer volume of 13.2 ml/m^2 . The flexo plate was made of nyloflex FAH digital, with a hardness of 60 ShA, and 1.14 mm of thickness.

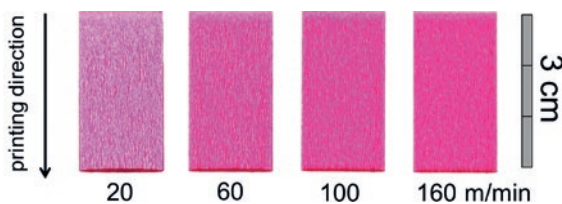


Figure 6: Flexo printed rectangles created with printing velocities of 20, 60, 100, and 160 m/min; the rectangles show a pronounced viscous fingering (ribbing), and ink seam at the edge in forward direction (i.e. at their bottom); the width of this rim scales with the printing velocity v_p

The printed rectangles exhibit two peculiar features: viscous finger formation, and ink squeezing. Ink squeezing resulted in a dense ink seam at the rectangle's border situated at the printing end. Here, the ink conducted in the nip zone is released from the rear edge of the printing area on the flexo plate, and deposited on the substrate. The width W (measured by digital evaluation of a 600 dpi scan of the printed samples, see Figure 6) of this seam is therefore essentially equal to the width $2\lambda_n(p_{visc})$ of the nip zone, or at least proportional to this length scale.

In the considered range of printing velocities we obtained seams of 0.5 to 0.7 mm in width. Plotting these values versus printing speed v_p we are thus able to check the scaling law implied by Eq. [21], which predicts that $\lambda_n(p_{visc}) \propto v_p^k$, with an exponent $k = -0.2$. Evaluating our printed samples we find that $k = -0.158 \pm 0.059$ which is indicated as the dash-dotted line in the logarithmic plot in Figure 7.

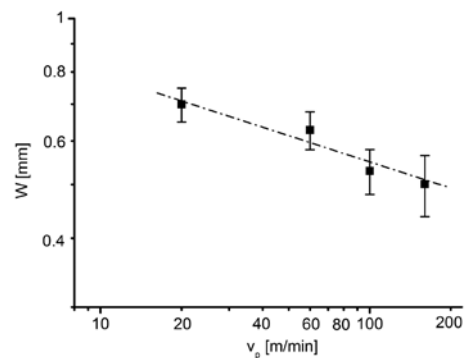


Figure 7: The width W of the seam as a function of printing velocity; the decrease of W corresponds to a scaling exponent $k = -0.158 \pm 0.059$ (dash-dotted line)

5. Stagnation points of viscous nip flow and how they affect the ink transfer

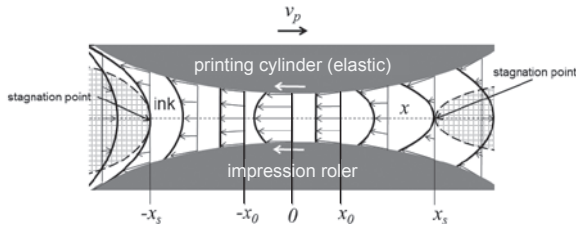


Figure 8: Ink flow velocity in the nip between two rotating cylinders, indicated by arrows and bold-printed curves; in the center region of the nip ($-x_0 < x < x_0$) the velocity of the ink exceeds the revolution speed of the cylinders (unless $x_0 = 0$), for $x > x_0$, and for $x < -x_0$, the ink flow is retarded in the middle between the cylinders and comes to rest the stagnation points $x = x_s$ and at $x = -x_s$; ink in the cross-hatched area never passes the nip but is trapped in circulating vortices before and after the nip

Ink squeezing is the consequence of a viscous ink flow in the microscopic gap between flexo plate and substrate, and here, we therefore have to consider ink velocity profile in the nip, using Eq. [6]. This equation describes an excess in flow velocity in the center between the two surfaces, with a Hagen-Poiseuille type velocity profile. This excess flow terminates at two stagnation points in a distance x_s in front of and behind the nip. This is depicted in Figure 8. The ink is apparently at rest here, i.e. $v_x(\pm x_s) = 0$. On the cylinder surfaces, the ink velocity is identical to v_p . In contrast, the ink velocity in the center of the nip, i.e. at $x = 0$, is:

$$v_x(x, z = 0) = v_p - \frac{3}{2} \int_{x_0}^x \frac{\dot{D}_p(x')}{D_p(x')} dx' = v_p + \frac{3v_p}{2} \log \frac{x_0^2 + \lambda_n^2}{x^2 + \lambda_n^2} + O(\dot{p})$$
[23]

The point x_0 corresponds to the position along the x axis where $v_x(x) = v_p$, and is an arbitrary parameter of the solution.

6. Viscous finger formation

We now consider the linear stability of a straight ink meniscus. As there is apparently more than one solution possible, distinguished by x_0 , we take account of capillary forces at the meniscus in order to decide which of the solutions is preferred by the surface forces, and whether this corresponds to a straight meniscus. We anticipate that the latter is not the case, specifically for the outgoing nip. Rather, the formation of finger-like patterns, viscous fingering, is usually observed. This is related to the Saffman-Taylor instability which is observed at retracting liquid surfaces. We shall not

The ink velocity approaches zero at positions $x = \pm x_s$, with

$$x_s \approx \pm \sqrt{1.9477 x_0^2 + 0.9477 \lambda_n^2}$$
[24]

These are the stagnation points of the ink flow. Ink outside these points, i.e. at positions $|x| > |x_s|$ will never pass through the nip. These ink portions will first approach the nip up to some minimum distance, but then reverse their movement in opposite direction. For this reason, the ink menisci located at $x = \pm x_m$ must coincide with the stagnation points in a steady-state situation, and the ink pressure must equal the atmospheric, in addition to the capillary pressure. In other words, $x_s = x_m$ holds here. The important point is that there is more than one solution of the hydrodynamic problem, and that these solutions are distinct in the position x_0 of shear-free flow, and in the stagnation points. The ink flow therefore is in an approximately indifferent equilibrium, and the flow and pressure distribution depend on the quantity of printing ink supplied to the nip, and on further forces such as capillary pressure. Moreover, the stagnation points, and therefore the menisci on both sides of the nip, are in mutual interaction. They cannot be shifted independently. Supplying more ink on the incoming side of the nip will move the stagnation points further apart from the nip. This, in turn, will increase the Poiseuille pressure, and squeeze additional ink portions through the nip, thereby widening the opening between the elastic printing plate surface and the substrate. This has an important consequence with respect to ink transfer: providing more ink to the printing plate by the anilox roller will also increase the transferred ink volume on the printing plate as the stagnation points of the ink flow will move outwards. One further aspect concerns the formation of possible ghost images: in spite of the intense shear of the ink in the nip the amount of ink deposited on the substrate depends on the excess ink that resides in the menisci of the nip since former contacts with substrate or anilox roller, as the excess ink will contribute to later ink transfer events.

discuss this here in detail, and we restrict to cylinders with hard surfaces. Our aim here is to demonstrate how viscous fingering instabilities principally appear in our model.

$$\frac{\partial p(x)}{\partial x_m} \Big|_x = p_{visk} \frac{x}{x_m^2} \left[\frac{x_m \lambda_n (x_m^2 - \lambda_n^2)}{(x_m^2 + \lambda_n^2)^2} + \arctan \frac{x_m}{\lambda_n} \right] = p_{visk} \frac{x}{x_m^2} \left[0.7586 + O\left(\frac{x_0}{\lambda_n}\right)^2 \right]$$
[25]

Taking the derivative of Eq. [20] with respect to the position x_m of the ink meniscus we find that at a given position x , with $-x_m < x < 0$ on the outgoing side behind the meniscus the ink pressure $p(x)$ is raising as the meniscus retracts towards the nip.

When considering elastic printing plates, one has, of course, to take the derivative of the full solution of Eq. [17] instead. As the derivative Eq. [24] is a negative on the outgoing side of the nip the solution cannot be stable: small fluctuations $\Delta x_m(y) = x_m(y) - x_{m,0}$ of the meniscus position $x_m(y)$ from the average position $x_{m,0}$ across the width of the printing plate will cause ink to be shifted from positions where the meniscus is retracting to positions where it is expanding. When we equilibrate these pressure fluctuations by the excess of surface energy related to the deformation of the meniscus as is given by

$$p_L = -\sigma \frac{\partial^2 x_m}{\partial y^2} \quad [26]$$

with σ as the surface tension of the ink, we obtain that periodic instabilities are possible for wavelengths larger than

$$\lambda_{\min}^{V.F.} = \sqrt{\frac{\sigma \lambda_n^3 x_{m,0}}{9.103 \eta v_p r_n^2}} \propto D_n \sqrt{\frac{\sigma}{4 \eta v_p}} \quad [27]$$

This is, up to minor numerical corrections, the well-known result from Saffman and Taylor (1958), and of the other authors cited above. In this manner it is possible to study viscous fingering phenomena between curved and elastic surfaces from solutions of the pressure equation [17], using capillary pressure at the meniscus as a boundary condition.

7. Conclusions

The specific benefit of our model is the following. It reduces the complex 3D hydrodynamic problem of ink splitting, at least under the assumptions of lubrication theory, to a still challenging but much better accessible 2D scalar potential problem. With respect to flexography, moreover, an essentially linear regime of this mathematical model is relevant, rendering many interesting questions into the range of analytic studies: the effect and significance of the elastic deformation of the printing

form, the systematical analysis of squeeze flows and ink splitting in the nip, on full-tone as well as on structured printing forms. Providing the surface profile of a printing form one can further define the complete boundary value problem for the calculation of pressure distribution, ink flows, and the ink distribution on the substrate. This could be of great help when designing high-resolution flexographic printing forms, as it is able to predict the ink flows as a function of the shape of the printing form.

Acknowledgements

We would like to appreciate the funding of this work by the German Federal Ministry of Research and Education (BMBF) under grant no. 13N10298 (NanoPEP).

Literature

- Behler, H., 1993. *Die Randstruktur von Druckpunkten – Eine experimentelle Untersuchung der Farbspaltungsströmung*, PhD thesis, TU Darmstadt.
- Ben Amar, M., 1991. Viscous fingering in a wedge, *Physical Review A*, 44(6), pp. 3673–3685.
- Bohan, M.F.J., Fox, I.J., Claypole, T.C. and Gethin, D.T., 2003. Influence of non-Newtonian fluids on the performance of a soft elasto-hydrodynamic lubrication contact with surface roughness, *Proceedings of the Institution of Mechanical Engineers, Part J: Journal of Engineering Tribology*, 217, pp. 447–459.
- Bornemann, N., Sauer, H.M. and Dörsam, E., 2011. Gravure printed ultrathin layers of small-molecule semiconductors on glass, *Journal of Imaging Sciences Technology*, 55(4), pp. 040201-1–040201-8.
- Bornemann, N., 2013. *Characterization and Investigation of Large-Area, Ultra-Thin Gravure Printed Layers*, PhD thesis, TU Darmstadt [online]. Available at: <<http://tuprints.ulb.tu-darmstadt.de/id/eprint/3847>> [Accessed 10 September 2015].
- Casademunt, J., 2004. Viscous fingering as a paradigm of interfacial pattern formation: recent results and new challenges, *Chaos*, 14(3), pp. 809–824.
- Fields, R.J. and Ashby, M.F., 1976. Finger-like crack growth in solids and liquids, *Philosophical Magazine*, 33(1), pp. 33–48.

- Gaskell, P.H., Innes, G.E. and Savage, M.D., 1998. An experimental investigation of meniscus roll coating, *Journal of Fluid Mechanics*, 355, pp. 17–44.
- Gingras, M.J.P. and Rácz, Z., 1989. Noise and the linear stability analysis of viscous fingering, *Physical Review A*, 40(10), p. 5960.
- Hopkins, M.R., 1957. Viscous flow between rotating cylinders and sheet moving between them, *British Journal of Applied Physics*, 8(11), p. 442.
- Landau, L.D. and Lifshitz, E.M., 1970. *Theory of Elasticity*, 2nd ed. Oxford: Pergamon Press.
- Lindner, A., Bonn, D., Ben Amar, M., Meunier, J. and Kellay, H., 1999. Controlling viscous fingering, *Europhysics News*, 30(3), pp. 77–78.
- Lindner, A., Coussot, P. and Bonn, D., 2000. Viscous fingering in a yield stress fluid, *Physical Review Letters*, 85(2), pp. 314–317.
- Maher, J.V., 1985. Development of viscous fingering patterns, *Physical Review Letters*, 54(14), p. 1498.
- Saffman, P.G. and Taylor, G., 1958. The penetration of a fluid into porous medium or Hele-Shaw cell containing a more viscous fluid, *Proceedings of the Royal Society of London, Ser. A*, 245(1242), pp. 312–329.
- Sauer, H.M., Bornemann, N. and Dörsam, E., 2011. Viscous fingering in functional flexo printing: an inevitable bug? In: *Large-area, Organic & Printed Electronics Convention (LOPE-C)*, Organic and Printed Electronics Association, Frankfurt, Germany.
- Varela López, F., Pauchard, L., Rosen, M. and Rabaud, R., 2002. Non-Newtonian effects on ribbing instability threshold, *Journal of Non-Newtonian Fluid Mechanics*, 103, pp. 123–139.
- Varela López, F. and Rosen, M., 2002. Rheological effects in roll coating of paints, *Latin American Applied Research*, 32, pp. 247–252.
- Voss, C., 2002. *Analytische Modellierung, experimentelle Untersuchung und dreidimensionale Gitter-Boltzmann-Simulation der quasistatischen und instabilen Farbspaltung*, PhD thesis, Universität Gesamthochschule Wuppertal.
- Whitacker, S., 1986. Flow in porous media I: A theoretical derivation of Darcy's law, *Transport in Porous Media*, 1(1), pp. 3.25.

JPMTR 064 | 1419
DOI 10.14622/JPMTR-1419
UDC 667.6 : 676.2

Research paper
Received: 2014-07-15
Accepted: 2015-08-28

Effect of coating pigment, binder type and binder amount on planar liquid wicking on coated substrates

Eveliina Jutila¹, Risto Koivunen¹, Patrick A. C. Gane^{1,2}

¹School of Chemical Technology,
Department of Forest Products Technology, Aalto University,
PL 16400, 00076 Aalto, Finland

E-mail: eveliina.jutila@aalto.fi
risto.koivunen@aalto.fi
patrick.gane@omya.com

²Omya International AG, Baslerstrasse 42,
CH-4665 Oftringen, Switzerland

Abstract

This study focuses on the development of highly wicking coated substrates for microfluidic devices with enhanced resolution compared to current filter paper-based devices. Four highly absorbing pigments, fumed silica (FS), modified calcium carbonate (MCC), natural diatomite (ND) and flux-calcined diatomite (FCD), as well as three binders, styrene-acrylate (SA) latex, polyvinyl alcohol (PVOH) and carboxymethyl cellulose (CMC), were used to form coating structures with different wicking properties. Studies include characterisation of the pigment particles and thin layer wicking (TLW) experiments, in which wicking height of liquid in coatings is measured as a function of time. The results show that the choice of coating pigment and binder as well as the binder amount has a significant effect on wicking characteristics of a coating. The introduction of diatomite pigments into blends with MCC improved the wicking capabilities of the coating, especially in the case of ND. Latex was found to inhibit wicking of liquid the least, followed by PVOH and CMC. Increased binder amounts reduce wicking due to reduced pore connectivity and binder-filled pores. It was found that the wicking resistance of pigment alone is too high for rapid analysis over long distances in thick coatings. Once optimised for binder type and amount, these coating structures could be utilised as high resolution microfluidic analysis elements, i.e. test cells, incorporated either into a wicking channel matrix or placed at junctions of microfluidic channels derived from controlled hydrophobic/oleophobic printing or designed shrinkage fracture geometries.

Keywords: microfluidic device, absorbent coating, microdiagnostics, hydrophilic channel, printed functionality

1. Introduction

Microfluidic analytical devices represent one of the most promising future applications in functional printing. Paper-based devices are not only inexpensive and portable, but they can be modified easily and can provide a fast and simple analysis through capillary absorption without external instrumentation. Furthermore, the microfluidic character of the devices enables small sample volumes and simultaneous multianalyte sensing (Abe, Suzuki and Citterio, 2008). Researchers contributing to the majority of the prior art utilise cellulose-based chromatographic and filter papers, in which the sample wicks along cellulose fibres (Khan et al., 2010; Martinez et al., 2010; Yetisen, Akram and Lowe, 2013). Despite the practical advantages, current paperfluidic devices have limitations such as accuracy and sensitivity (Liana et al., 2012). By adopting porous coated substrates it may be possible to fabricate narrower, better spatially resolved channels, and so enhance the resolution and enable smaller volumes of sample to be applied, as well

as provide better colour contrast during optical sensing. The term resolution in this context refers to the degree of control of the spreading of liquids and printing inks, such as containment channel walls and sites used as test cells containing analytes in reaction areas, on the substrate used in microfluidic devices. Speciality coated substrates provide better resolution than uncoated filter paper devices, due to increased control over spreading via detailed design of pore structure and surface free energy. Previous attempts to use coated paper in paperfluidics, however, have proven unsatisfactory due to heterogeneous colour distribution in the reaction area and low wicking capabilities of coated paper (Määttänen et al., 2011; Zhong, Wang and Huang, 2012).

1.1 Background

A plain paper substrate can be transformed into a diagnostic device by printing functional components, such as

hydrophilic channels that guide polar fluid flow through analysis regions, points or cells to perform chemical assays, and by depositing chemical reagents into those test stations, the resultant components of which may even flow further into detection zones (Martinez et al., 2007; Mukhopadhyay, 2010). The main advantages of employing paper as a base material include its low cost, availability, portability and ease of modification. In addition, paper-based microfluidics function without external pumps, instrumentation or power, and provide a fast and simple analysis (Martinez et al., 2007), even remotely, if combined with an imaging device (Martinez et al., 2008; Yetisen, Akram and Lowe, 2013).

Low cost diagnostics are especially needed in underprivileged and developing countries, where people suffer from high levels of infectious diseases such as HIV, malaria and tuberculosis (Lee et al., 2010; Lisowski and Zarzycki, 2013) as well as in remote or other resource-limited areas distanced from healthcare establishments or electricity (Maxwell, Mazzeo and Whitesides, 2013). The microfluidic character of the devices enables reducing sample volume down to microlitres and, therefore, these devices offer a superior solution compared to conventional diagnostic tools, which often require large reagent and sample quantities as well as specific laboratory conditions and accomplished professionals for the analysis (Whitesides, 2013).

The basic principle of paperfluidic devices embodies the following three phases (Mukhopadhyay, 2010). First, a drop of sample, for example a bodily fluid, such as blood, is either placed on the device (planar laminar flow) or the device is dipped into the sample (wicking vertical flow). Secondly, the paper wicks the fluid through walled channels, derived from hydrophobic containment. Finally, the sample is guided into discrete detection zones. Most researchers utilise enzymatic or colour detection (Lisowski and Zarzycki, 2013),

though adopting gold nanoparticles (Mukhopadhyay, 2010) or electrochemical analysis offers an alternative detection method (Maxwell, Mazzeo and Whitesides, 2013; Yetisen, Akram and Lowe, 2013). Several research groups, including George Whitesides' research group at Harvard University (Martinez et al., 2007; 2010), Wei Shen's research group at Monash University (Khan et al., 2010; M. Li et al., 2012), as well as the Sentinel Bioactive Paper Network in Canada (Sentinel, 2015), amongst others, are actively developing simple devices for paper-based point-of-care (POC) diagnosis, food monitoring and environmental screening. Figure 1 shows a prototype of a paper-based device developed at Harvard University.

Despite the promising future of paper-based diagnostics and their many advantages, limitations such as accuracy and sensitivity still show that further development is required (Liana et al., 2012). The hydrophobic walled channels guiding the fluid flow are relatively wide, often greater than 200 μm , hindering the liquid flow length for limited volume application. In addition, sample retention and evaporation during liquid transport result in insufficient sample delivery (Glavan et al., 2013; Li, Ballerini and Shen, 2012), and the resolution of the cellulose-based chromatographic or filter paper utilised by most researchers depends on the size and rather unstable dimensional stability of cellulose fibres in contact with water. Furthermore, swelling of cellulose fibres may further inhibit capillary flow (Yetisen, Akram and Lowe, 2013). By adopting coated substrates it may be possible to fabricate narrower, better spatially resolved channels, and so enhance the resolution and enable smaller volumes of sample to be applied. Also, paper thickness and colour may play a significant role in the analysis of the results (Yetisen, Akram and Lowe, 2013).

Previous attempts to use coated paper as a base material in printed microfluidic diagnostics have, however,

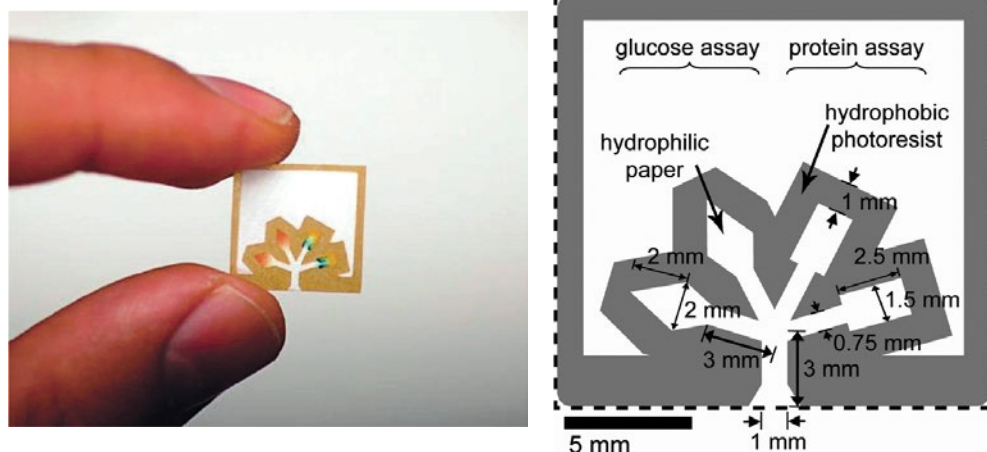


Figure 1: A prototype microfluidic device fabricated on filter paper for simultaneous analysis of glucose and proteins from urine (Reprinted with permission from Martinez et al., 2008; 2010. Copyright (2015) American Chemical Society)

proven unsatisfactory. Määttä et al. (2011) tested the performance of different hydrophilic paper substrates, including a highly permeable Whatman Grade 1 filter paper, an intermediate air permeance surface sized office copy paper, and a slow water and air permeance multilayer-coated paper substrate, for colorimetric glucose detection. The coated paper proved unsuitable for the colorimetric detection due to the heterogeneous colour distribution in the reaction area, caused by slow evaporation of the analyte solution. This phenomenon led to a considerable standard deviation in the calibration curve preventing accurate determination. However, coated paper was best suited for electrical applications, because it offers good print resolution compared to copy paper and filter paper. Zhong, Wang and Huang (2012) investigated the wicking potential of, and wax compatibility with, different paper substrates, including printing paper, paper napkins and paper towel. Their experiments showed that the printing paper had low wicking capability and suggested that this was due to its low porosity and adverse surface tension effects.

1.2 Principles of absorption

Paper-based diagnostics rely on wicking of liquid into the porous medium driven by capillary pressure, which is created by the difference in the surface energies of the dry and wetted solid matrices. Two approaches are commonly combined to model wicking mathematically: the classical Lucas–Washburn (L–W) equation combines the wetting force driving imbibition and the viscous drag opposing it. The viscous drag is related to the permeability defined by Darcy's law (Masoodi and Pillai, 2013). The L–W model assumes an hydraulic flow in an average single capillary derived from a bundle of aligned capillary tubes having the range of radii equivalent to the assumed pores in the sample (Lucas, 1918; Washburn, 1921), whereas Darcy's law describes permeation of an incompressible fluid through a saturated material under pressure as (i) a single-phase flow or (ii) two-phase flow through the porous substrates

2. Materials and methods

Coatings are constructed of various highly wettable pigments, bonded together and to the glass slide using a range of binder types.

2.1 Coating pigments, dispersants and binders

The chosen coating pigments consist of a highly porous form of *modified calcium carbonate* (MCC), typically used in the design of coated inkjet papers (Omyjet 5372 ME) provided by Omya International AG, Oftringen, Switzerland, *fumed silica* (FS, CAB-O-SPERSE PG002) provided by Cabot Corporation, Heverlee, Belgium, and two diatomaceous earths, *a natural diatomite* (ND,

where one phase replaces another (Masoodi and Pillai, 2013). Both of the phenomena constituting the L–W model assume equilibrium laminar flow. In complex micro and nano porous network structures, such as in coating structures, however, equilibrium is rarely established except after very long timescales and after relatively long wicking distances in respect to Darcy permeation behind the wetting front. This is because the liquid becomes accelerated and decelerated within the geometrically rapidly changing pore structure. To account for this, workers invoke either inertial effects via, for example, the Bosanquet equation (Bosanquet, 1923, Schoelkopf et al., 2000) or energy loss during pore entry flow (Szekely, Neumann and Chuang, 1971). The effect is to fill the finest pores in a given layer of the structure preferentially under linear time rate, and the larger pores slower under square root time rate, which in turn act as reservoirs for the next set of finest pores and so on (Ridgway and Gane, 2002). Once equilibrium is reached between these phenomena, a square root of time emerges as the macroscopic observation related to flow under permeation conditions (Ridgway and Gane, 2002). Yetisen, Akram and Lowe (2013) suggest that the most important parameters regarding wicking in porous materials include pore size, pore size distribution, porosity and surface area of the chosen substrate, as well as capillary flow rate, i.e. the migration speed of the liquid front moving along the test sample. Permeability is also needed to provide access to the differentiating mechanism of fine pores, and this contains the important factor of pore connectivity, which is strongly reduced by increasing binder content (Ridgway, Gane and Schoelkopf, 2006).

This study focuses on the development of highly wicking pigment coated substrates for microfluidic devices with enhanced resolution compared to current filter paper-based devices. Various highly absorbing coating pigments and different binders are used to form coating structures with different properties in regards to porosity, surface area and permeability.

Clarcel 78) and *a flux-calcined diatomite* (FCD, Clarcel FD), both supplied by Ceca Arkema, La Garenne-Colomber Cedex, France. MCC (52 % solids) and FS (20 % solids) were delivered as aqueous dispersions, whereas the diatomite pigments exist in powder form. The diatomite slurries were dispersed using *sodium polyacrylate salt* (Polysalz S, BASF, Ludwigshafen, Germany). *Carboxymethyl cellulose* (CMC, Finnfix 10, CP Kelco Oy, Äänekoski, Finland) was added to support dispersing and to provide both thickening and, at high dose, binding. CMC was prepared at 6 % solids by adding the required amount of CMC to cold water under agitation and heating the mixture in a slow cooker (Fiskars

Home, Hackman, Helsinki, Finland) to 50–60 °C. The solution was held at this temperature until the CMC had dissolved completely. The solution was allowed to cool down to room temperature before adding to the pre-slurried pigments under slow agitation.

The binders included a *styrene-acrylate latex* (SA latex, Acronal S 505, BASF, Ludwigshafen, Germany), having a particle size of approximately 0.2 µm and a T_g of < 1 °C, a *fully hydrolysed polyvinyl alcohol* (PVOH, BF-05 provided by Omya International AG), which has a degree of hydrolysis 98.5–99.2 mole %, and a molecular weight of 22 000–27 000 g·mol⁻¹ (Limpan et al., 2012), and CMC. PVOH was prepared at 10 % solids by adding the required amount of PVOH to cold water under agitation and heating the mixture in a slow cooker (Fiskars Home, Hackman, Helsinki, Finland) to 95–98 °C. The solution was held at this temperature until the PVOH had dissolved completely. The solution was allowed to cool down to room temperature before adding to the slurried pigments at a slow rate of agitation.

2.2 Substrates

Super premium microscope slides with ground edges (90°) made from low iron clear glass and having a thickness of 0.8–1.0 mm (25 × 75 mm, VWR International BVBA, Leuven, Belgium) were used as substrates in thin layer wicking (TLW) tests. The glass slides were attached to a 300 g·m⁻² liquid packaging board sheet (Stora Enso, Imatra, Finland) with double sided tape

(Scotch®, Suomen 3M Oy, Espoo, Finland) to ensure an even coating result. In addition, two commonly used filter papers, Whatman grades 1 and 4 (GE Healthcare Europe GmbH, Suomen sivuliike, Helsinki, Finland), were used as a comparison.

2.3 Coating colour formulations

The effect of different coating pigments on the wicking of liquid was tested using MCC and combinations of MCC with ND and FCD in a latex binder system. Table 1 presents the properties of the coating colours as well as the coating thickness and coat weight of coated samples. The coating thickness and coat weight were calculated by measuring thickness and the weight of the glass slides before and after coating. First, ND and FCD were blended with water to as high solids content as possible while retaining good “coatability”, after which MCC and binder was added to the diatomite-water mixture. In the case of ND this meant a solids content of 15.8 % (ND + MCC; 25 : 75) and 10.9 % (ND + MCC; 50 : 50), and in the case of FCD 37.7 % (FCD + MCC; 25 : 75) and 29.5 % (FCD + MCC; 50 : 50).

The effect of different binders and binder amounts on wicking of liquid was tested by using three different binders: SA latex and PVOH, which are commonly used binders, and CMC which is widely used as a co-binder in coating structures. Table 2 presents the properties of the coating colours as well as the thickness and coat weight of coated samples.

Table 1: Coating colour properties – different coating pigments with 4 pph latex; Brookfield spindle #4 was used with MCC, spindle #2 with other coating formulations

Coating formulation	Solids (%)	Thickness (µm)	Coat weight (g·m ⁻²)	Brookfield visc. (mPa·s @ 100 min ⁻¹)	pH	Zeta poten. (mV)	Conductivity (µS·cm ⁻¹)
MCC (100)	52.00	50	60	402	8.49	-17.60	51.0
ND + MCC (25 : 75)	34.90	51	43	208	8.23	-18.60	39.7
ND + MCC (50 : 50)	19.20	46	43	66	8.03	-18.03	34.6
FCD + MCC (25 : 75)	48.60	72	63	130	8.49	-19.03	40.4
FCD + MCC (50 : 50)	39.50	71	49	42	8.83	-22.37	40.5

Table 2: Coating colour properties – different binders and binder amounts; Brookfield spindle #4 was used with all coating formulations

Coating formulation	Solids (%)	Thickness (µm)	Coat weight (g·m ⁻²)	Brookfield visc. (mPa·s @ 100 min ⁻¹)	pH	Zeta poten. (mV)	Conductivity (µS·cm ⁻¹)
MCC	52.00	50	62	566	8.80	-16.57	43.4
MCC + 4 pph latex	51.92	74	62	402	8.49	-17.60	51.0
MCC + 8 pph latex	51.85	51	43	348	8.31	-17.80	41.3
MCC + 2 pph PVOH	48.00	42	52	884	8.50	-8.81	34.7
MCC + 10 pph PVOH	37.62	75	43	678	8.33	-7.47	40.2
MCC + 1 pph CMC	48.35	67	55	952	8.81	-18.30	38.4
MCC + 4 pph CMC	40.11	68	48	742	8.49	-22.70	45.9

2.4 Equipment

The particle size distributions of the coating pigments were determined by laser diffraction (Mastersizer 2000, Malvern Instruments Ltd., Malvern, UK), and the surface structures of the pigment particles were imaged with scanning electron microscopy (SEM). The surface area was supplied using an equivalent spherical particle model derived from the particle size distribution data as calculated from the Mastersizer.

For the SEM imaging, the coating samples were coated with a thin layer of gold using a table-top sputtering device (Leica EM SCD050, Leica Microsystems GmbH, Wetzlar, Germany) and analysed using a Hitachi TM-1000 SEM (Hitachi High-Technologies Europe GmbH, Krefeld, Germany).

The PVOH and CMC dispersions were prepared using a Heidolph RZR 1 mixer (Heidolph Instruments GmbH & Co, Schwabach, Germany). The coating colours were prepared in small sample containers and mixed by hand. The viscosity of the coating colours was measured using a Brookfield DV-II+ viscometer (Brookfield Engineering Laboratories, Inc., Massachusetts, USA) using spindles #2 and #4 and a rotation speed of 100 min^{-1} , the pH using a pH meter (Orion 420A, Thermo Scientific, Cambridgeshire, England), conductivity and zeta potential using a Zetasizer Nano-ZS90 (Malvern Instruments Ltd., Malvern, UK).

The glass slides were coated with the various test formulations using a K202 Control Coater (RK PrintCoat Instruments Ltd., Herts, UK) adopting the brown labelled wire-wound rod, which applies an $80 \mu\text{m}$ thick wet film onto the substrate, with a speed setting of $6 \text{ m} \cdot \text{min}^{-1}$. The latex containing coated glass plates were dried in an oven at $105 \text{ }^\circ\text{C}$ for 2 minutes to ensure proper latex film formation. The glass slides were weighed with a balance (Precisa XT 320M, Precisa Gravimetrics AG, Dietikon, Switzerland) and their

thickness measured with a caliper thickness tester (I&W Micrometer SE 250D, Lorenzen & Wettre, SE 164 93 Kista, Sweden) before and after coating to obtain coat weight and coating thickness.

A digital camera (Sony Cyber-shot DSC-HX20V, Sony Europe Limited, Espoo, Finland) was used to record images of the thin layer wicking tests as a function of time. The images were analysed using PowerPoint Picture and Drawing Tools (Microsoft Oy, Espoo, Finland). The coated glass slides were analysed with a light microscope (Leica DM750) coupled with a high definition digital camera (Leica ICC50 HD, Leica Microsystems GmbH, Wetzlar, Germany) and scanned with Epson Expression 1680 (Epson, Suwa, NGN, Japan).

2.5 Test set-up for thin layer wicking experiments

In thin layer wicking (experiments, a coated glass slide with 1 mm scaling marked on one side is lowered vertically into contact with the test liquid (10 % red food dye, Dr. Oetker Suomi Oy, Helsinki, Finland) and the wicking height (mm) is determined as a function of time (s).

Figure 2 shows a schematic of the wicking test set-up including the digital camera, a petri dish filled with dyed water to act as a liquid supersource, a transparent plastic support, e.g. a simple cup, holding the sample, the coated sample with 1 mm scale markings, and a light source (flashlight). Three repeats were made for each test. Wicking tests were conducted under standard paper testing conditions ($23 \pm 1 \text{ }^\circ\text{C}$ and $\text{RH } 50 \pm 2 \%$).

2.6 Test set-up for droplet wicking tests

Horizontal wicking was tested by placing a droplet of dyed water onto the coated samples with a pipette, as shown in Figure 3. The samples were scanned after reaching equilibrium and drying. The tests were conducted under standard paper testing conditions ($23 \pm 1 \text{ }^\circ\text{C}$ and $\text{RH } 50 \pm 2 \%$).

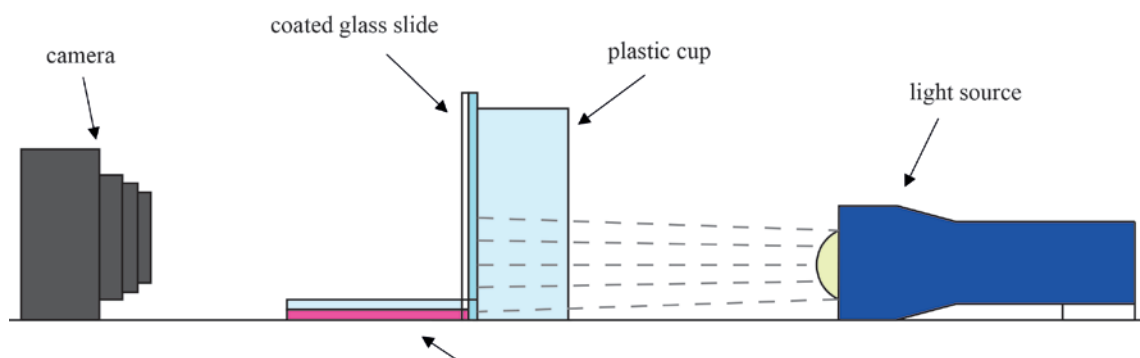


Figure 2: Schematic of the wicking test set-up

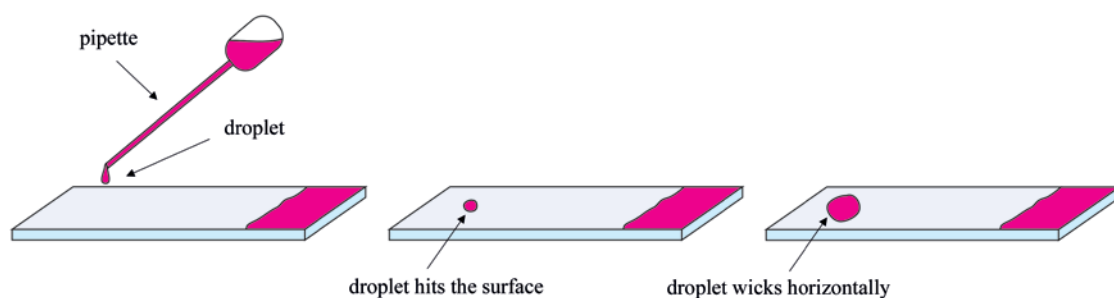


Figure 3: Schematic of the drop test set-up; additionally, the supersource wicking from the vertical test is also shown on the right side of each sample

3. Results

The findings from the experimental procedures are reported, beginning with the characterisation undertaken to define the likely properties of the pigments responsible for the surface interaction with liquid, followed by the direct observation of that interaction in respect to wicking in the porous structure of the resultant coatings, including the study of binder type and quantity used.

3.1 Characterisation of the coating pigments

The volume frequency based particle size distributions of the coating pigments are shown in Figure 4, and the differences in particle size distributions are summarised in Table 3. Particle size distribution relates ultimately to the particle packing in the coating structure and affects the porosity and the permeability of the coating layer (Gane and Ridgway, 2007), thus influencing wicking of liquids in coatings containing the pigments. Fumed silica as coating pigment has a narrow particle size distribution and the individual pigment particles are the smallest of the four pigments studied. Silica, due to its micro-agglomerated nature, therefore, forms a less densely packed structure than either MCC, which has a spherical shape in a narrow size distribution, or diatomite pigments, having a broader particle size distribution, respectively, corresponding to a more tightly packed structure where small particles fill pores defined by the larger particles (Mueller, Osterhuber and Donigian, 2006). Studies have shown that smaller pores can be obtained using

fine broad particle size distribution pigment particles (Burri et al., 2004) and that the use of larger monosize particles results in both increased porosity and pore size in the final coating structure (Rousu et al., 2000).

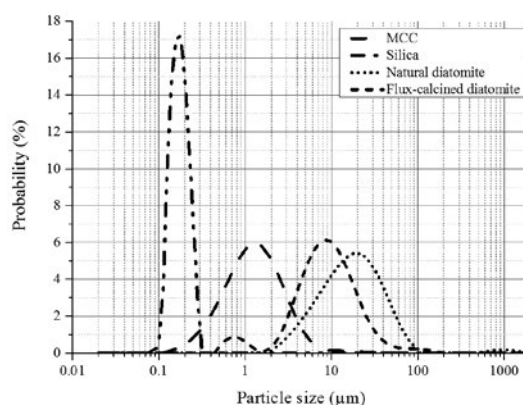


Figure 4: Volume frequency based particle size distribution of coating pigments

As we see in Table 3, the use of the equivalent spherical model for particle surface area, derived from the light scattering cross-section, greatly underestimates the true micro and mesoscale surface. To access the surface detail in this way would require the use of gas adsorption, e.g. nitrogen adsorption using the method BET of Brunauer, Emmett and Teller (1938). For example, the MCC is reported in the supplier's speci-

Table 3: Particle size and equivalent sphere model specific surface area of the coating pigments

Pigment	Specific surface area ($\text{m}^2 \cdot \text{g}^{-1}$)	Fine particle limit, d_{10} (μm)	Median particle size, d_{50} (μm)	Coarse particle limit, d_{90} (μm)
MCC	6.20	0.47	1.33	3.445
FS	33.70	0.14	0.18	0.251
ND	0.36	5.88	18.25	49.604
FCD	0.88	3.32	9.16	24.429

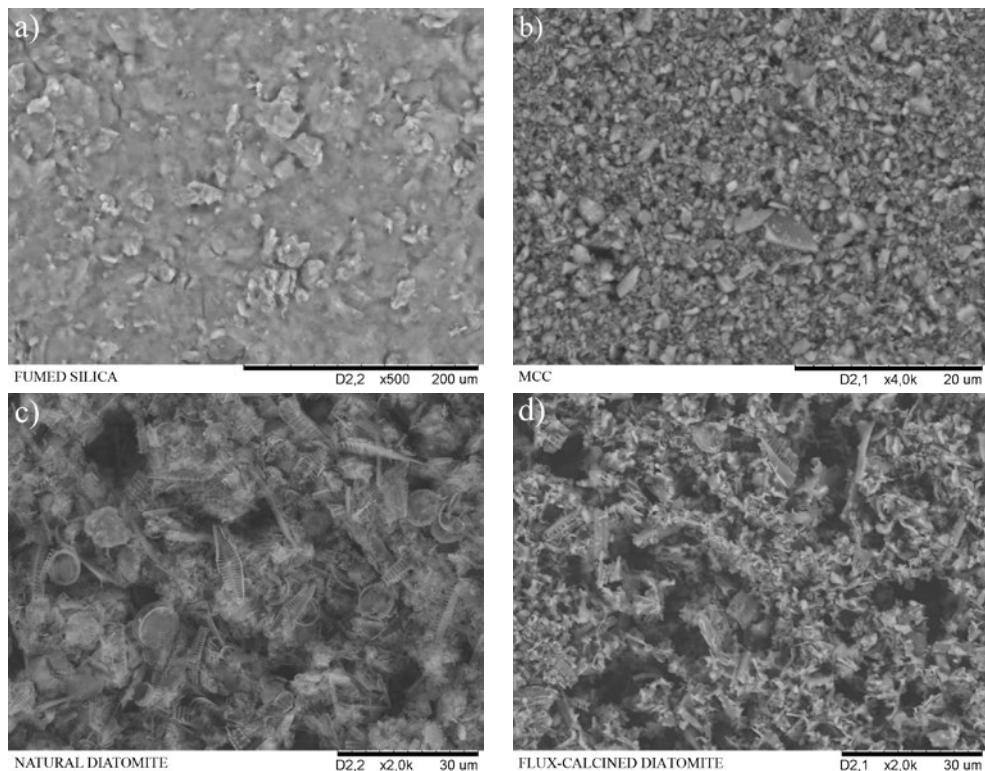


Figure 5: SEM images of the coating pigments: a) fumed silica, b) porous modified calcium carbonate (MCC), c) natural diatomite, and d) flux-calcined diatomite

cation to have a specific surface area ranging between $\sim 30\text{--}40\text{ m}^2\cdot\text{g}^{-1}$ (Lamminmäki et al., 2009), and it is typical that fumed silica can have a specific surface area greater than or approximately $100\text{ m}^2\cdot\text{g}^{-1}$.

SEM images of the coating pigments are shown in Figure 5. Clear visual differences can be seen in the pigment particle size and shape. The diatomite pigment particles, especially the ND, are significantly larger than the finer MCC pigment and much finer silica particles, though the silica particles are seen to be partly clustered. The shape and size of the pigment particles also influence the void structure of the coating together with the chosen binder and binder amount.

3.2 Effect of pigment type on wicking

FS was selected as one of the coating pigments due to its known capacity to absorb large amounts of liquid in ratio to the solid volume as a result of its fine particle size and high level of microporosity generated in the clustered structure (Wu et al., 2012).

However, due to the ultrafine fraction and the resulting extremely high capillary forces during drying, shrinkage cracks formed in the coating and the coating layer peeled off upon drying, indicating adhesion failure when latex and PVOH were used as binders. Even the addition of MCC into the coating colour did not solve the problem

and therefore the silica pigment was discarded from the wicking experiments at this stage of the investigation.

The diatomite pigments were selected based on their potential absorption capabilities, although they are not conventionally used in paper coatings, being more commonly applied as filtration aids. However, experiments revealed that the chosen dispersing agent was not able to stabilise the coarse diatomite pigments against sedimentation. To overcome this, extensive amounts of CMC were required to retain the particles in suspension: 10 pph for ND and 12 pph for FCD. Although CMC solved the problem of pigment particle sedimentation, and improved the flow uniformity of the coating formulations, and hence coating coverage, it failed to prevent the formation of induced clumps during the coating process. This indicates that even CMC does not stabilise the pigment completely against shear-induced aggregation, and this can be considered as a characteristic of these pigments. The high amounts of CMC were seen, not unexpectedly, to interfere significantly with the wicking capabilities of the diatomite pigments. To achieve more stable coating colours while still utilising the diatomite pigments, ND and FCD were mixed with MCC.

Figure 6 shows the wicking height as a function of time when the various coating pigments or their combinations were tested with latex binder. Further, the impact of different binders and binder amounts, with MCC

pigment alone, was tested. The error bars represent the standard deviation of the observation. Three observations were made for each test. The wicking height was calculated from the difference between the final wicking height of the liquid and the initial wetting front.

The addition of diatomite pigments to MCC increased the wicking capabilities of the coatings significantly, especially in the case of the coarser ND. The MCC and ND + MCC coatings have similar thickness values, but ND containing coatings have significantly lower coat weight indicating a lower coating density. Furthermore, the solids content of the coatings containing diatomite are much lower than that of a coating consisting of MCC, but the formulations still produce thick coating layers. These factors indicate that the addition of larger diatomite particles creates a coating structure with larger voids compared to MCC. Although faster absorption of liquid is normally seen with finer pore structures over short distances (Gane, Matthews and Schoelkopf, 2000), in the case of diatomite a coating structure consisting of larger pigment particles led to greater wicking over the distances required for microfluidics, especially in these relatively thick coating layers. Diatomite structures internally have a low permeability, but they possess a very high porosity and the particles pack loosely together to provide well-connected flow pathways for wetting fluid resulting in low resistance to the flow generated by the capillary wall wetting forces (Akin et al., 2000). It is reported that the fine intraparticle pores and high surface area of the MCC act to provide strong wetting forces, which drive the meniscus forward (Ridgway and Gane, 2002), while the diatomite with its open interparticle packing reduces the resistance to viscous flow through the coating structure.

As we see in Figure 6, expressing the absorption/wicking height as a function of the square root of time does not deliver perfect straight lines, as would be the case if the traditional Lucas–Washburn model alone had

applied. We see first of all a short delayed rate of wicking, which reflects the likely depression of the contact meniscus as the sample is lowered into the supersource of liquid, which depends on the dynamic advancing contact angle, which becomes bigger as the sample is moved against the direction of wicking. Once equilibrium is reached, then a short period of linear root time behaviour is seen, followed by a slowing toward an eventual plateau. The plateau is defined as the equilibrium between wicking and evaporation at the far-reaches of the wetting meniscus. As we see from the optical analysis in Figure 7, this series of behaviours results in various concentration regions of dyestuff as the structure surface acts via adsorption, and the pore volume permits a balance between diffusion, bulk liquid flow and evaporation over the surface of the sample.

Figure 7 shows the wicking front and droplet spreading on and in the MCC and MCC-diatomite combination coating structures. The pigment surface interacts with certain dissolved materials, such as vegetable or insect dye, and thus the coating acts as a surface sorptive chromatographic column through surface and pore wall adsorption. This was evident during the experiments as a water front could be clearly observed ahead of the colorant front. The chromatographic effect was most prominent in the case of ND + MCC; 50 : 50, which showcased a series of lighter and darker areas. The lighter areas show incomplete pore filling or depletion of dye, whereas the darker coloured areas show saturated pores or concentration of dye. The innermost dark ring during droplet spreading marks the point at which there is no more surface liquid and the spreading proceeds subsurface due to the coating pore structure. The band of diffuse colour thereafter marks the adsorption of the dye onto the pore walls. The outermost intensely coloured ring is caused by evaporation of the liquid, which takes place faster than the onward wicking of the liquid, and so dye becomes concentrated – the so-called coffee stain effect. Similar layering effects can

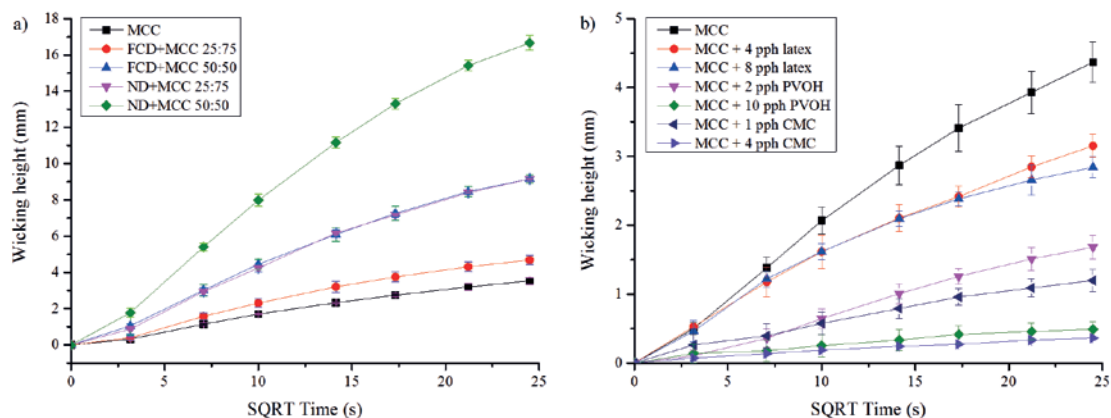


Figure 6: Wicking height as a function of square root of time ($t^{0.5}$); a) when different coating pigment combinations were tested with 4 pph latex and b) when different binders and binder amounts were tested with MCC alone

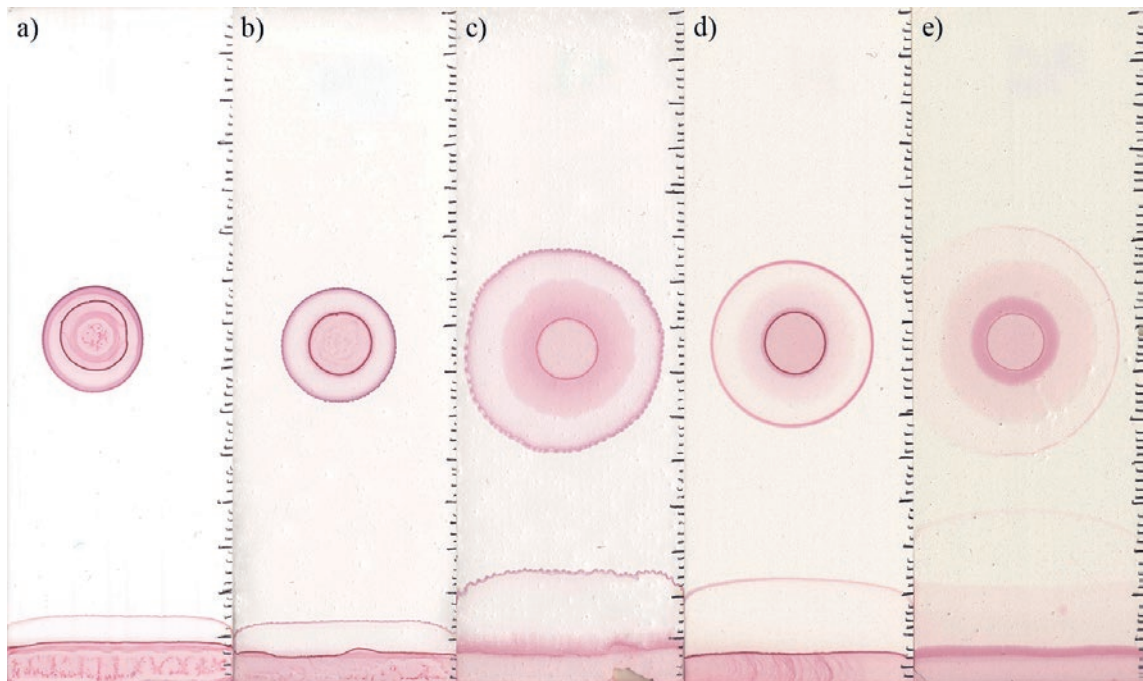


Figure 7: Wicking front and droplet spreading in a) MCC, b) FCD + MCC (25 : 75), c) FCD + MCC (50 : 50), d) ND + MCC (25 : 75) and e) ND + MCC (50 : 50) coating structures

be seen during the vertical wicking based on the identical series of events.

3.3 Effect of binder type and binder amount on wicking

The choice of a binder and the binder amount have a significant effect on wicking of liquid in a coating structure (as can be seen from Figure 6b), which presents the wicking height in the variously bound structures as a function of the square root of time. The highest wicking distance in the binder-containing coating systems was achieved with latex. An addition of 4 pph of latex provided sufficient binding to maintain the integrity of the coating and hindered the wicking remarkably less than PVOH and CMC. Further addition of latex (8 pph) reduced the wicking distance, but not too greatly. Latex may either change the pore structure by filling the pores and blocking the entrances affecting the capillary absorption (Burri et al., 2004) or at these lower doses actually undergoes depletion flocculation in the presence of pigment (Husband and Adams, 1993; Ridgway and Gane, 2007). Thus, a low level of suitable latex binder may lead to preservation of the total pore volume and permeability of the coating structure to a large extent (Ridgway, Kukkamö and Gane, 2011).

Even a low addition of PVOH (2 pph) reduced the wicking height noticeably, and the liquid front progressed even slower when a higher amount of PVOH (10 pph) was used, as expected. Significantly higher amounts of

PVOH would have been required to bind the coating properly onto the glass slides, but were not investigated since they would have inhibited wicking even more. The reason for low wicking distances in PVOH containing coatings most probably lies in PVOH's tendency to absorb water and swell, thus reducing the pore volume, especially affecting the fine high capillary pores and so reducing the pore network connectivity (Lamminmäki et al., 2011; Ridgway, Kukkamö and Gane, 2011). CMC also prevented liquid wicking significantly, but in addition failed to provide the required binding power to secure the coating onto the glass slide, even at higher dosage. This is probably due to the long timescale solubility of CMC in water.

Figure 8 shows the droplet spreading in the MCC coatings, when latex, PVOH and CMC were used as binders. The addition of a binder reduces the droplet spreading and dye migration by either filling some of the pores or, more particularly in the case of soluble binders, reducing the connectivity of the pore network as the soluble binders concentrate at the interstices of the pigment particle contact points due to capillary forces during the drying of the coating layer. Higher binder amounts result in less spreading and the dye concentrates in the edge areas. Once again, it can be seen that the dye does not spread homogeneously. The original equilibrium surface spread droplet size can be seen in the case of plain MCC (without binder) and in latex-containing coatings as an “inner ring”. As previously, the outer ring is related to the coffee stain effect

and associated Marangoni behaviour during evaporation. This delineation between surface equilibrium and internal pore wicking did not occur when soluble PVOH and CMC were used, although dye spreading was still not uniform, suggesting that the use of these soluble binders prevented a defined meniscus pinning line on the surface via a prevention of rapid evapora-

tion, such that the dye could continue to diffuse to the outer limit. This effect is thus related to the water swelling and dissolution properties of soluble binders. A more clearly visible outer coffee ring stain effect is seen as the soluble binder level is increased: the dye migrates and concentrates to the “outer rings” as the water evaporates.

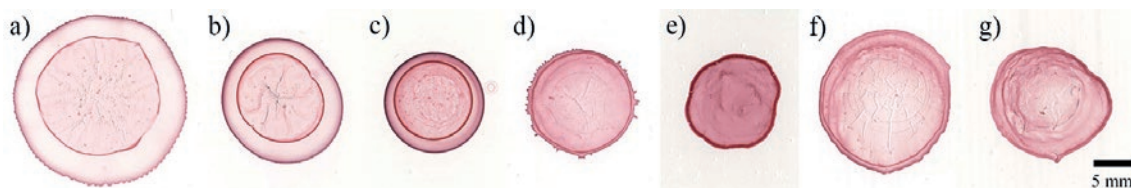


Figure 8: Droplet spreading in a) MCC, b) MCC + 4 ppb latex, c) MCC + 8 ppb latex, d) MCC + 2 ppb PVOH, e) MCC + 10 ppb PVOH, f) MCC + 1 ppb CMC and g) MCC + 4 ppb CMC

4. Discussion

A number of interesting observations provide a deeper understanding of the relationship between the coating structure formation and the subsequent wicking tendency. Of perhaps greatest importance is the recognition of the role of wicking rate, and surface and binder chemistry, in respect to the distribution of soluble or carried substances in the liquid vehicle being wicked through the structure. On the one hand, surface adsorption by chromatography would prevent delivery to a diagnostic station, whilst, on the other hand, it could allow for valuable material separation to be undertaken. Similarly, the diffusion potential of dissolved constituents in the vehicle through soluble polymer binders, such as PVOH and CMC, could allow for

a more uniform deposition of a given solute, captured within the polymer matrix and then potentially eluted at a later date.

It is revealing to visualise the differences in macro and microstructure of the various resulting substrate materials. Figure 9 illustrates a comparison using optical microscopy between the large scale porous structure of a filter paper and the contrasting variation in microstructure seen between the fine MCC and the blends of MCC and the two diatomites. The lower permeability of the finer structures limits the long range wicking when considering using the complete coating layer as the absorbing structure.

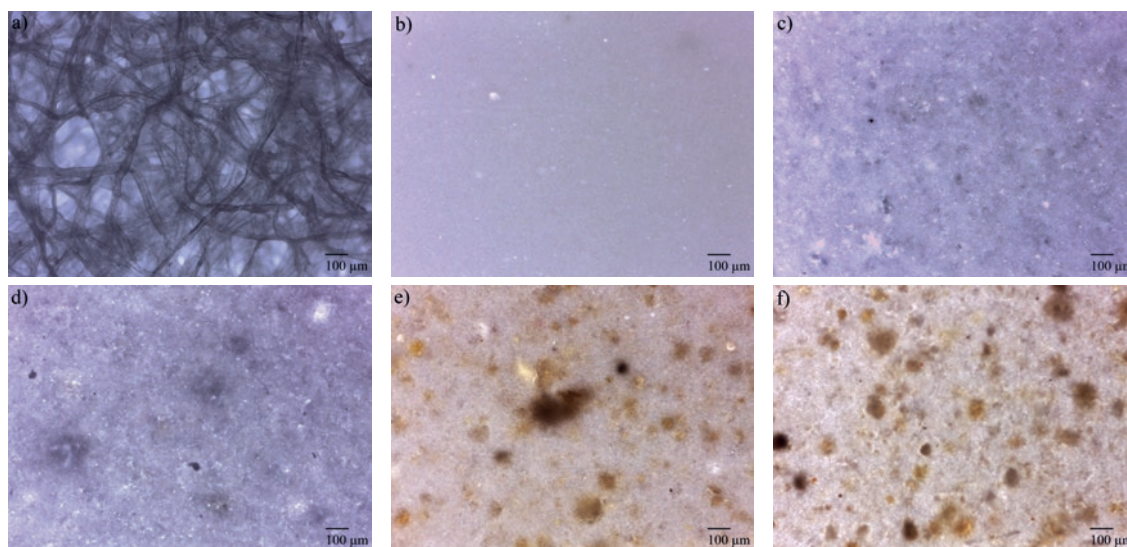


Figure 9: Light microscopy images of a) Whatman Grade 1 filter paper, b) MCC with 4 ppb latex, c) FCD + MCC (25 : 75), d) FCD + MCC (50 : 50), e) ND + MCC (25 : 75), and f) ND + MCC (50 : 50)

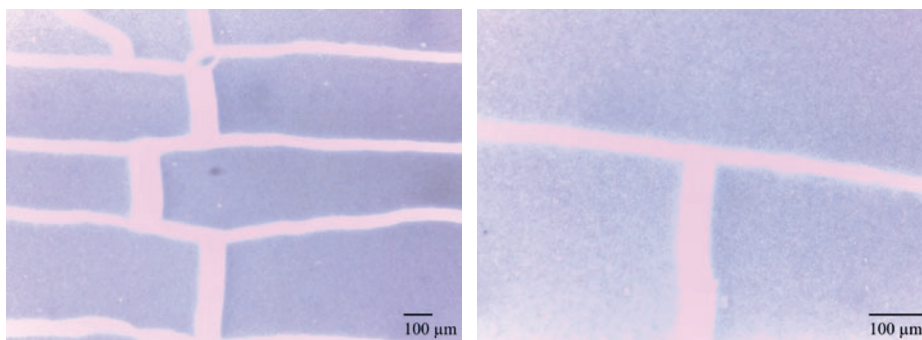


Figure 10: Light microscopy images of glass slides coated with fumed silica FS + MCC (25 : 50)

In the following discussion we concentrate on the direct physical relations between the wicking behaviour and the constituent formulations employed.

4.1 Fumed silica

Neither latex nor PVOH were suitable for binding the silica onto the glass slides, and therefore the wicking capabilities of FS could not be studied at this point. Surface treatment of the glass slides or the use of other binders, especially inorganic binders, such as sodium silicate, could perhaps provide a worthwhile alternative, which could be studied. The cracking phenomenon of silica coatings could also perhaps be exploited by designing a certain substrate patterning that could lead to a coating structure that might provide geometrical “mud cracks” formed during shrinkage (Figure 10). The phenomenon could potentially be controlled by using different pigment and binder combinations, but would require further investigation.

4.2 Dispersing diatomite pigments

Other stabilising agents against sedimentation and shear-induced aggregation could be researched to find an optimum to achieve a stable coating formulation whilst retaining the high wicking capabilities of the diatomite pigments. For example, the influence of using microfibrillated (MFC) or nanofibrillated (NFC) cellulose instead of CMC could be explored (Dimic-Misic et al., 2014). Alternatively, size selective sedimentation could be used to remove the coarsest (oversize) particles in a water-pigment mixture prior to coating to reduce the development of coating lumps.

4.3 Effect of pigment type, binder type and amount on wicking

The coating structure, especially the packing, porosity, permeability and pore connectivity of the coating, can be altered significantly by using different pigments in combinations with different binders. In these experiments, the ND pigment containing coatings resulted in most wicking of the fluid, followed by FCD and MCC,

the latter itself being known to promote rapid absorption and high liquid uptake capacity (Ridgway, Gane and Schoelkopf, 2006). However, the challenge of fully utilising diatomite pigments lies in making the dispersions stable, as discussed earlier.

Liquid wicks up the coating structure faster when no binder is present, because binders fill or block some of the pores and/or pore connections in the coating structure, but nonetheless sufficient amounts of binder are required to bind the coating layer to the glass slide. The results agree with previous studies, in which higher binder levels of latex and PVOH reduce the absorption capabilities of the coating (Lamminmäki et al., 2009; Ridgway, Kukkamö and Gane, 2011).

The droplet spreading experiments of coated samples show that the spreading dye droplets does not result in a homogeneous distribution of the solute dye. The dye separates from the water chromatographically in the presence of different pigments (Figure 7) and binders (Figure 8). However, in the case of uncoated filter paper a more uniform solute distribution is seen (Figure 11), although some of the dye concentrates at the “outer ring”. This confirms the importance of understanding the interactive properties of the solute and the surface chemistry of the pore walls, as well as the distribution of liquid between the macroscopic coating surface and the microscopic pores. Similar observations about heterogeneous spreading on coated substrates have also been made by Määttä et al. (2011).

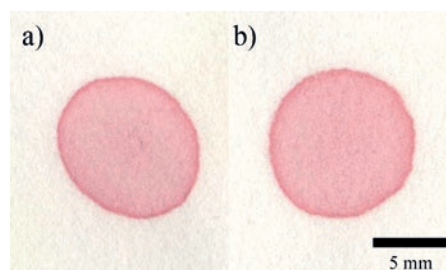


Figure 11: Droplet spreading on a) Whatman Grade 1 filter paper, b) Whatman Grade 4 filter paper

Furthermore, the thin layer wicking experiments showed that the wicking resistance of pigmented coatings, even without binder, is normally too high for rapid analysis over long distances in thick coatings. Zhong, Wang and Huang (2012) also concluded that coated paper did not possess good wicking properties. However, such coated papers are usually designed to prevent bleeding and spreading of ink. The selection of targeted coating formulation components, such as the coating pigments, binders and additives studied here, could be used to create a suitable coating for paperfluidic devices, especially when attention needs to be given to the potential for improved resolution at analysis/diagnostic stations when compared to uncoated fibrous substrates. Figure 12 shows an example of printed channel patterns on coated paper and on filter paper. It is evident that the ink spreads much less on the coated sample than on filter paper. This enables the printing of smaller channels and designs and, as a result, using smaller reagent volumes. Furthermore, advantageous use could be made of the surface chemistry and structure potential of coatings as media for solute or particulate suspension separation.

4.4 Impact of the results on future applications

This study demonstrated how different pigments, binders and binder amounts affect wicking on coated sam-

ples. The desired wicking characteristics depend on the end purpose. In a microfluidic device, for example, the fluid needs to wick through the narrow channels all the way to the detection zones, and the spreading of the reagents printed/spotted onto the detection zones should be controlled so that the reagents do not migrate by further spreading to the channels. Also, homogeneous spreading of the reagent would be preferable. These both can be controlled by changing the point of assay design or using different coating formulations. Future publications will focus on studying wicking and drop spreading in such narrow coated channels and test designs.

Paper-based microfluidic devices offer a simple and an affordable option to existing laboratory-based tests. Furthermore, using coated paper as a substrate enables cost savings compared to filter paper due to decreased reagent and sample volumes and smaller device designs. The reagents and the sample will only have to penetrate through a thin coating layer, which can be followed by a barrier layer, instead of penetrating through the whole paper structure as in the case of filter paper. The resultant increased spatial resolution will greatly enhance the application in diagnostics and microfluidic devices, including microfluidic switches, for example.

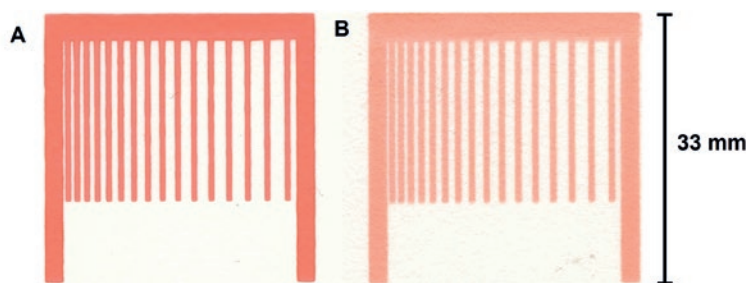


Figure 12. An example channel pattern printed on a) coated paper and b) filter paper (Koivunen et al., 2015)

5. Conclusions

The results show that the wicking characteristics of a coating can be greatly influenced by the choice of mineral coating pigment and binder – absorbent or non-absorbent. Using dyed water it could be shown that there is potential for using coatings to steer chromatographic or particulate separation of chosen solute components, as the coatings act as surface sorptive chromatographic columns through surface adsorption. Additionally, soluble binders can be used to provide potential differential

absorption for water and solute. Generally, however, the wicking resistance of pigment coatings is too high for rapid analysis over long distances. Once optimised for binder type and amount, these coating structures could be utilised as high resolution microfluidic analysis elements, i.e. test cells, incorporated either into a wicking channel matrix or placed at junctions of microfluidic channels derived from controlled hydrophobic/oleophobic printing or designed shrinkage fracture geometries.

Acknowledgements

The fumed silica sample used in this study was provided free of charge by Cabot Corporation.

Funding for the project was provided by Omya International AG. Particle size distribution measurements were performed by Anu Anttila of Aalto University.

References

- Abe, K., Suzuki, K. and Citterio, D., 2008. Inkjet-printed microfluidic multianalyte chemical sensing paper. *Analytical Chemistry*, 80(18), pp. 6928–6934.
- Akin, S., Schembre, J.M., Bhat, S.K. and Kovscek, A.R., 2000. Spontaneous imbibition characteristics of diatomite. *Journal of Petroleum Science and Engineering*, 25(3–4), pp. 149–165.
- Bosanquet, C.M., 1923. On the flow of liquids into capillary tubes. *Philosophical Magazine Series 6*, 45(267), pp. 525–531.
- Brunauer, S., Emmett, P.H. and Teller, E., 1938. Adsorption of gases in multimolecular layers. *Journal of American Chemical Society*, 1938, 60(2), pp. 309–319.
- Burri, P., Bluvoil, G., Gane, P.A.C. and Carlsson, R., 2004. Optimizing ink setting properties on double coated woodfree papers. In: *Proceedings of TAPPI Coating and Graphic Arts Conference*, May 16–19, 2004, Baltimore, USA: Tappi Press, pp. 201–216.
- Dimic-Misic, K., Ridgway, C., Maloney, T., Paltakari, J. and Gane, P., 2014. Influence on pore structure of micro/nanofibrillar cellulose in pigmented coating formulations. *Transport in Porous Media*, 103(2), pp. 155–179.
- Gane, P.A.C., Matthews, G.P. and Schoelkopf, J., 2000. Coating imbibition rate studies of offset inks: a novel determination of ink-on-paper viscosity and solids concentration using the ink tack force-time integral. In: *Proceedings of TAPPI International Printing & Graphic Arts Conference*, Atlanta, 3-10-2000, Savannah, US: Tappi Press, pp. 71–88.
- Gane, P.A.C. and Ridgway, C.J., 2008. Moisture pickup in calcium carbonate coatings structures: role of surface and pore structure geometry. In: *Proceedings of TAPPI 10th Advanced Coating Fundamentals Symposium*, June 10–13, 2008, Montreal, Canada, Atlanta, USA: Tappi Press, 13 p.
- Glavan, A.C., Martinez, R.V., Maxwell, E.J., Subramaniam, A.B., Nunes, R.M., Soh, S. and Whitesides, G.M., 2013. Rapid fabrication of pressure driven open-channel microfluidic devices in omniphobic R(F) paper. *Lab on a Chip*, 13(15), pp. 2922–2930.
- Husband, J.C. and Adams, J.M., 1993. Interactions in clay-based rotogravure coating colours. *Nordic Pulp and Paper Research Journal*, 8(1), pp. 195–199.
- Khan, M.S., Thouas, G., Shen, W., Whyte, G. and Garnier, G., 2010. Paper diagnostics for instantaneous blood typing. *Analytical Chemistry*, 82(10), pp. 4158–4164.
- Koivunen, R., Jutila, E., Bollström, R. and Gane, P., 2015. Inkjet printed reaction arrays on pigment coated substrates. In: *Proceedings of the 42nd International LARIGAI Conference*, Helsinki, Finland.
- Lamminmäki, T., Kettle, J.P., Puukko, P., Ridgway, C. and Gane, P.A.C., 2009. Inkjet print quality: the role of polyvinyl alcohol in speciality CaCO₃ coatings. *Journal of Pulp and Paper Science*, 35(3–4), pp. 137–147.
- Lee, W.G., Kim, Y-G., Chung, B.G., Demirci, U. and Khademhosseini, A., 2010. Nano/microfluidics for diagnosis of infectious diseases in developing countries. *Advanced Drug Delivery Reviews*, 62(4–5), pp. 449–457.
- Li, M., Tian, J., Al-Tamini, M. and Shen, W., 2012. Paper-based blood typing device that reports patient's blood type “in writing”. *Angewandte Chemie International Edition*, 51(22), pp. 5497–5501.
- Li, X., Ballerini, D.R. and Shen, W., 2012. A perspective on paper-based microfluidics: current status and future trends. *Biomicrofluidics*, 6(1), pp. 11301–1130113.
- Liana, D.D., Raguse, B., Gooding, J.J. and Chow, E., 2012. Recent advances in paper-based sensors. *Sensors*, 12(9), pp. 11505–11526.
- Limpan, N., Prodpran, T., Benjakul, S. and Prasarnpran, S., 2012. Influences of degree of hydrolysis and molecular weight of poly(vinyl alcohol) (PVA) on properties of fish myofibrillar protein/PVA blend films. *Food Hydrocolloids*, 29(1), pp. 226–233.
- Lisowski, P. and Zarzycki, P.K., 2013. Microfluidic paper-based analytical devices (μ PADs) and micro total analysis systems (μ TAS): development, applications and future trends. *Chromatographia*, 76, pp. 1201–1214.
- Lucas, R., 1918. Rate of capillary ascension of liquids. *Kolloid-Zeitschrift*, 23, pp. 15–22.
- Martinez, A.W., Phillips, S.T., Butte, M.J. and Whitesides, G.M., 2007. Patterned paper as a platform for inexpensive, low-volume, portable bioassays. *Angewandte Chemie International Edition*, 46(8), pp. 1318–1320.

- Martinez, A.W., Phillips, S.T., Carrilho, E., Thomas III, S.W., Sindi, H. and Whitesides, G.M., 2008. Simple telemedicine for developing regions: camera phones and paper-based microfluidic devices for real-time, off-site diagnosis. *Analytical Chemistry*, 80(10), pp. 3699–3707.
- Martinez, A.W., Phillips, S.T., Whitesides, G.M. and Carilho, E., 2010. Diagnostics for the developing world: microfluidic paper-based analytical devices. *Analytical Chemistry*, 82(1), pp. 3–10.
- Masoodi, R. and Pillai, K.M., eds., 2013. *Wicking in Porous Materials: Traditional and Modern Modeling Approaches*. Boca Raton: CRC Press/Taylor & Francis Group. 380 p.
- Maxwell, E.J., Mazzeo, A.D. and Whitesides, G.M., 2013. Paper-based electroanalytical devices for accessible diagnostic testing. *MRS Bulletin*, 38(04), pp. 309–314.
- Mueller, K., Osterhuber, E. and Donigian, D., 2006. When optimizing paper print performance, minerals matter. *Pulp & Paper*, 80(4), pp. 39–43.
- Mukhopadhyay, R., 2010. Paper-based diagnostics. *Chemistry World*, November 2010, pp. 50–53.
- Määttä, A., Fors, D., Wang, S., Valtakari, D., Ihalainen, P. and Peltonen, J., 2011. Paper-based planar reaction arrays for printed diagnostics. *Sensors and Actuators B: Chemical*, 160(1), pp. 1404–1412.
- Ridgway, C.J. and Gane, P.A.C., 2002. Dynamic absorption into simulated porous structures. *Colloids and Surfaces A: Physicochemical and Engineering Aspects*, 206(1–3), pp. 217–239.
- Ridgway, C.J. and Gane, P.A.C., 2007. Effect of latex and pigment volume concentrations on suspension and consolidated particle packing and coating strength. *Journal of Pulp and Paper Science*, 33(2), pp. 71–78.
- Ridgway, C.J., Gane, P.A.C. and Schoelkopf, J., 2006. Achieving rapid absorption and extensive liquid uptake capacity in porous structures by decoupling capillarity and permeability: nanoporous modified calcium carbonate. *Transport in Porous Media*, 63(2), pp. 239–259.
- Ridgway, C.J., Kukkamo, V. and Gane, P.A.C., 2011. Effects of binders and additives on inkjet coating pigment pore structures. In: *Proceedings of the TAPPI Coating and Graphic Arts Conference*, May 2011, Covington, USA: Tappi Press, pp. 1305–1319.
- Rousu, S.M., Gane, P.A.C., Spielmann, D.C. and Eklund, D., 2000. Separation of offset ink components during absorption into pigment coating structures. *Nordic Pulp and Paper Research Journal*, 15(5), pp. 527–535.
- Schoelkopf, J., Gane, P.A.C., Ridgway, C.J. and Matthews, G.P., 2000. Influence of inertia on liquid absorption into paper coating structures. *Nordic Pulp and Paper Research Journal*, 15(5), pp. 422–430.
- Sentinel Bioactive Paper Network. [online] Available at <www.bioactivepaper.com> [Accessed 12 September 2015].
- Szekely, J., Neumann, A.W. and Chuang, Y.K., 1971. The rate of capillary penetration and the applicability of the Washburn equation. *Journal of Colloid and Interface Science*, 35(2), pp. 273–278.
- Washburn, E.W., 1921. The dynamics of capillary flow. *Physical Review*, 17(3), pp. 273–283.
- Whitesides, G.M., 2013. Viewpoint on “Dissolvable fluidic time delays for programming multi-step assays in instrument-free paper diagnostics”. *Lab on a Chip*, 13(20), pp. 4004–4005.
- Wu, Y.-J., Lovell, V., Pekarovicova, A., Fleming, P.D. and Joyce, M., 2012. Influence of coating pigment porosity on inkjet color and lightfastness performance. *International Circular of Graphic Education and Research*, 5, pp. 6–17.
- Yetisen, A.K., Akram, M.S. and Lowe, C.R., 2013. Paper-based microfluidic point-of-care diagnostic devices. *Lab on a Chip*, 13(12), pp. 2210–2251.
- Zhong, Z.W., Wang, Z.P. and Huang, G.X.D., 2012. Investigation of wax and paper materials for the fabrication of paper-based microfluidic devices. *Microsystem Technologies*, 18(5), pp. 649–659.

List of abbreviations

CMC	carboxymethyl cellulose	NFC	nanofibrillated cellulose
FCD	flux-calcined diatomite	POC	point-of-care
FS	fumed silica	PVOH	polyvinyl alcohol
MCC	modified calcium carbonate	SA	styrene-acrylate
MFC	microfibrillated cellulose	SEM	scanning electron microscopy
ND	natural diatomite	TLW	thin layer wicking

JPMTR 065 | 1443
DOI 10.14622/JPMTR-1443
UDC 655 : 621.798

Research paper
Received: 2014-12-09
Accepted: 2015-09-01

Formation and photoluminescent properties of nanophotonic elements with nanosized ZnO for smart packaging, deposited by screen printing

Olha Sarapulova, Valentyn Sherstiuk

National Technical University of Ukraine,
Kyiv Polytechnic Institute, Institute of Publishing and Printing,
03056, Ukraine, Kyiv, 1/37 Yangel Str.

E-mail: olhasarapulova@gmail.com
sherstyukv@ukr.net

Abstract

Smart food packaging (active and intelligent packaging), which indicates and/or prevents changes in the packaged food product, traces the history of its storage etc., is becoming more popular due to the fact that it enhances safety of packaged food storage, transportation and consumption. It is convenient to use printing techniques to produce active elements of smart packaging, including the elements which respond to the changes in packaged food, which occur as the result of food spoilage or aging. However, issues concerning technological aspects arise when the compositions are printed onto materials such as paper or polymer films, especially if these compositions contain functional nanoparticles with luminescent properties. There has been conducted technological research of formation of luminescent coatings containing nano-sized ZnO, for active and intelligent packaging, using screen printing. Photoluminescent properties of the obtained nanophotonic elements are studied and the factors that affect their properties are defined. It was determined that by manipulating coating thickness, molecular weight of the polymer and the concentration of nanophotonic component in the composition it is possible to increase photoluminescent intensity of the screen-printed coatings and obtain different colors of photoluminescence.

Keywords: screen printing, nanophotonics, photoluminescence, nanomaterial, zinc oxide

1. Introduction

In respect to the global trend of increasing requirements for food safety, increasing the functionality and environmental safety, packaging containing nanoscale materials and nanotechnology in food packaging seems to be perspective to provide special properties, that is to create active and intelligent packaging. Achievements of nanotechnology are beginning to be used in all areas of production, including printing and packaging printing.

Active and intelligent packaging are able to respond to the changes in condition of packaged product in various ways: the first ones ensure the safety of content of a packaging for a longer time without increasing heat treatment parameters or other processing procedures for the product, the second ones monitor the status of a product or the environment in which the product is stored and inform consumers about the safety of consumption of the product (Suppakul et al., 2003; Sekhon, 2010). Informing consumers may be carried out by changing certain properties of packaging elements such as optical, electrical, geometrical properties and so on (Yam, Takhistov and Miltz, 2005). Therefore, the use of luminescent tags or sensors that respond to changes in the packaged product by changing the intensity of photoluminescence is quite promising. These elements,

for instance, based on nanosized zinc oxide (ZnO), are an example of the use of nanophotonic systems for printed active and intelligent packaging.

The use of ZnO nanoparticles has several advantages over the use of other luminescent compounds as nano-ZnO is primarily a safe, possess antimicrobial properties, absorbs UV radiation (Li et al., 2010; Seo et al., 2011) and changes the intensity of luminescence in contact with decomposition products of organic matter: carbon dioxide, organic acids (lactic, acetic acid), alcohols (ethanol), aldehydes, hydrogen sulfide, ammonia, biogenic amines formed by the interaction of ammonia with carboxylic acids and amino acid decarboxylation in result of bacteria (cadaverine, lysine, histamine) due to destruction of nano-ZnO crystals and the formation of aggregates without luminescent properties (Emamifar et al., 2010). Experimental studies showed that ZnO nanocrystals in polymers react to the presence of decomposition products of organic matter almost the same way as without polymer, presumably due to migration of such substances into the upper layers of the composition. This enables the use of printed layers of nano-ZnO with polymers for application to smart packaging. Yet as a result of introduction of ZnO nanoparticles in

a solvent for the purpose of printing application onto a packaging material there is often a loss of luminescent properties of nano-ZnO, so the selection of polymers that can serve as a matrix for nanoparticles of ZnO is necessary. We have determined that the introduction of colloidal solution of ZnO nanocrystals in ethanol to polyvinylpyrrolidone (PVP) (safe for consumption polymer) leads to no considerable loss of nano-ZnO photoluminescence intensity. However, in the process of manufacturing compositions and applying coatings there is a number of factors that affect the luminescent properties of the obtained printed labels which should be considered when producing photoactive printed packaging elements.

Despite a rather extensive research of the process of incorporating ZnO nanoparticles in polymeric materials,

2. Methods

Colloidal solution of ZnO nanoparticles in ethanol was prepared from zinc acetate ($\text{Zn}(\text{CH}_3\text{COO})_2$), sodium hydroxide (NaOH), and 100 % ethanol ($\text{C}_2\text{H}_5\text{OH}$) (Shvalagin, Stroyuk and Kuchmii, 2004). Polyvinylpyrrolidone (PVP) was added to the colloidal solution of ZnO in ethanol (concentration of $2 \cdot 10^{-3}$, $1 \cdot 10^{-2}$ and $2 \cdot 10^{-2}$ mol/L) at room temperature and intensive stirring (molar weight 10 000, 40 000 and 360 000 g/mol).

The coatings were obtained using screen printing of the produced nanophotonic compositions on polypropylene substrates. For the depositions of layers, hand screen printing was used under standard press conditions with controlled room temperature. The mesh #21 (52 tpi) with the thickness of the thread 144 μm was used to print 20×20 mm areas. The layers with thickness of 20 μm were printed onto each other several times (up to

3. Results

There was investigated the formation of coatings containing ZnO nanoparticles in PVP using screen printing and the influence of several factors on the intensity of photoluminescence of the obtained films.

It was found that with the inclusion of ZnO nanoparticles in PVP and subsequent application of the coating films two peaks in the luminescence spectra are displayed: one at 400 nm and the other at 530 nm (Figure 1, curve 2). Peak at 530 nm is typical for ZnO nanoparticles (Figure 1, curve 1) and a small peak at 400 nm is observed when irradiating PVP (Figure 1, curve 3).

By increasing the molar mass of PVP, the luminescence intensity of the samples increases (Figure 2). The peak

the issues of producing compositions for printed photoactive elements of smart packaging with nanoscale substances, such as ZnO, is practically not disclosed in the literature. Given this, the study of the features of printing production of photoactive elements for novel packaging with nanoscale luminescent substances is an important and urgent task, which is to enable the use of varnish and ink compositions based on nano-ZnO for production of printed smart packaging that respond to the state of packaged food by changing the luminescent properties.

The aim of this work is to study the factors and parameters of manufacturing process of photoluminescent coatings based on nanosized zinc oxide applied by screen printing onto the surfaces for producing active and intelligent packaging.

5 times to obtain layer thicknesses up to 100 μm). The layer thicknesses were measured with a thickness gauge based on the use of profilogram, measuring the increase in thickness with each print and calculating the average for 15–20 printed impressions. The printed impressions were cured under room temperature conditions without special equipment.

Photoluminescence spectra were recorded using luminescence spectrometer (Perkin Elmer, LS 55) and excited by light with a wavelength of 330 nm (λ_{ex}). The results for photoluminescence intensity in arbitrary units are obtained with the luminescence spectrometer with the same conditions of the measurements – spectral width of apertures (15 nm and 2.5 nm), speed of measurement (600 nm/min), filters (at 350 nm). The absorption spectra (optical density) were recorded using a spectrophotometer (Analytic Jena, Specord 210).

at 400 nm, which is typical for the polymer, increases most likely as a result of the participation of functional groups at the ends of the polymer chains of PVP in emissive processes in the polymer, and efficient capture of electronic excitation of ending groups of ZnO nanoparticles, followed by the emission in the natural region of the polymer. The number of functional groups increases with the decrease of molecular weight of the polymer and leads to a decrease of the luminescence band of nano-ZnO and an increase of the luminescence intensity of PVP.

Therefore, for maximum luminescence intensity of the films in the long-wave region (typical for nanocrystalline ZnO), it is optimal to use PVP with the highest

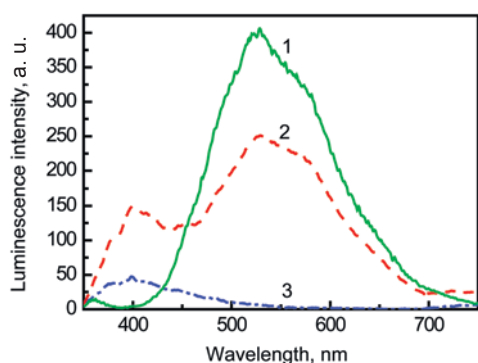


Figure 1: Luminescence spectra of colloidal solution of ZnO nanoparticles (1), coatings of ZnO nanoparticles in PVP (2) and PVP without ZnO nanoparticles (3);
 $M(\text{PVP}) = 360\,000 \text{ g/mol}$, $[\text{ZnO}] = 2 \cdot 10^{-2} \text{ mol/l}$,
 $\lambda_{\text{ex}} = 330 \text{ nm}$

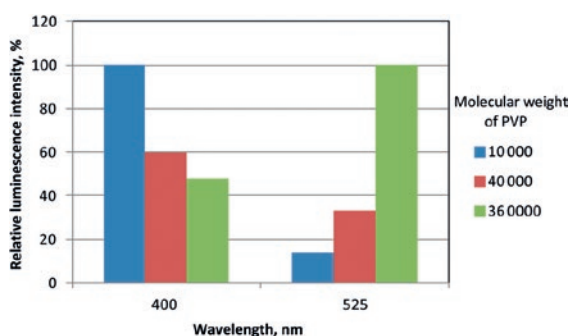


Figure 2: Influence of molecular weight of PVP on the height of the luminescence peaks of the coatings (400 and 525 nm)

molecular weight ($M = 360\,000 \text{ g/mol}$). However, the change in molecular weight of PVP allows changing the color of luminescence from blue to green and yellow, which might be useful for creation of various colors of luminescent emission for active and intelligent packaging. That is, with the increase of molecular weight of PVP the peak at 400 nm decreases and the peak at 525 nm increases. Consequently, if for higher luminescence intensity at 525 nm zone, PVP with a molecular weight of 360 000 g/mol should be used; if peaks need to be about the same, PVP with a molecular weight of 40 000 should be used; and for a more distinguished peak at 400 nm, PVP with a molecular weight of 10 000 g/mol should be used.

The study of the influence of the film thickness of PVP containing nano-ZnO on the intensity of luminescence of films is important for film deposition on the surface by printing techniques. Figure 3 shows that in order to increase total luminescence intensity the thickness of the coating layer should be increased. It is possible to use different printing techniques (screen printing, flexography, inkjet, pad printing, etc.). By increasing the layer thickness, the peak at 400 nm can be increased to the level of the peak at 525 nm. In this case, the peak

at 525 nm (a concentration of ZnO is $2 \cdot 10^{-2} \text{ mol/L}$) is always higher than the peak at 400 nm (Figure 4).

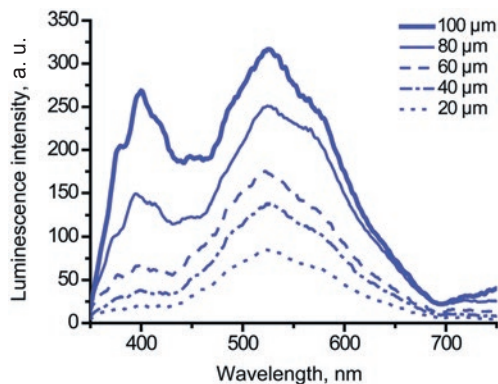


Figure 3: Luminescence spectra of the coatings depending on the thickness; $M(\text{PVP}) = 360\,000 \text{ g/mol}$,
 $[\text{ZnO}] = 2 \cdot 10^{-2} \text{ mol/L}$, $\lambda_{\text{ex}} = 330 \text{ nm}$

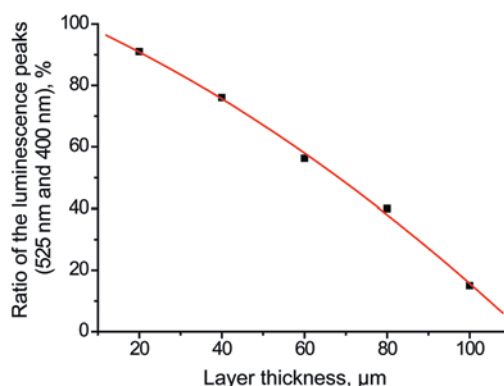


Figure 4: Effect of layer thickness on the ratio of the luminescence peaks (400 and 525 nm); $M(\text{PVP}) = 360\,000 \text{ g/mol}$, $[\text{ZnO}] = 2 \cdot 10^{-2} \text{ mol/L}$, $\lambda_{\text{ex}} = 330 \text{ nm}$

Figure 5 shows the relative change in luminescence intensity depending on the thickness of the coating layer. Relative luminescence intensity is calculated dividing the luminescence intensity of the analyzed sample by the primary luminescence intensity (or the luminescence intensity of the basic sample). Thus, in the Figure 5, the last sample (with layer thickness of 100 μm) has the luminescence intensity (in the short-wave region – 400 nm) about 7 times higher than the first sample (with layer thickness of 20 μm) does.

For different concentrations of nano-ZnO, relative change in luminescence intensity with the thickness of the coating layer is almost the same. With the increase of thickness of the coating layers, the increase of the peak at 400 nm (typical for the polymer) is more significant than the increase of the peak at 525 nm. Total luminescence intensity increases with the increase of coating layer thickness, therefore for the highest total luminescence of the films it is appropriate to use the highest technologically achievable thickness of the coating layer.

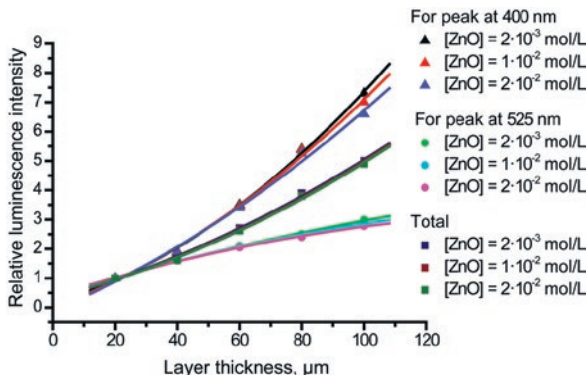


Figure 5: Effect of layer thickness on the luminescence intensity of coatings with different concentrations of nano-ZnO; $M(PVP) = 360\,000\text{ g/mol}$, $\lambda_{ex} = 330\text{ nm}$

The observed pattern is related to the fact that the increase of the thickness of the layer takes place due to the polymer component, as shown in Figure 6.

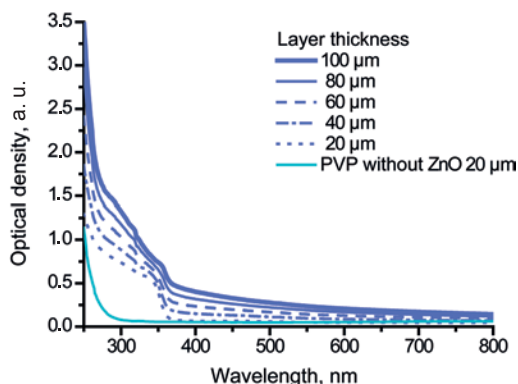


Figure 6: Absorbance spectra of the coatings depending on the thickness; $M(PVP) = 360\,000\text{ g/mol}$, $[ZnO] = 2 \cdot 10^{-2}\text{ mol/L}$

This phenomenon can be explained by the processes of luminescence quenching caused by the presence of oxygen in the deposited layers. With the increase of thickness of a coating layer, the intensity of absorption of

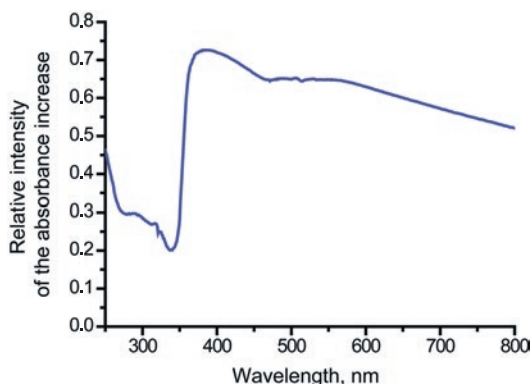


Figure 7: The relative intensity of the absorbance increase with increasing coating thickness of the layer 4 times; $M(PVP) = 360\,000\text{ g/mol}$, $[ZnO] = 2 \cdot 10^{-2}\text{ mol/L}$

the layer in the region of nano-ZnO absorption (250–350 nm) increases less significantly than in the region of absorption of the polymer (350–800 nm) – on average of 30 % and 60 %, respectively, with the thickness 4 times higher (Figure 7).

The increase in absorbance depending on the thickness of the coating layer in the shortwave (300 nm) and longwave (500 nm) regions of the spectrum is linear (Figure 8). Relative optical density is calculated dividing the optical density of the analyzed sample by the primary optical density (or the optical density of the basic sample). Thus, in the Figure 8, the last sample (with layer thickness of 100 μm) has the optical density (in the longwave region – 500 nm) almost 5 times higher than the first sample (with layer thickness of 20 μm) does.

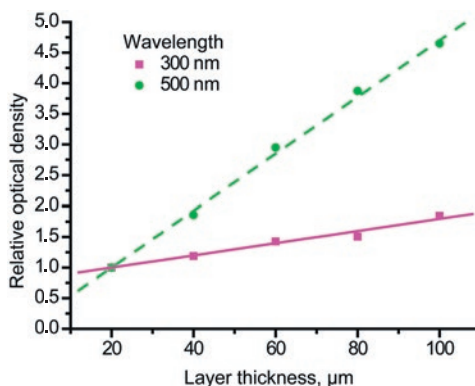


Figure 8: The influence of layer thickness on the change of the optical density of the coatings; $M(PVP) = 360\,000\text{ g/mol}$, $[ZnO] = 2 \cdot 10^{-2}\text{ mol/L}$

The influence of the concentration of ZnO nanoparticles on the luminescent properties of PVP films was also studied (Figure 9).

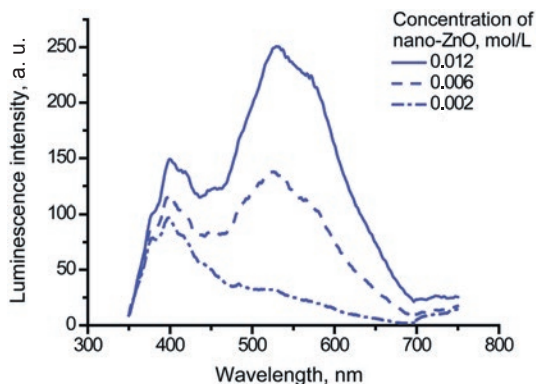


Figure 9: Luminescence spectra of the coatings depending on the concentration of ZnO nanoparticles; $M(PVP) = 360\,000\text{ g/mol}$, $\lambda_{ex} = 330\text{ nm}$

Figure 10 shows that with the increase of concentration of nano-ZnO in the composition the luminescence peak at 525 nm can be reduced to the level of peak at

400 nm and lower or the peak at 525 nm can be raised above the peak at 400 nm. Thus the peak at 525 nm may be lower than the peak of 400 nm, in contrast to the case of changing the thickness of the coatings.

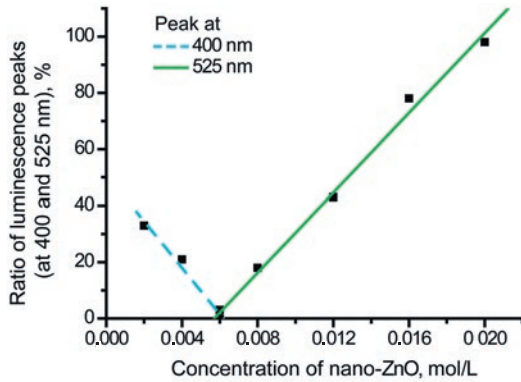


Figure 10: The influence of the concentration of ZnO nanoparticles on the ratio of luminescence peaks (at 400 and 525 nm); $M(\text{PVP}) = 360\,000 \text{ g/mol}$, $\lambda_{\text{ex}} = 330 \text{ nm}$

The integrated luminescence intensity of coatings increases with the increase of concentration of ZnO nanoparticles (Figure 11). Therefore, for the highest total luminescence intensity it is appropriate to use the highest concentration of ZnO nanocrystals in ethanol, which is limited to $2 \cdot 10^{-2} \text{ mol/L}$ (Shvalagin, Stroyuk and Kuchmii, 2004). Figure 11 also shows that with the increase of concentration of nano-ZnO in the composition the luminescence peak at 525 nm increases more significantly than the peak at 400 nm. It allows the manipulation of the ratio of luminescence peaks and, consequently, its color not only by the initial choice of molecular weight of the polymer and change of the layer thickness, but also by changing the concentration of the luminescent component in the composition.

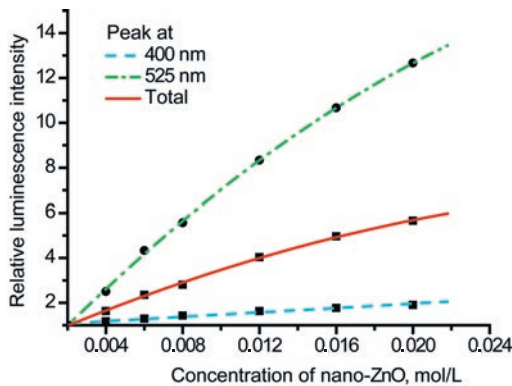


Figure 11: Effect of the concentration of ZnO nanoparticles on the luminescence intensity of the coatings; $M(\text{PVP}) = 360\,000 \text{ g/mol}$, $\lambda_{\text{ex}} = 330 \text{ nm}$

The rapid growth of the luminescence peak at 530 nm, typical for nano-ZnO, can be explained by the increased concentration of ZnO nanoparticles and, consequently,

the optical density in the UV area of the spectrum, as shown in Figure 12. A slight increase of the peak at 400 nm, typical for the polymer, can be explained by the capture of increased emission of ZnO nanocrystals by functional groups at the ends of the polymer chains.

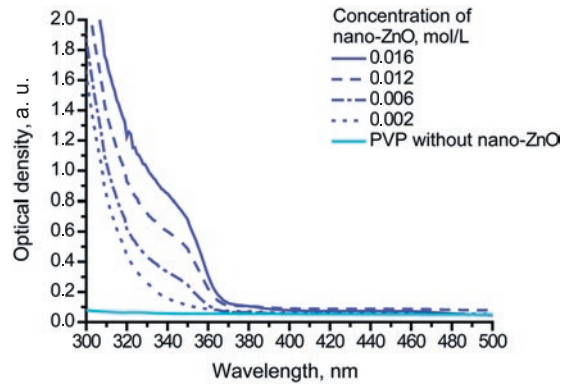


Figure 12: Absorbance spectra of coatings depending on the concentration of ZnO nanoparticles; $M(\text{PVP}) = 360\,000 \text{ g/mol}$

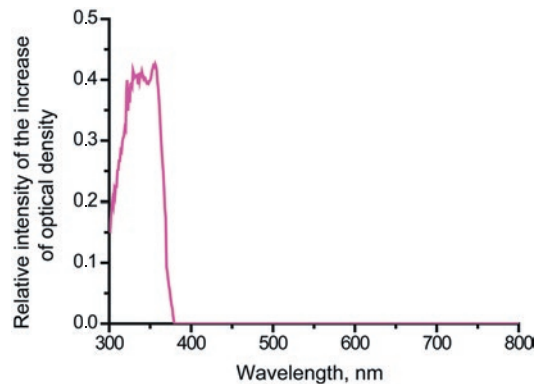


Figure 13: The relative intensity of the increase of optical density of the coatings with the twice increase of concentration of ZnO nanoparticles; $M(\text{PVP}) = 360\,000 \text{ g/mol}$

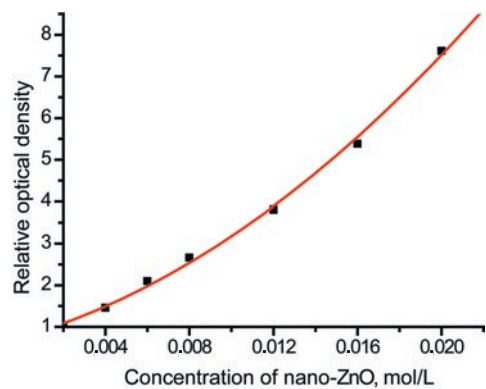


Figure 14: Influence of the concentration of ZnO nanoparticles on the change of optical density in the shortwave region of the spectrum; $M(\text{PVP}) = 360\,000 \text{ g/mol}$

Figure 13 shows that the intensity of absorption in the region of absorption of nano-ZnO (250–350 nm) increases significantly, while in the region of polymer absorption (250–800 nm) it is virtually unchanged. Figure 14 shows that with the increase of concentra-

4. Discussion

In the presented research work the factors and parameters of manufacturing process of photoluminescent coatings based on nanosized ZnO and PVP applied by screen printing onto the surfaces for producing active and intelligent (smart) packaging has been studied.

It was found that the highest intensity of photoluminescence of the coatings can be obtained by increasing thickness of the coatings (up to 100 μm), molecular weight of PVP (up to 360 000 g/mol) and concentration of ZnO nanoparticles (up to 0,02 mol/L) in the initial composition.

The developed compositions based on nano-ZnO and PVP displays two peaks of luminescence in different regions of the visible spectra, which allows controlled changes in luminescent color by manipulation of the peaks ratio. The research has shown that such manipulation is possible by changing the molecular weight of PVP in the composition.

It was determined that for higher luminescence intensity at 525 nm zone (yellow color of luminescence) PVP with a molecular weight of 360 000 g/mol should be used; if peaks need to be about the same (green color of luminescence), PVP with a molecular weight of 40 000

5. Conclusions

As a result of the study, the formation of luminescent coatings by screen printing on polypropylene films was carried out, the parameters of the process of film deposition were defined and the photoluminescence properties of obtained coatings were studied. Optimum parameters of applying the luminescent compositions based on nano-ZnO to the surfaces of smart packaging by screen printing were defined to maximize total luminescence intensity. The possibility to manipulate color of the luminescence by changing molecular weight of the polymer (PVP), concentration of nano-ZnO and layer thickness was studied in detail.

tion of ZnO nanoparticles the absorption intensity of PVP films in the UV region of the spectrum increases proportionally. The relative change in optical density is exponential due to the changes in the concentration of ZnO nanoparticles.

should be used and for a more distinguished peak at 400 nm (blue color of luminescence) PVP with a molecular weight of 10 000 g/mol should be used.

The manipulation of color is also possible by changing film thickness. It was shown that with the increase of the layer thickness the peak at 400 nm can be increased to the level of the peak at 525 nm. Therefore, for relatively thin layer thicknesses (20 μm), blue shades of luminescence color could be obtained. With the increase of layer thickness the color of luminescence gradually changes to green.

The experiments showed that manipulation of color is also possible by changing concentration of nano-ZnO in the composition. It was determined that with the increase of concentration of nano-ZnO in the composition the luminescence peak at 525 nm can be reduced to the level of the peak at 400 nm and lower; or the peak at 525 nm can be raised above the peak at 400 nm. Therefore, for low concentration of nano-ZnO (0,002 mol/L), blue color of luminescence could be obtained, and with the increase of concentration of nano-ZnO up to the maximum possible 0,02 mol/L the color of luminescence gradually changes to green and then to yellow.

The study contributes to the development of smart packaging – a novel method to inform consumers, producers and distributors about various changes in the food packaging during transportation and storage. Smart food packaging is able to notify customers whether the product is safe for consumption. Resulting signal is based on the analysis of chemical content – due to the presence of substances which reveal the degradation and aging processes taking place in packaged foodstuffs. The study will allow the use of existing equipment and technological lines of printing companies to produce the new product – smart packaging with printed nanophotonic elements.

Acknowledgements

This investigation was supported by the Ministry of Education and Science of Ukraine (grant 2873p).

References

- Emamifar, A., Kadivar, M., Shahedi, M. and Soleimani-Zad, S., 2010. Preparation and evaluation of nanocomposite LDPE films containing Ag and ZnO for food-packaging applications. *Advanced Materials Research*, 129–131, pp. 1228–1232.
- Li, X.H., Xing, Y.G., Li, W.L., Jiang, Y.H. and Ding, Y.L., 2010. Antibacterial and physical properties of poly(vinyl chloride) -based film coated with ZnO nanoparticles. *Food Science and Technology*, 16(3) pp. 225–232.
- Sekhon B.S., 2010. Food nanotechnology – an overview. *Nanotechnology, Science and Applications*, 3, pp. 1–15.
- Seo, J., Jeon, G., Jang, S., Khan, S.B. and Han, H., 2011. Preparation and properties of poly(propylene carbonate) and nanosized ZnO composite films for packaging applications. *Journal of Applied Polymer Science*, 122(2), pp. 1101–1108.
- Shvalagin, V.V., Stroyuk, A.L. and Kuchmii, S.Y., 2004. Role of quantum-sized effects on the cathodic photocorrosion of ZnO nanoparticles in ethanol. *Theoretical and Experimental Chemistry*, 40(6), pp. 378–382.
- Suppakul, P., Miltz, J., Sonneveld, K. and Bigger, S.W., 2003. Active packaging technologies with an emphasis on antimicrobial packaging and its applications. *Journal of Food Science*, 68(2), pp. 408–420.
- Yam, K.L., Takhistov, P.T. and Miltz, J., 2005. Intelligent packaging: concepts and applications. *Journal of Food Science*, 70(1), pp. R1–R10.



JPMTR 066 | 1415
DOI 10.14622/JPMTR-1415
UDC 582.763 : 667.5

Research paper
Received: 2014-07-15
Accepted: 2015-08-19

Formulation of drop on demand soy inkjet inks

Alexandra Pekarovicova, Zabra Mashbadi Khodabakhsh, Paul D. Fleming III

Western Michigan University, Center for Ink and Printability,
4601 Campus Drive, A-213 Parkview, Kalamazoo,
MI 49008-5462, USA

E-mail: a.pekarovicova@wmich.edu

Abstract

Soy protein has a complex 3-D shape and contains 19 different amino acids, which are held together in a coiled structure by peptide bonds. The basic application of industrial-grade soy protein is for a use as a binder in paper coatings. In this work, soy polymer Pro-Cote 4610E was used for formulation of drop on demand piezoelectric inkjet inks. Soy drop on demand inks performance was compared to ones of inks formulated with acrylic polymer Joncryl 678 and commercial inkjet ink. During formulation, sodium hydroxide was more successful in solubilizing of soy polymer than ammonium hydroxide. Preliminary soy ink formulations were made, and based on these results, a design of experiments (DOE) was carried out to optimize ink formulations. The DOE was executed with another aim to compare soy and acrylic based chemistry performance. A combination measure of ink density, surface tension and viscosity was used to assess inkjet printability. Drop behavior was controlled by Reynolds, Weber and Ohnesorge numbers. Reciprocal value of Ohnesorge number (Z number) was calculated, and used for prediction of soy protein inks and acrylic inks jettability. The print design for Dimatix Material Printer DMP-2800 consisted of solid patches and lines of varied width and orientation. At first, even inks with proper Z number were creating satellite drops and were puddling, which was removed by increasing the drop velocity from $0.2 \text{ m} \cdot \text{s}^{-1}$ to around $4 \text{ m} \cdot \text{s}^{-1}$. Thus, it was found that higher voltage is crucial for proper drop formation. The quality of printed lines was evaluated by measuring their width and raggedness using image analysis. Print mottle was evaluated on solid patches. All inks, soy, acrylic and commercial, exhibited printed line widths greater than their nominal widths, which was expected, due to printing on plain inkjet paper. There were no significant differences in quality of print lines between soy and acrylic inks and commercial ink. Soy ink achieved the best print uniformity of solids, when compared to formulated acrylic or commercial inkjet ink.

Keywords: soy polymer, acrylic ink, ink formulation, jetting, Z number

1. Introduction

Acrylic polymers are used in the automotive industry, medical devices, coatings, paints, and adhesive industries. With the development of disposable diapers, much of acrylic chemistry is consumed in diaper manufacture. Often times, the ink industry competes for acrylic polymers, which inspired this work on alternative inks based on renewable soy based raw material.

Soybeans, the material used to extract soy protein from, are composed of about 40 % proteins and 20 % oil (Xu et al., 2011). Soy oils have been employed in ink manufacture for a long time. They are used mainly in offset litho newsprint inks, as well as heatset offset inks. Recently, eco-friendly pigment and soy oil were applied in formulating heat resistant soy inks (Liu et al., 2014). The paper industry continues to use soy protein for paper coatings. Currently, soy protein is intensely researched for viability for green packaging application alone or in blends with other green polymers (Garrido et al., 2014; Ciannamea, Stefani and Ruseckaite, 2014; Leceta et al., 2014).

Soy protein features a complex 3-D shape which contains 19 different amino acids. These acids are held together in a coiled structure by peptide bonds (Kinsella, 1979). The major functional groups found in soy protein consist of amino, carboxyl, hydroxyl, phenyl and sulfhydryl ones. Soy proteins can be obtained from soybeans through the extraction of soybean oil (Xu et al., 2011; Kinsella, 1979). It is an excellent raw material for formulating environmentally friendly adhesives, asphalts, resins, cleaning materials, cosmetics, paints, plastics, polyesters and textile fibers (Smith, 1996). The basic application of industrial-grade soy protein is for a use as a binder in paper coatings (Graham and Krinski, 1983; Zhou et al., 2013; Merrifield, 1998). Soy protein is extracted from soy meal under neutral or alkaline conditions, because its water solubility is very closely related to pH, and it drops with decreasing pH, reaching minimum at pH around 4.2–4.6 (Kumar et al., 2002). Fractionation of soy polymer can be also done by ultra centrifugation based on sedimentation constants of proteins. The principal soy protein is glycinin with molecular weight

around 320–360 kDa (Kumar et al., 2002). Glycinin contains mainly acidic amino acids and their amides. Soy protein is manufactured from concentrates, which contain denatured insoluble proteins, and isolates, which are water soluble, and useful for industrial application, such as plastic films, composite materials or adhesives.

In general, a base inkjet ink is prepared with four main raw materials: resins, colorants, solvents, and additives (Magdassi, 2010; Kipphan, 2001). Resins, solvents, and additives create a varnish, which can be mixed with a pigment dispersion to make the final ink system. Resin is usually added to provide cohesive forces between materials and adhesive forces between materials and substrate. It enhances abrasion resistance, gloss, rub resistance, and also the durability of the ink. Colorant is either a soluble dye or insoluble pigment. Dyes provide transparent and vivid colors. They have lower cost in comparison to pigments, and at the same time, they do not need to be ground or filtered. Dyes also provide a larger color gamut than pigments. Their disadvantage is their low light stability and permanence (Chovancova et al., 2005). Pigments on the other hand

are fade resistant, thus they are gaining popularity for inkjet ink formulations (Chovancova et al., 2005). Due to their chemical nature, pigments are inorganic or organic. They are ground into submicron particles in the process of pigment dispersion preparation. Solvent is used in printing ink to adjust the viscosity. Water is the main solvent in water-based inks. Additives are used to give special properties to printing inks and they should be added to ink in amounts not exceeding 5 %. There are several types of additives that have different functions in a printing ink. The main groups of additives are waxes, defoamers, surfactants, humectants, biocides, pH adjusters, cross linkers, and anti-corrosion agents (Leach et al., 1993). To prevent ink contamination, the use of deionized water in the ink formulation is essential. The finished ink should be able to keep its properties such as ink color stability, stable viscosity, surface tension, pH, pigment content, and particle size for a prolonged time (Kipphan, 2001), but also during printing (Frimova et al., 2005). Information on formulating inkjet inks can be found (Magdassi, 2010), but there has not been much work found on formulating inks based on soy protein, thus it became the main goal of this work.

2. Methods

2.1 Ink formulations

Resins Pro-Cote 4610E soy polymer with glass transition temperature of $T_g > 160$ °C (DuPont), and acrylic polymer Joncryl 678 (BASF); $T_g = 101$ °C, molecular weight $MW = 800$, acid number 216 were used to formulate soy and acrylic based inks. NaOH and NH_4OH were used to solubilize soy polymer and keep alkaline pH of solubilized resins. The Joncryl 678 acrylic resin was in powdered form, and a liquid resin needed to be made. The process to make Joncryl 678 resin solution was as follows (total weight 100 g): add 59 ml 50 °C water into a beaker; add 9 g ammonia (27 % as NH_3), then add Joncryl 678 solid resin in small increments (total 32 g) into solution while dispersing.

Surfynol CT-231 and Carbowet 300 (Air Products) were used as ink surfactants. Soy based inks were formulated with the addition of a biocide. Ethylene glycol was applied as humectant for inkjet inks. Commercial cyan pigment dispersion (Hostajet PT, Clariant) was employed to formulate both acrylic and soy based inks. Ink formulating was done similarly for soy and acrylic polymers. First, resins were solubilized in alkali, surfactants and water, then the pigment dispersion and further additives were blended in.

2.2 Printing

A Dimatix Material Printer DMP-2800 was used to print inkjet inks. The print head permits users to fill cartridges

with any jettable fluid and print directly with the DMP-2800. The cartridge reservoir has a capacity of 1.5 ml and each single-use cartridge has 16 piezoelectric nozzles linearly spaced at 254 μm with 21.5 μm openings to produce typical drop sizes of 10 pl. Plain inkjet paper was used for printing.

2.3 Analytical

A combination measure of density, surface tension and viscosity was used to assess inkjet printability. Thus, drop behavior is controlled by Reynolds, Weber and Ohnesorge numbers. Ohnesorge number (Oh) can be calculated as follows:

$$Oh = We^{1/2} / Re = \eta / (\gamma \cdot \rho \cdot a)^{1/2} \quad [1]$$

Where ρ is the density, η is the dynamic viscosity, γ the surface tension, and a is the characteristic length (nozzle diameter).

Reciprocal value of Ohnesorge number is then calculated (Fromm, 1984) and designated as the Z number:

$$Z = 1 / Oh \quad [2]$$

The density, surface tension and viscosity were measured in order to calculate the Z number. Density was determined using a 25 ml pycnometer and analytical balance. Contact angle and surface tension measurements were performed using a FTA200 dynamic contact

angle measurement device. The change in contact angle with time was measured for DI water and methylene iodide on the paper substrate and printed ink films to enable their surface energies to be determined by use of the Owens-Wendt (1969) method. The equilibrium contact angle for each liquid (contact angle where no further change with time was observed) was used in these calculations (Owens and Wendt, 1969). Viscosity of inks was determined with RA 2000 dynamic stress rheometer (TA Instruments, DE) (Yumeizhi, Pekarovicova and Fleming, 2013). Cone-plate couette geometry was used. Viscosity measurements were performed at a fixed temperature of 25 °C while increasing the shear rate from 0 to 1500 s⁻¹. The solids content of inks was measured by a Smart Turbo-Moisture/Solids Analyzer.

3. Results and discussion

Commercial soy polymer was implemented into alkaline water based slurries. Different alkalis, such as Na₂CO₃, NaOH and NH₄OH were tested for soy powder solubilization. It was found that soy polymer dissolves to different extent in various alkalis, resulting in particle size ranging from 800 to 400 nm. Moreover, it dissolves best in ammonium hydroxide, in which the particle size reached 400 nm (Khodabakhsh, 2013). Dispersed soy protein was then blended with pigment dispersion and surfactants. The particle size of such polymer dispersion decreased even further after mixing with pigment dispersion to 150–160 nm depending on ink formulation and pH environment. Rheology, surface tension and density of these inks were measured. These data were used to calculate Z numbers, combining influence of density, surface tension and viscosity on ink jettability (Owens and Wendt, 1969; Yumeizhi, Pekarovicova and Fleming, 2013; Derby, 2011). Applying Weber and Ohnesorge calculations, Fromm used the reciprocal

The particle size of ink and ink ingredients was measured by Submicron Particle Sizer Model 370 Nicomp (Particle Sizing Systems, Santa Barbara, California) based on photon correlation spectroscopy. The ImageXpert (KDY Inc.) image analysis system was used for measurement of average width and raggedness of printed lines. ImageXpert image analysis system consisted of a motion table for sample positioning, two calibrated cameras for image capture and ImageXpert image analysis software (IX 10.0b63). Five readings were taken for every feature measured on each sample. For color and optical density characterization, an X-Rite 530 SpectroDensitometer was employed. Specular gloss was measured by Novo-Gloss 20°/60°/75° meter at 60 degree geometry.

value of Oh number and came to conclusion that the Z number should be in the range $2 \leq Z \leq 14$, in order for ink formulations to be suitable for ink jetting (Fromm, 1984; Derby, 2011; Reis, Ainsley and Derby, 2005).

According to preliminary formulations with appropriate Z number (data not shown), a design of experiments was employed to optimize formulation of soy and acrylic based inks (Table 1). Print design is illustrated in Figure 1.

Commercial inkjet ink extracted from a cartridge, and formulated soy and acrylic inks were printed using a Dimatix Material Printer DMP-2800. Even with inks with Z number in the optimum range, it took formulation changes and surfactant amount optimization as well as Dimatix waveform modification to reach proper jetting. At first, inks created satellite drops and puddled (Figure 2). Also, it seemed like the drop velocity was very slow, thus, it was decided to measure the velocity

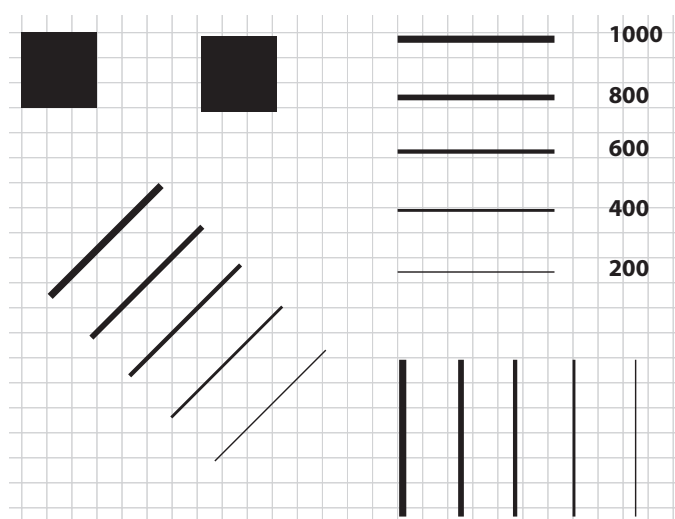


Figure 1: Design for printing acrylic and soy inks on Dimatix printer

of the drops and then compare with required velocity of ink for a proper ejection and without breakup. The drop velocity was calculated using the video system on Dimatix (data not shown). From these data the Weber number We and $We_{critical}$ (Pilch and Erdman, 1987) were calculated:

$$We_{critical} = 12 \cdot (1 + 1.077 \cdot Oh^{1.6}) \quad [3]$$

It was shown previously that, in the case where the We number is smaller than the $We_{critical}$, there would not be

any breakup nor satellite drop formation (Lim et al., 2013). Also, it was found that the required velocity to achieve proper drop formation was around $4 \text{ m} \cdot \text{s}^{-1}$, while the velocity of inkjet ink jetted as shown in Figure 2 was $0.2 \text{ m} \cdot \text{s}^{-1}$. Thus, it is clear that ink needs to be jetted at higher voltages to get higher drop velocity. Another challenge was to avoid nozzle clogging (Figure 3). Nozzle clogging reduction was enabled using humectant, such as ethylene glycol up to 10 % wt., in the ink formulation. Appropriate jetting of acrylic and soy based ink is illustrated in Figure 4 and Figure 5.

Table 1: Design of Experiment for soy inkjet inks optimization (AWoutS – acrylic without surfactant, AWS – Acrylic w/surfactant, SWoutS – Soy without surfactant; SWS – Soy with surfactant)

Formula No.	AWoutS (1)	AWS (2)	SWoutS (3)	SWS (4)	AWoutS (5)	AWS (6)	SWoutS (7)	SWS (8)
Acrylic Joncryl 678 (g)	12	12	–	–	12	12	–	–
Soy polymer solution (g)	–	–	12	12	–	–	12	12
Pigment dispersion (g)	15	15	15	15	10	10	10	10
Surfactant (Carbowet 300) (g)	–	0.1	–	0.1	–	0.1	–	0.1
Humectant (Ethylene Glycol) (g)	10	10	10	10	10	10	10	10
DI water (g)	63	62.9	63	62.9	63	62.9	63	62.9

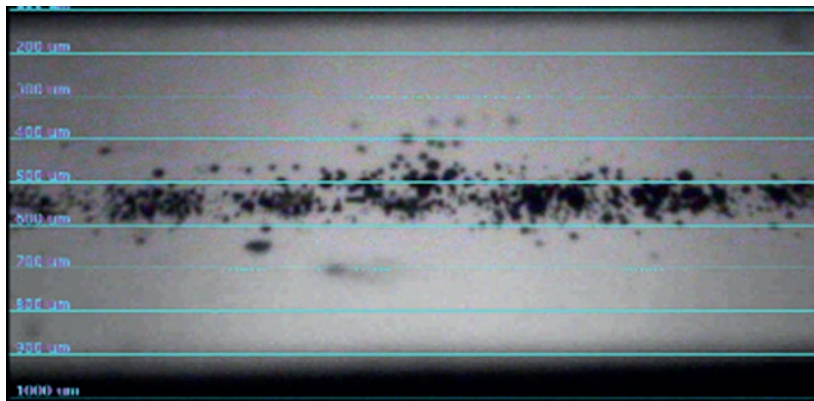


Figure 2: Soy ink puddling while printed on Dimatix Material Printer DMP-2800

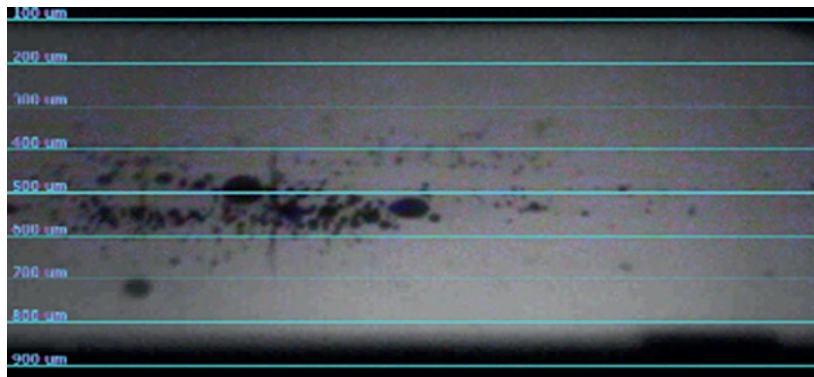


Figure 3: Soy ink clogging nozzles on Dimatix Material Printer DMP-2800

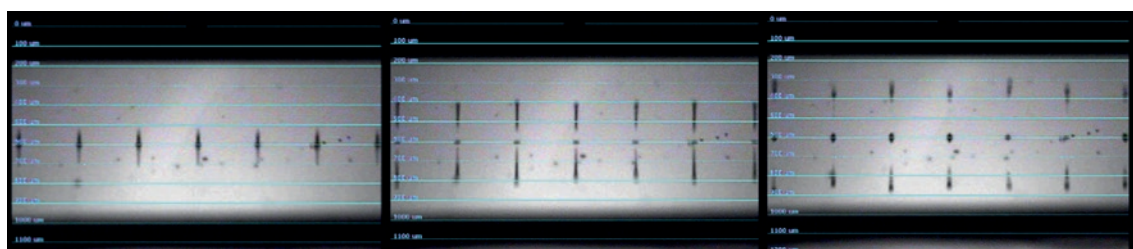


Figure 4: Jetting of acrylic based inks on Dimatix

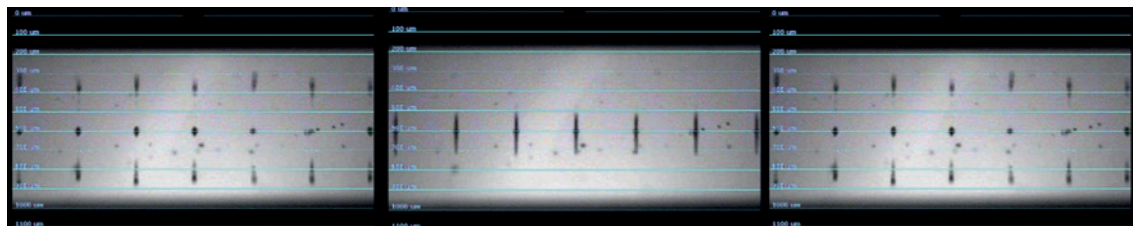


Figure 5: Jetting of soy based inks on Dimatix

The viscosity versus shear rate for acrylic-based inkjet ink and soy-based inkjet ink was studied. The viscosity curves suffer from noise in the region $0.1\text{--}4\text{ s}^{-1}$ and then again from 300 s^{-1} (acrylic) and 400 s^{-1} (soy), data not shown. Both soy and acrylic inks behave as Newtonian fluids in the region of shear rate $4\text{--}300\text{ s}^{-1}$ (acrylic AWS) and $4\text{--}400\text{ s}^{-1}$ (soy SWS). It is obvious that the acrylic ink has slightly lower viscosity ($2.4\text{ mPa}\cdot\text{s}$) than the soy ink ($3.9\text{ mPa}\cdot\text{s}$). Similarly, viscosities of all formulated inks were measured. Figure 6 shows comparison of viscosity of all inks with/without surfactant and with varying amount of pigment dispersion. As expected, the ones with lower pigment load had lower viscosity (Figure 6).

According to rule of thumb, the surface tension of inks should be at least $10\text{ mN}\cdot\text{m}^{-1}$ lower than the surface energy of the substrate, in order to achieve proper print quality and adhesion. The substrate surface energy is defined as the sum of the excess energies at the surface of the substrate compared to the bulk (Whiting et al.,

2011). In inkjet printing, it is very important to obtain an accurate drop placement and a uniform dried film, which can be controlled by adjusting the surface energy of the substrate (Whiting et al., 2011). It was found that acrylic-based inkjet inks have larger surface tension than the soy-based inkjet inks, maybe because soy protein is a natural surfactant. It was also found that the surface tension values of inks with 15 g of pigment dispersion are lower than of inks with 10 g pigment dispersion. It is most likely because commercial pigment dispersion contains wetting agent blended in, which may reduce the surface tension. Also, surfactant has a slight effect on surface tension of acrylic-based inkjet inks, while it has no effect on soy-based inkjet inks. It was also shown that the surface tension of soy-based inkjet inks with 10 g pigment dispersion with or without surfactant was very close to that of commercial inkjet ink (Figure 7). Soy inks had slightly lower surface tension $32.5\text{--}34.8\text{ mN}\cdot\text{m}^{-1}$ than acrylic inks $35.3\text{--}39.3\text{ mN}\cdot\text{m}^{-1}$ as compared to commercial ink having surface tension $34.0\text{ mN}\cdot\text{m}^{-1}$. Soy inks particle size was slightly larger

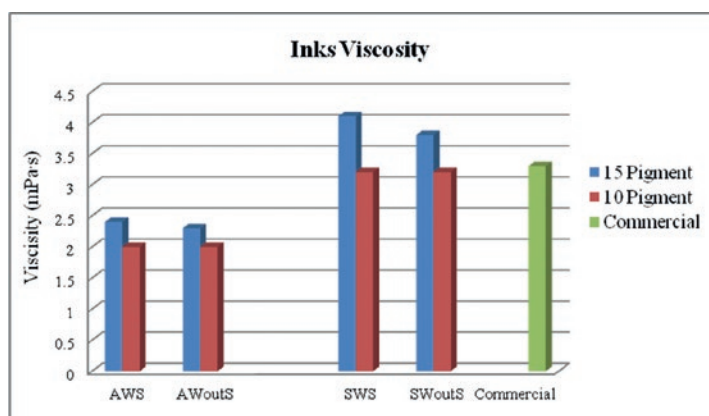


Figure 6: Comparison of viscosity of formulated and commercial inkjet inks

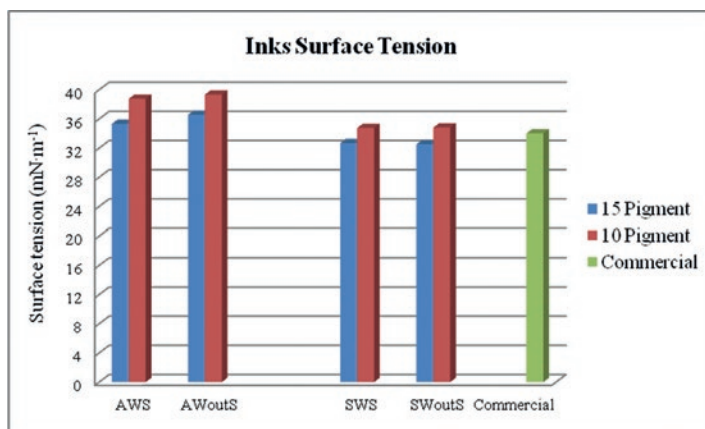


Figure 7: Comparison of surface tension of formulated and commercial inkjet inks

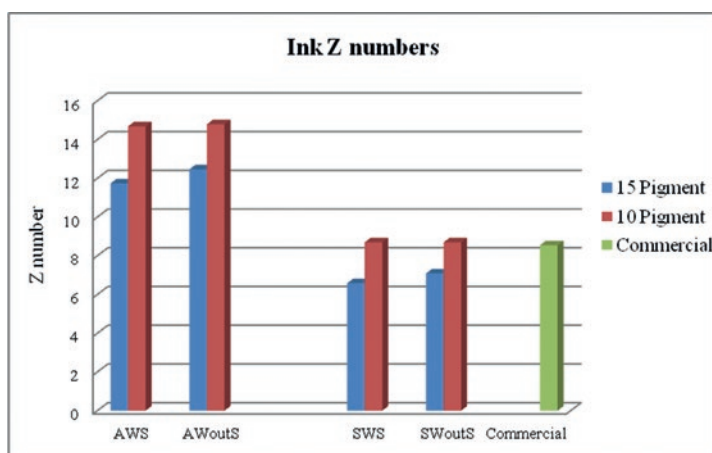


Figure 8: Comparison of Z numbers of formulated and commercial inks

(range of 188–197 nm) than that of the acrylic inks (range of 160–174 nm), data not shown.

Acrylic-based inkjet inks had larger Z numbers than soy-based inkjet inks (Figure 8). Inks with 10 g pigment dispersion had larger Z number than those with 15 g of pigment dispersion. Also, the Z number for soy-based inkjet inks with 10 g pigment dispersion (with and without surfactant) was very close to that of the commercial inkjet ink (Figure 8). It was found that increased level of surfactant in ink does not affect the Z number for both acrylic-based and soy-based inkjet inks.

A print done with one of the successful formulations of soy ink is illustrated in Figure 9 and a print of commercial ink is illustrated in Figure 10. The quality of printed lines was evaluated by measuring their width and raggedness using image analysis. There were five lines with different nominal widths: 200, 400, 600, 800, and 1000 μm measured for each ink formula. Only lines parallel to print direction were measured. It was found that all line widths are greater than their nominal widths

(Figure 11). It is due to ink spreading, which would be observed as tone value increase, or dot gain, if measured on individual printed dots. The type of paper, in this case plain uncoated paper, has a significant effect on spreading. The plain paper pulls liquid into its body or moves it laterally along the surface, while paper with a coating tends to hold the ink at the surface and does not allow adsorbing into or wicking along its surface (Briggs, 2002; Forrest et al., 1998).

The raggedness of both sides of the lines was measured to consider the line quality. Again, only lines parallel to print direction were measured. The more feathering occurs, the more ragged the line is. It was found that some prints suffered from overspray and smearing. Figure 12 illustrates line raggedness for all acrylic and soy inks and commercial ink and Figure 13 shows detail of line raggedness for acrylic, soy and commercial ink and how it was measured.

Overall, Figure 12 shows that acrylic ink with or without surfactant printed less ragged lines than soy ink. Also, ink formulations without surfactant printed less ragged

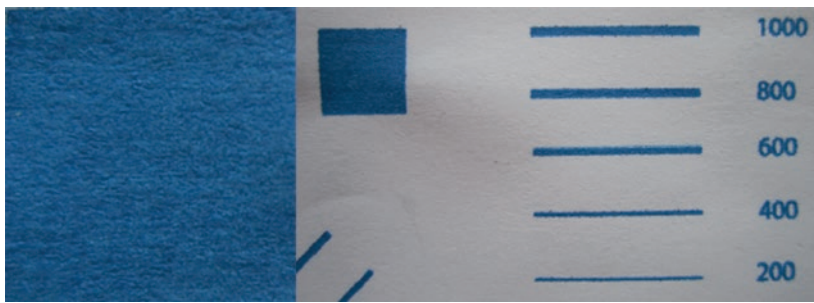


Figure 9: Print of soy based ink with viscosity $4.1 \text{ mPa} \cdot \text{s}$, surface tension $32.7 \text{ mN} \cdot \text{m}^{-1}$, and Z number 6.58

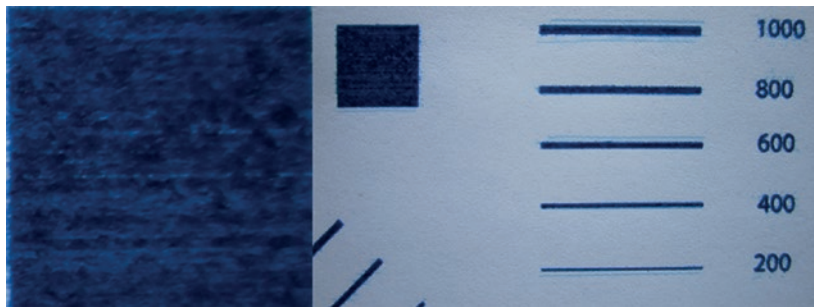


Figure 10: Print of commercial ink with viscosity $3.3 \text{ mPa} \cdot \text{s}$; surface tension $34.0 \text{ mN} \cdot \text{m}^{-1}$ and Z number 8.54

lines than the formulations with surfactant. Also, more viscous inks with 15 g of pigment dispersion were less ragged than those with 10 g of pigment dispersion. It may indicate that lower viscosity encourages spreading and raggedness. Overspray and smearing were observed with all of these three types (acrylic, soy and commercial) of inkjet inks (Figure 13), thus these problems can be also related to selection of ink viscosity and printing conditions of Dimatix printer as well as quality of the paper surface. It can be concluded that line raggedness of commercial and formulated acrylic and soy inks are comparable, which pinpoints the need of further optimization of Dimatix waveform printing conditions.

Optical properties and print quality were then analyzed. Both soy and acrylic inks achieved low specular gloss around 2–3 %, (data not shown), maybe due to surface roughening because of alkaline pH of inks and low quality of paper substrate. Optical densities of all soy inks were lower (1.11–1.21) than that of commercial ink (1.36). However, optical density can be modified with pigment dispersion addition. Soy ink achieved the best print uniformity of solids, when compared to formulated acrylic or commercial ink (Khodabakhsh, 2013).

CIELAB data of all inks are shown in Figure 14. All inks with 15 g pigment dispersion had lower L^* value than

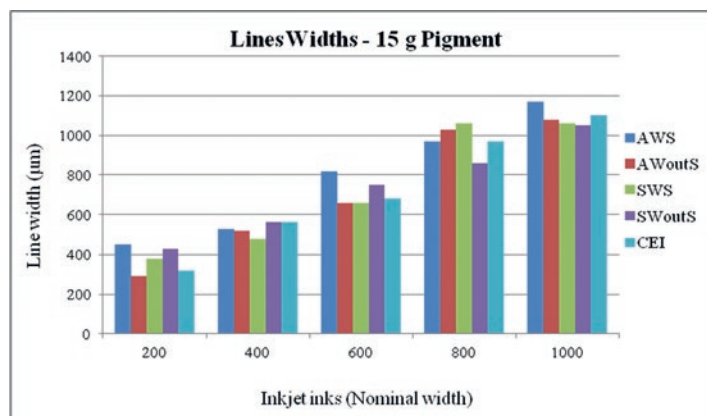


Figure 11: Line width of inkjet inks with 15 g of pigment dispersion (CEI – commercial)

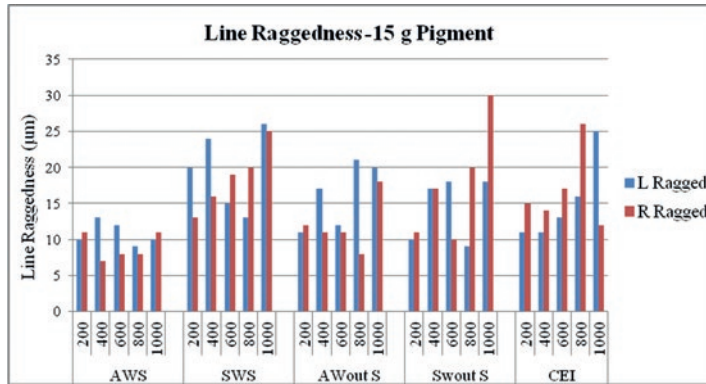


Figure 12: Raggedness of both left and right sides of line of all inkjet inks with 15 g of pigment dispersion

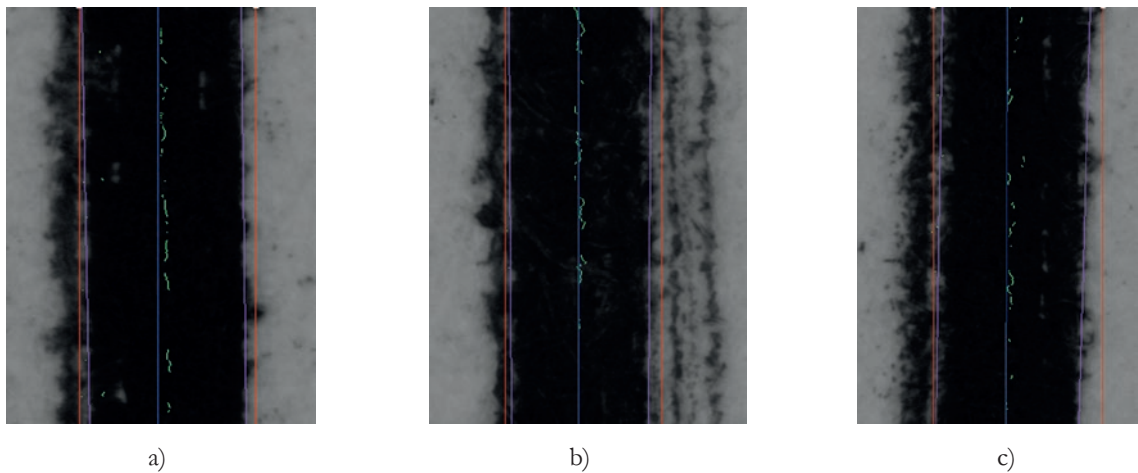


Figure 13: Line raggedness of acrylic, soy and commercial inks (15 g of pigment dispersion); a) AWoutS (#1), b) SWoutS (#3), c) CEI (#9)

those with 10 g pigment dispersion. Formulated acrylic inks had lower CIE L^* values (L^* range 28 to 31) than soy inks (L^* range 35 to 37). Commercial ink had lowest CIE L^* value of 25.8. Commercial ink was also redder (CIE $a^* = 16.2$), while our formulated inks were greener (CIE a^* in range of -0.5 to -10.6), which indicated that

different crystalline structure cyan pigment was used. CIE b^* value of commercial ink was -41.5 , while formulated inks had CIE b^* value in the range of -44.6 to -52.4 ; acrylic had lower b^* values, than soy inks, which indicates that acrylic resin developed bluer cyan than the soy resin.

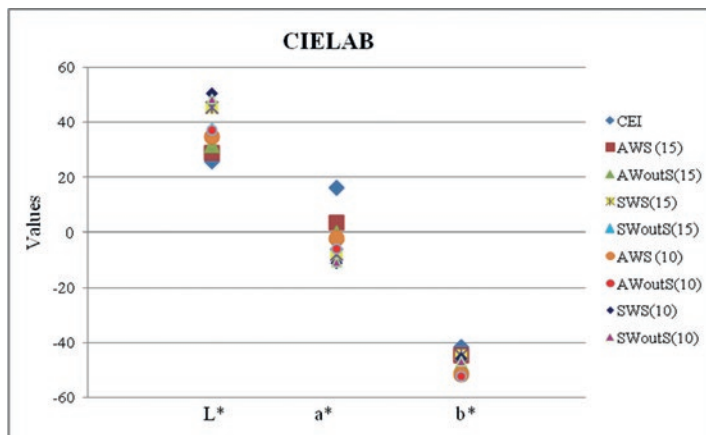


Figure 14: CIELAB values of commercial and formulated cyan inks

4. Conclusion

The aim of this work was to determine if the soy polymer can be used to formulate drop on demand inkjet inks. First, preliminary formulations were made and printing on the Dimatix Material Printer DMP-2800 was tested. Based on these preliminary results, a design of experiment was prepared for formulation of soy protein inks. Inks were designed so that their combined performance regarding viscosity, density and surface tension would give a certain value of Z number, predicted to be jettable. All inks formulated according to design of experiment were successfully jetted using the Dimatix printer. It was confirmed that both soy and acrylic inks behaved as Newtonian fluids in the region of shear rate $4\text{--}300\text{ s}^{-1}$ (acrylic AWS) and $4\text{--}400\text{ s}^{-1}$ (soy SWS). Acrylic ink had slightly lower viscosity ($2.4\text{ mPa}\cdot\text{s}$) and particle size (range of $160\text{--}174\text{ nm}$) than the soy ink

($3.9\text{ mPa}\cdot\text{s}$ and $188\text{--}197\text{ nm}$). However, soy inks exhibited slightly lower surface tension ($32.5\text{--}34.8\text{ mN}\cdot\text{m}^{-1}$) than acrylic inks ($35.3\text{--}39.3\text{ mN}\cdot\text{m}^{-1}$) maybe because soy polymer acts as a natural surfactant. Printability of soy ink jet inks was comparable to acrylic based ink jet inks and commercial drop on demand ink. The quality of printed lines was evaluated by measuring their width and raggedness using image analysis. Print motile was evaluated on solid patches. All inks, soy, acrylic and commercial, exhibited printed line widths greater than their nominal widths, which was expected, due to printing on plain inkjet paper. There were no significant differences in quality of print lines between soy, acrylic inks and commercial ink. Soy ink achieved the best print uniformity of solids, when compared to formulated acrylic or commercial inkjet ink.

References

- Briggs, J.C., 2002. *Application Note: Inkjet Media Print Quality Analysis*, Quality Engineering Associates (QEA), Inc., Burlington MA/USA. [online] Available at: <http://www.qea.com/upload/files/products/AppNote_QEA_InkJet_Media.pdf> [Accessed 11 September 2015].
- Chovancova, V., Fleming, P.D., Howell, P. and Rasmusson, A., 2005. Color and lightfastness of different Epson ink sets. *Journal of Imaging Science and Technology*, 49(6), pp. 652–659.
- Ciannamea, E.M., Stefani, P.M. and Ruseckaite, R.A., 2014. Physical and mechanical properties of compression molded and solution casting soybean protein concentrate based films, *Food Hydrocolloids*, 38, pp. 193–204.
- Derby, B., 2011. Inkjet printing ceramics: From drops to solid, *Journal of the European Ceramic Society*, 31(14), pp. 2543–2550.
- Forrest, D.J., Briggs, J.C., Ming-Kai, T. and Barss, S.H., 1998. Print quality analysis as a QC tool for manufacturing inkjet print heads, *ISE&T NIP14 International Conference on Digital Printing Technologies*, Oct. 18–23, Toronto, Canada.
- Frimova, A., Pekarovicova, A., Fleming, P.D., and Pekarovic, J., 2005. Ink stability during printing, *TAGAJ*, 2, pp. 122–131.
- Fromm, J.E., 1984. Numerical calculation of the fluid dynamics of drop-on-demand jets, *IBM Journal of Research and Development*, 28(3), pp. 322–333.
- Garrido, T., Etxabide, A., Leceta, I., Cabezudo, S., de la Caba, K. and Guerrero, P., 2014. Valorization of soya by-products for sustainable packaging, *Journal of Cleaner Production*, 64, pp. 228–233.
- Graham, P.M. and Krinski T.L., Ralston Purina Company, 1983. *Heat coagulable paper coating composition with a soy protein adhesive binder*; USA. US patent 4421564.
- Khodabakhsh, Z.M., 2013. *Soy Based Inkjet Ink*. M.S. Thesis, Western Michigan University, Kalamazoo.
- Kinsella, J. E., 1979. Functional properties of soy proteins, *Journal of the American Oil Chemists' Society*, 56(3), pp. 242–258.
- Kipphan, H., 2001. *Handbook of Print Media: Technologies and Production Methods*. Berlin, Heidelberg: Springer-Verlag.
- Kumar, R., Choudhary, V., Mishra, S., Varma, I.K. and Mattiason, B., 2002. Adhesives and plastics based on soy protein products, *Industrial Crops and Products*, 16(3), pp. 155–172.
- Leach, R.H., Pierce, R.J., Hickman, E.P., Mackenzie, M.J. and Smith, H.G., eds., 1993. *The Printing Ink Manual (5th edition)*. Dordrecht, The Netherlands: Springer.
- Leceta, I., Etxabide, A., Cabezudo, S., de la Caba, K. and Guerrero, P., 2014. Bio-based films prepared with by-products and wastes: environmental assessment, *Journal of Cleaner Production*, 64, pp. 218–227.
- Lim, S., Fleming, P.D., Joyce, M. and Lee, M., 2013. A Study of the jetting evolution of nanocopper ink and nanosilver ink with inkjet, *Journal of Imaging Science and Technology*, 57(2) pp. 20506-1–20506-8.
- Liu, Z., Liu, Q., Yang, L., Sun, J.Y., Ma, G.Y. and Zhang, B.L., 2014. Preparation and study of temperature resistance environmentally friendly ink based on natural pigment and soy oil, *Applied Mechanics and Materials*, Vol. 469, pp. 13–16.

- Magdassi S., 2010. *The Chemistry of Inkjet Ink*. Singapore, Hackensack: World Scientific Publishing Co.
- Merrifield, T.B., 1998. Soy polymer use in coated paper and paperboard production. In: *Proceedings of the 1998 TAPPI Notes*; Norfolk, VA, USA, 16.
- Owens, D.K. and Wendt, R.C., 1969. Estimation of surface free energy of polymers, *Journal of Applied Polymer Science*, 13(8), pp. 1741–1747.
- Pilch, M. and Erdman, C.A., 1987. Use of breakup time data and velocity history data to predict the maximum size of stable fragments for acceleration-induced breakup of a liquid-drop, *International Journal of Multiphase Flow*, 13(6), pp. 741–757.
- Reis, N., Ainsley, C. and Derby, B., 2005. Ink-jet delivery of particle suspensions by piezoelectric droplet ejectors, *Journal of Applied Physics*, 97, p. 094903.
- Smith, K., 1996. Industrial uses of soy protein: new ideas. In: *87th AOCs Annual Meeting & Expo*, Inform, 7(11) pp. 1212–1215.
- Whiting, G.L., Lujan, R.A., Krusor, B.S., Russo, B., Daniel, J.H., Arias, A.C. and Street, R.A., 2011. Surface-energy patterning for ink-jet printed flexible electronics. In: *2011 Spring Meeting of the Materials Research Society*, San Francisco, CA.
- Xu, Q., Nakajima, M., Liu, Z. and Shiina, T., 2011. Soybean-based surfactants and their applications, In: Ng, T.-B., ed., *Soybean-Applications and Technology*. [online] Available at: <<http://www.intechopen.com/books/soybean-applications-and-technology/soybean-based-surfactants-and-their-applications>> [Accessed 11 September 2015].
- Yumeizhi, J., Pekarovicova, A., and Fleming, P.D., 2013. Inkjet printability of phthalocyanine dye ink. In: *TAGA 65th Annual Technical Conference*, Portland, OR.
- Zhou, G.F., Ma, J.X., Lin, G.Q., Zhai, H.M. and Richard, G., 2013. Effects of soy protein polymer Pro-cote[®] 4610 on properties of coated paperboard, *China Pulp and Paper*, 32(1) pp. 19–22.

JPMTR 067 | 1430
 DOI 10.14622/JPMTR-1430
 UDC 003.29 : 004.93/7.061

Research paper
 Received: 2014-07-30
 Accepted: 2015-07-26

Image analysis as a tool to discriminate counterfeit from true 2D printed codes

Nadège Reverdy-Bruas, Lionel Chagas, Jean-Pascal Poletti, Raphaël Passas

Univ. Grenoble Alpes, LGP2, F-38000 Grenoble, France
 CNRS, LGP2, F-38000 Grenoble, France
 Agefpi, LGP2, F-38000 Grenoble, France

E-mail: nadega.reverdy@pagora.grenoble-inp.fr
lionel.chagas@pagora.grenoble-inp.fr

Abstract

The general context of this study is to establish recommendations for the development of digital models in the framework of counterfeiting. To achieve this goal, printed 2D codes were investigated. Visual Basic tools have been developed in order to automate tasks. The present paper allows characterizing the printing process used (conventional and waterless offset); sensitive results were also obtained regarding the kind of printed substrate (coated and uncoated paper). Histograms of area classes were plotted and they revealed that the printing process induced the raise of a new class of small dots not present on the digital file. In addition, two types of counterfeiting methods were carried out and they pointed out that the histograms of the counterfeit codes were different from the original printed code, whatever the attempt of counterfeiting. Furthermore, in these cases, small dots tend to agglomerate and form new area classes of bigger size. The method developed in this study thus allows the identification of the printing process as well as the distinction of true and counterfeit 2D codes.

Keywords: 2D codes, counterfeiting, security, automation, image analysis

1. Introduction and background

The general context of this study is to establish recommendations for the development of digital models in the framework of counterfeiting (Jotcham, 2005). The first step of the research was to characterize the similarity between a printed 2D code and the corresponding numerical file (Chagas et al., 2013). The present article summarizes the second phase of characterization of 2D printed codes.

Even if they are similar to stacked 1D barcodes, 2D codes work in a very different way. They require a 2D scanner to be read, consisting of a camera – generally a smartphone – that acquires a picture of the substrate. In a second step, the picture is analysed for the purpose of restoring the original code and decrypting the

information contained in it. These steps require complex mathematical treatment to be applied on the picture (Chu et al., 2011; Wang and Zou, 2006).

In 1994, Denso Wave, a subsidiary of the Japanese company Toyota, developed a 2D code to mark components. This code can be quickly read by cameras, so they can identify and sort the components automatically, quickly and without ambiguity (DENSO WAVE, 2013). It is rightly called QR code – for Quick Response Code – and has been subject to several standards, in particular ISO 18004 in June 2000, after Denso published QR code as a royalty-free license in 1999. This permitted its global expansion and use in various application fields.



7 % redundancy



30 % redundancy



Stylized



Logo

Figure 1: Various QR code features encoding the same web link

QR code (Figure 1) public success is due to its high-speed readability, high-capacity data storage and reliability (from 7 % to 30 % of redundancy). Moreover it is not only a conveyer of characters as part of numbers or texts, but also contains various kinds of content. It is possible to create QR codes containing business card information, web link, Wi-Fi settings, pre-filled SMS... Free QR code generators are available on internet (UNITAG, 2013). The size of this code depends on the information encoded and the rate of redundancy, which results from Reed-Solomon theory (Swetake, 2013). Thanks to this system, one can integrate logos or drawings into a QR code: even if it hides a part of the code and redundancy is decreased, it is still correctly decodable (Figure 1).

As QR codes are widely used by general public, other 2D codes have been developed such as Data Matrix, for the applications rather industrial than public (Stevenson, 2005). This one was invented in October 2005 by a subsidiary of Siemens. It is similar to a QR code (Figure 2) and uses Reed-Solomon algorithm too. Covered by ISO 16022, Data Matrix can encode various kinds of information (text, web link, SMS...); however, it is mostly used for marking small electronic components. One of the advantages of this code is its readability with a very low contrast – 20 % is sufficient. In addition, Data Matrix has become mandatory on every medicine box since 1st of January 2011 in France (Lemaire, 2011).



Figure 2: Data Matrix encoding a web link to Google

There is also a possibility of encoding information in clustered-dot halftones, a system that uses the properties of this kind of printing in order to avoid black-and-white pixel-like blocks on an advertisement (Ulichney, Gaubatz and Simske, 2010).

The ANR Estampille project, of which this study is a part, fits into a global strategy of prevention and deter-

rence in regard to the fight against counterfeiting. In this context there are two key concepts to take into account: authenticity and traceability.

- The authenticity of a product is the correspondence between its description and its characteristics. Detecting a counterfeit item requires to define relevant characteristics, so that controls can be done in a reasonable time – most of the time they involve technical parameters quickly recognizable. It is important not to confuse identification and authentication: identification helps to visually recognize the protected product (brand, logos, various indications...), whereas authentication consists in checking this identity, the correspondence between the product and the indications.
- Traceability means collecting information – by single product or product batch – about the production stages and location data. Such indication can be consulted on demand but it is not a mean of authentication (anomalies in traceability can still trigger suspicion).

There are a lot of technologies meeting these requirements that are used as security systems. They all have assets and drawbacks, so they have to be chosen regarding the product: target market, difficulty of counterfeiting, cost of implementation, etc.

There are many technologies to secure documents: Cryptoglyph[®], microtaggants, geometrical distortion analysis, multilayer stickers, selective varnish, Bokode[®], special paper, etc. Among this variety of security systems, 2D codes present the advantage of being really cheap and easy to implement in a production line. Moreover, the large amount of free generators available on the web promotes the global expansion of their use in various domains. But because they are visible and easily printable, they are likely to be counterfeited.

In this context, 2D codes composed of very small modules (down to 10 μm) corresponding to the smallest dots printable at high resolution (up to 2400 dpi) are under development. This parameter makes it really different from classical 2D codes such as QR codes. Table 1 summarizes the orders of magnitude of widely used 1D and 2D codes.

Table 1: Orders of magnitude – storage for selected code sizes – of 1D and 2D codes

Code	Storage capacity	Module size	Code size
1D barcode (EAN-13)	13 digits – 46 bits	1 mm \times 15 mm	30 mm \times 20 mm
QR code	Up to 7089 digits or 4296 alphanumeric data – 24800 bits	1 mm \times 1 mm	20 cm \times 20 mm
Data Matrix	Up to 3119 digits or 2335 alphanumeric data – 10900 bits	1 mm \times 1 mm	10 mm \times 10 mm
High resolution codes	About 60000 bits	20 μm \times 20 μm	5 mm \times 5 mm

The high resolution codes, discussed in this paper, exhibit a 250 times higher data storage capacity than traditional 2D codes. It is therefore obvious that the challenge is to minimize the module size (and the code size) while keeping the robustness of the code. The small size of the modules makes these kinds of codes nearly impossible to copy.

2. Methods

The analyzed codes are made of single dots and groups of dots on matrixes 100×100 , printed by different printing processes. It is therefore possible to compare the deformation of 2D codes due to the variability of printing parameters: substrate – coated and uncoated, elementary dot size or printing resolution – dot size from 10.2 to 42.4 μm , printing process – conventional and waterless offset; the print area coverage is maintained at the same level (20 %) in this study.

The successive steps carried out to analyse the printed codes consist of:

- developing methods of image analyses by creating macros with VBA (Visual Basic for Applications) on Visolog[®],
- choosing an automatic threshold method,
- establishing histograms showing the number of elements in a class of area.

Finally, two counterfeiting strategies were tested:

- a second print of an original printed code after its digitalization,
- a second print from the digitally reconstructed printed code.

2.1 Printing process

In this study, investigations were focused on the prints obtained with waterless offset, and to a small extent, to conventional offset for the original printed code. Then, counterfeit code was printed using a Ricoh electrophotography press.

Therefore, the present study focuses attention on the characterization of 2D codes printed by different printing processes on different substrates and for different resolutions (dot size). The final aim is to point out the reliability of the 2D code after a first print and after a copy. This is performed by studying the histograms of the number of elements in a class of area.

2.2 Printing substrate

Two kinds of substrates were printed: a coated paper and an offset uncoated paper. Measurements were performed on 10 samples of each kind of paper to characterize their main properties. Table 2 summarizes the results.

The main difference among these two substrates that has a direct impact on the reproduction of the 2D code is the roughness. It is about 0.8 μm for the coated paper and about 6.3 μm for the uncoated one which is typical for these grades.

2.3 Dot size

On the digital test chart, four series of squares of increasing coverage percentages were designed. Each one was printed with a unique printing resolution: 2400, 1200, 800 and 600 dots per inch (dpi).

The hardware resolution corresponds to the size of the smallest dot that it can print. A hardware resolution of 2400 dpi means that it can print dots that are 10.6 μm wide (1 inch = 2.54 cm, 2400 dots in 1 inch implies that 1 dot measures $2.54/2400 = 0.00106 \text{ cm} = 10.6 \mu\text{m}$ in width). In computer science, the equivalent is the pixel: it is the smallest element that can be displayed by a device (screen). The dimension of the elemental dots in the 2D code varies regarding the printing resolution. It is respectively 10.6, 21.2, 31.8 and 42.4 μm for 2400, 1200, 800 and 600 dpi resolutions.

Table 2: Main characteristics of the two studied papers

Paper		Basis weight (g/m ²)	Thickness (μm)	Specific volume (cm ³ /g)	CIE whiteness	PPS Roughness (μm)
Coated paper	Mean	88.90	64.00	0.72	118.06	0.78
	Standard deviation	0.20	0.90	0.01	1.03	0.05
Uncoated paper	Mean	150.90	169.90	1.13	131.45	6.27
	Standard deviation	0.50	2.40	0.02	0.71	0.08

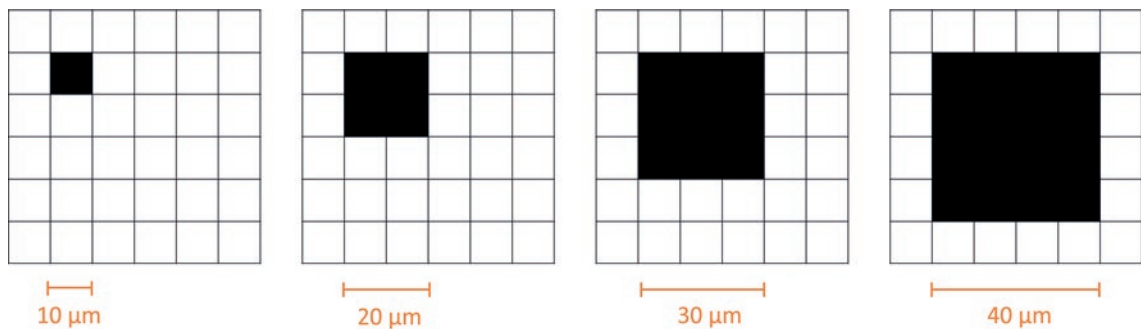


Figure 3: Principle pattern of a 2400 dpi hardware printing a dot at 2400, 1200, 800 and 600 dpi (from left to right) – approximated sizes

A hardware that has a 2400 dpi resolution can also print at lower resolution: in this case, it combines dots at 2400 dpi to have groups of dots that have the size of the desired printing resolution (Figure 3).

2.4 Picture acquisition

2.4.1 Hardware

In order to analyse pictures as clean as possible at very high resolution – and therefore to minimize the influence of the acquisition in the image analysis – the samples were digitalized by an optical Zeiss Microscope Axio Imager.M1m, with associated software Axio Visio, Release 4.8.

2.4.2 Image acquisition protocol

Each printed sample has been digitalized according to the following acquisition protocol on the microscope, to have the same acquisition condition and so to minimize the influence of this step.

- 100-fold magnification (adapted to acquire the smallest squares, printed at 2400 dpi; for the others, it is necessary to make four or nine pictures and combine them into mosaic)
- Reflection light with the highest level of intensity and black background
- Shading process to have an homogeneous light
- Exposure time: 6.40 s
- Pictures: RGB in TIFF format, standard size: 2584 × 1936 pixels

2.5 Image analysis

2.5.1 Software

All the image treatments of the project have been done with Visilog® 7.0, image analysis software of the company Noesis. It is a powerful tool including a lot of functions to analyse complex and even 3D images (VISILOG, 2015). Moreover this software is highly customizable and VBA (Halvorson, 2008) can be used

to create macros, in order to improve the protocols of image analysis and to automate a lot of tasks.

Microsoft® Excel® 2013 has been used to gather data of the samples studied and plot graphs.

2.5.2 Surface of interest

In this study, analyses were focused on 100 × 100 pixels matrixes and did not take into account the printed borders in order them not to influence the measurements. Figure 4 shows the targeted area (4b) selected on the picture taken with the microscope (4a).

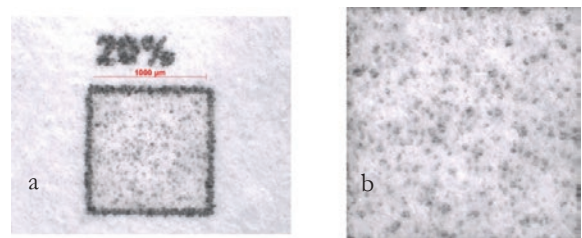


Figure 4: Acquisition of the original picture (a) and corresponding surface of interest (b)

2.5.3 Thresholding

To perform image analysis, binary images are required. It is therefore necessary, from the RGB pictures, to separate the color layers of the image and to threshold one of them. Several thresholding methods can be carried out from the histogram of grey levels.

The manual method consists in creating two value ranges from the color intensity values of each pixel. Pixels which have an intensity value between 0 and the chosen threshold – the darkest – will be converted into black, and pixels which have an intensity value between the chosen threshold and 255 – the brightest – will be converted into white. The threshold can be chosen in regard to the image histogram. Some images clearly show two peaks, so the approximate limit between the peaks is an adapted value for the threshold. When the

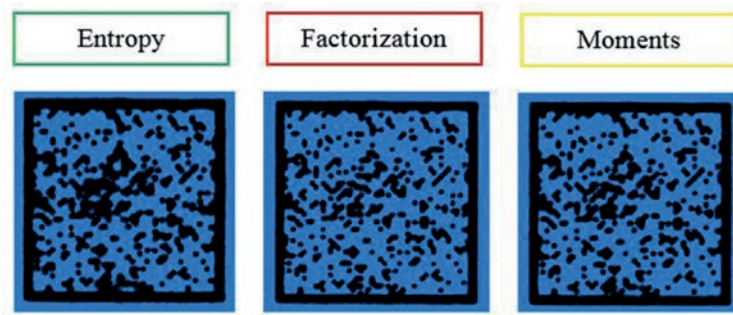


Figure 5: Example of automatic thresholding methods applied on the same 2D code

histogram do not have such appearance, it is more difficult to choose an accurate threshold.

The interactive manual method allows visualizing the result of the thresholding and therefore, the chosen threshold value is adjustable.

Finally, the threshold can be performed automatically using algorithms. Three algorithms available on Visilog[®] were evaluated: entropy, factorization and moments. The function generates a spreadsheet containing the calculated threshold, depending on the chosen algorithm. An example of pictures obtained using these three methods is depicted in Figure 5.

The visual methods – manual and interactive manual – are not adapted because they do not allow an automation of tasks. The fidelity method (that adjusts the threshold with the known 2D code) implies that the digital file is known. Therefore, it cannot be applied to counterfeiting realized on a printed code.

The factorization method was selected because it was the one that gave, on several tested samples, the best satisfying visual results. Furthermore, it is an automated method allowing carrying out a constant protocol.

2.5.4 Histogram of area distribution

On the binary picture obtained after thresholding, the Visilog[®] software allows to count the groups of pixels

of the same intensity (taking the value 0 or 1 depending on if they represent the inked part or the non-inked part of the code).

2.5.5 Comparison of pictures

In order to compare the printed 2D code to the digital file, a first step is required. Indeed, they must be of the same size. The theoretical picture – 100×100 matrix – is a 100×100 pixels image, whereas the pictures captured from the microscope have a variable size ranging from 1000×1000 pixels to 2500×2500 pixels.

The image from the microscope cannot be resampled, to avoid the loss of information; so it is the theoretical square (extracted from the test chart file) that must be resampled.

There are several methods to achieve this: Photoshop[®] and Visilog[®] include functions to resample an image, based on complex algorithms. But they deteriorate the shape of the original pixels, so another method has been developed: decoding and reconstructing the image thanks to a complex macro.

Each pixel of the original 100×100 pixels matrix is scanned; the value is stored in an Excel[®] sheet; a new image of the same size as the sample is created; then the information is reported onto this new image without any deterioration, i.e. the aspect ratio is kept (Figure 6).

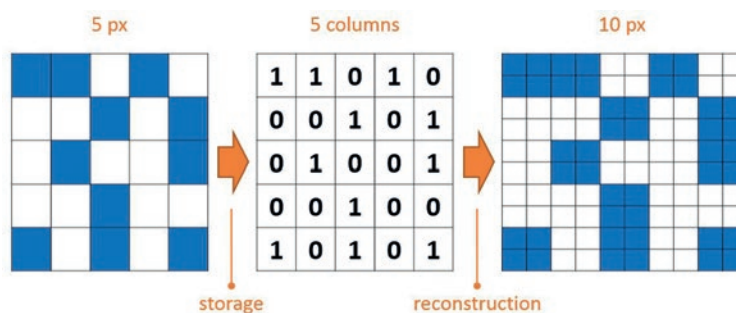


Figure 6: Resampling a theoretical image without any deterioration (px – pixel)

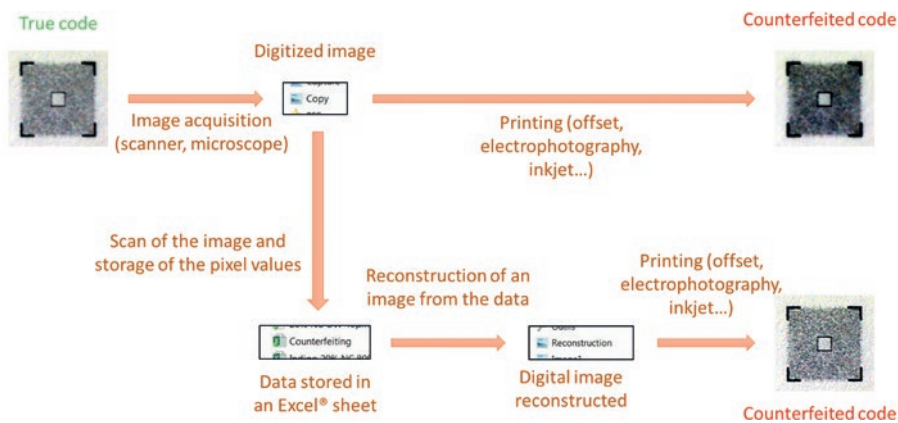


Figure 7: Different steps realized to compare an original print to a second print of a same 2D code – two strategies of counterfeiting studied

2.6 Simulation of counterfeiting – two strategies

2.6.1 General overview

In this part, the possibility to counterfeit a 2D code is studied. Two strategies were considered (Figure 7):

- the direct counterfeiting: second print after digitalization of a printed code,
- the indirect counterfeiting: second print with integration of an intermediate step of reconstructed image.

2.6.2 Image reconstruction

Image reconstruction in the context of counterfeiting has some similarities with the resampling of the theoretical image formerly presented (Chap. 2.5.5. and Figure 6). The major difference is that in counterfeiting, the input image is a 1 000 × 1 000 pixels to 2 500 × 2 500 pixels, and the output image is of the same size. Therefore, it is necessary to resample the input image, but because of the deterioration due to printing and acquisition, the data in the image cannot be easily read.

To decode the information, a method has been developed. It deals with the superimposition of a layer of 100 squares × 100 squares, each square corresponding to 1/(100 × 100) = 0.01 % of the total surface of the image. From there, two parameters are configurable: the square width and the coverage percentage; this parameter corresponds to the coverage percentage of the

square from which one can consider that on the corresponding theoretical image, there was a dot (Figure 8). This method scans the entire image, stores the data in an Excel® sheet and then reconstructs an intermediate theoretical image the same way as the former resampling method.

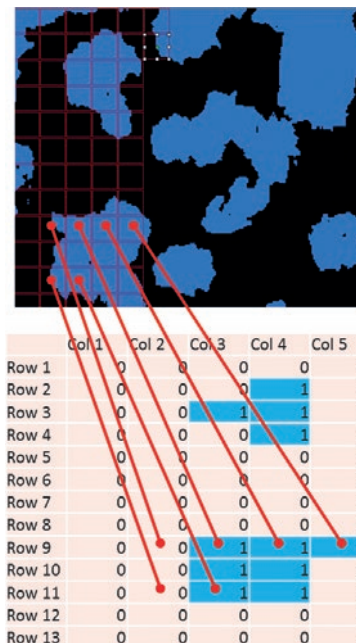


Figure 8: Example of decoding a 1 600 × 1 600 pixels image: square width = 90 %, coverage percentage = 95 %

3. Results

As previously mentioned, the thresholding method by factorization was selected. The Visilog® software thus allows analyzing the surface of each element.

On a 1 600 × 1 600 pixels image of 100 modules × 100 modules, if no deterioration due to printing of acqui-

sition would occur, an isolated dot would have a (1 600 × 1 600)/(100 × 100) = 256 pixels surface. This surface A is the reference used for the classification (it depends on the size of the studied sample). On the histograms below (Figures 9–16), X elements in the class N means that there are X elements which surface is in

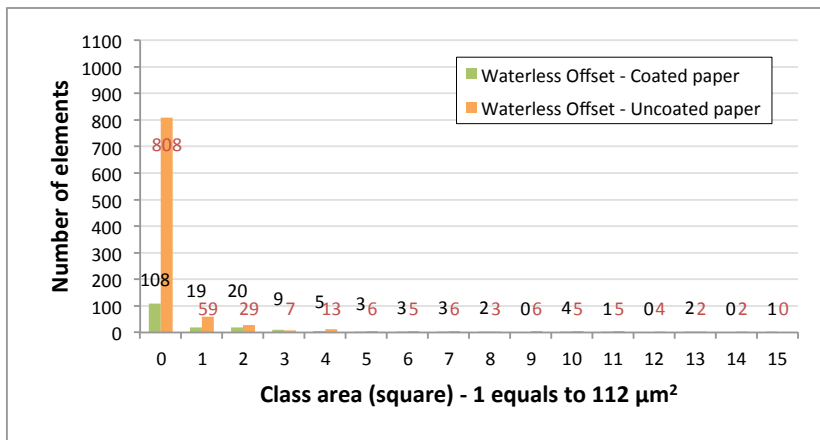


Figure 9: Size distribution histogram of a 2D code – 20 % of coverage, 10.6 μm dot – waterless offset on coated and uncoated paper

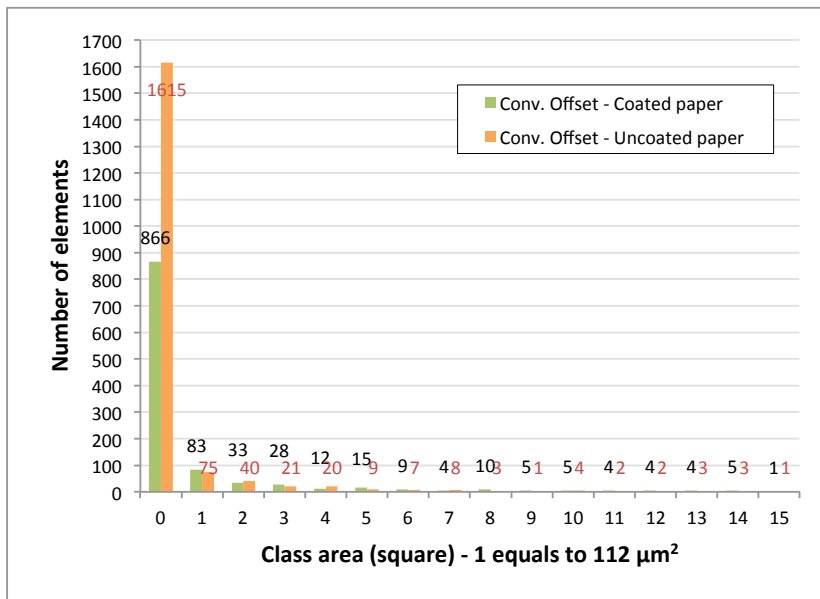


Figure 11: Size distribution histogram of a 2D code – 20 % of coverage, 42.4 μm dot – waterless offset on coated and uncoated paper

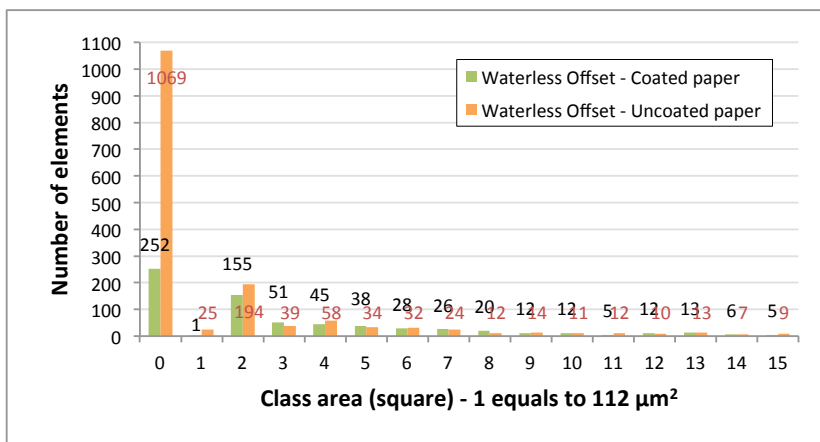


Figure 10: Size distribution histogram of a 2D code – 20 % of coverage, 10.6 μm dot – conventional offset on coated and uncoated paper

the range $[(N - 0.5) \times A; (N + 0.5) \times A]$. The class of surface 0 corresponds to elements which surface is in the range $[0; 0.5 \times A]$.

3.1 Case of the first print

3.1.1 Size distribution histogram of the printed code

Figures 9 and 10 represent the size distribution histogram of a code with a 20 % of coverage, 10.6 μm dots and printed by waterless or conventional offset on coated or uncoated paper, respectively.

From these histograms (Figure 9 and 10), it is important to notice the number of elements in the class 0 that represent the smallest printed elements but that can also be “parasite” dots.

The main key points to underline are:

- the number of elements in the class 0 is far higher for the uncoated paper compared to the coated one whatever the printing process,

- the number of elements in the class 0 is lower for waterless offset (Figure 9) than for conventional offset (Figure 10), whatever the substrate.

A similar analysis was performed for waterless offset with a 42.4 μm dot (Figure 11). The same tendency is observed with the raise of the class 0 and the higher number of elements on the uncoated paper

3.1.2 Size distribution – comparison with the digital file

On Figures 12 and 13 and on Figures 14 and 15, the comparison between printed code and digital file is pointed out for waterless and conventional offset, respectively.

For the digital file, there is no element in the class 0 because the smallest element of the code is a multiple of the basis surface (A); therefore, no element can have a surface size in the range 0 to $0.5 \times A$. With waterless, as well as with conventional offset, and for a 10.6 μm dot, a lot of small elements are generated on the printed code.

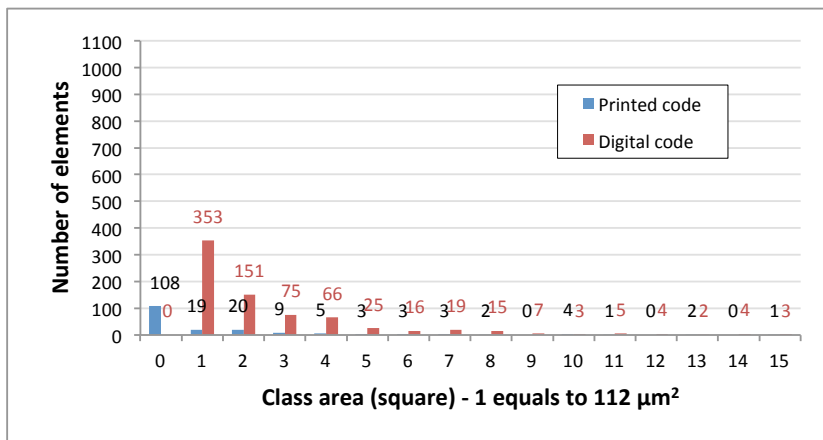


Figure 12: Size distribution of a 2D code – 20 % of coverage, 10.6 μm dot, waterless offset on coated paper – comparison with the digital file

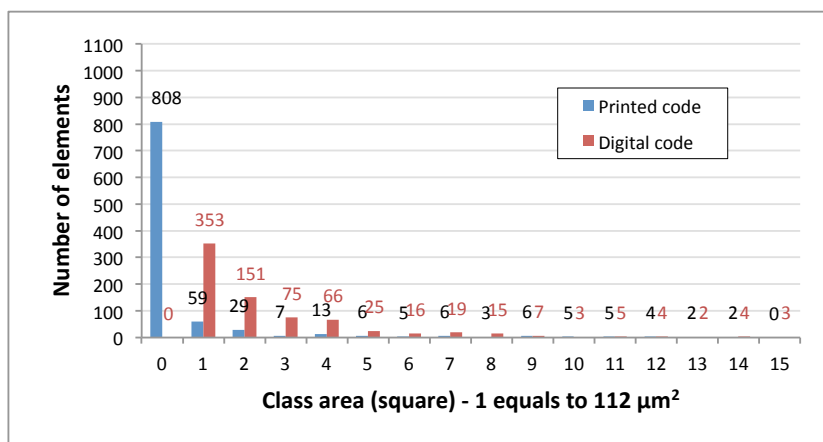


Figure 13: Size distribution of a 2D code – 20 % of coverage, 10.6 μm dot, waterless offset on uncoated paper – comparison with the digital file

3.2 Case of the second print

In order to apply the reconstruction method to the code, samples were printed with a Ricoh electrophotography press for a 20 % of coverage code, on uncoated paper, with dot size of 21.2 μm, 31.8 μm and 42.4 μm. The maximum resolution of the press being 1200 dpi, it was

not possible to print 10.6 μm dots. The different cases are depicted on Figure 16. In the class 0, there are more than 3 333 elements for the true code and for the one counterfeit with the direct method (Visilog® cannot analyse more than 3333 elements). For the counterfeit code with the image reconstruction method, only 1 875 elements are counted.

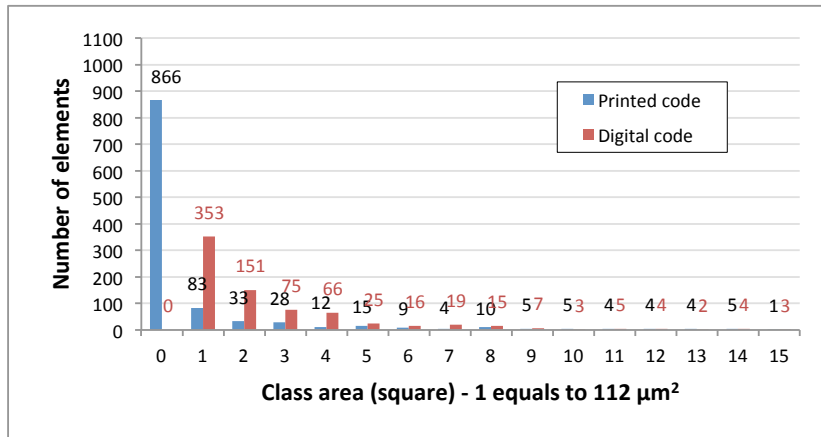


Figure 14: Size distribution of a 2D code – 20 % of coverage, 10.6 μm dot, conventional offset on coated paper – comparison with the digital file

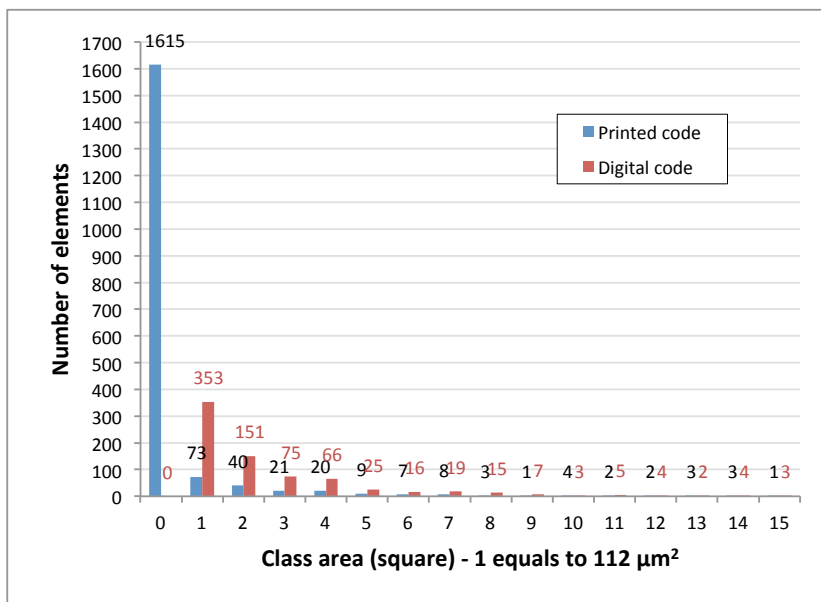


Figure 15: Size distribution of a 2D code – 20 % of coverage, 10.6 μm dot, conventional offset on uncoated paper – comparison with the digital file

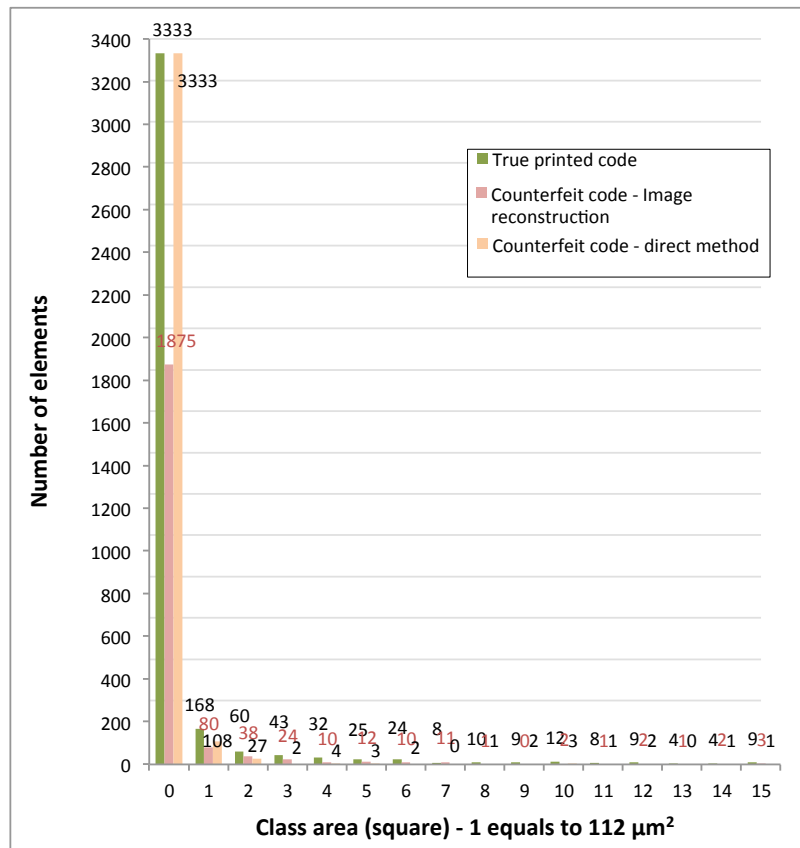


Figure 16: Size distribution histogram of a 2D code – 20 % of coverage, 42.4 μm dot, electrophotography printed on uncoated paper – comparison of the different counterfeiting strategies

4. Discussion

4.1 Case of the first print

The class area 0 corresponds to the smallest elements composing the image. It includes some elements resulting from the acquisition and pre-analysis treatment; taking into consideration that almost all the tasks have been automated, these factors are common to all the samples. Therefore, the class 0 characterizes mainly the smallest printed elements such as satellite ink drops and interferences (Table 3).

There is a sensitive difference between coated and uncoated papers: if the other parameters are identical, the number of elements in the class area 0 is 2 to 7.5 times higher for uncoated paper than for coated paper. The surface finish of the uncoated paper is less adapted to a clean printing than the coated one. These results can be explained by the lower surface state quality of the uncoated paper that exhibits a higher roughness: 6.3 compared to 0.8 μm for coated paper. Indeed, this roughness value is of the same order of magnitude than the size of the smallest dot (10.6 μm). If the printed

codes were perfectly identical to the digital file, no elements would be detected in the class 0.

In addition to this raise of the class 0, it must be underlined that there are 4 to 19 times less elements in the classes 1 to 5 in the printed code than in the digital file. This criterion is also a way to discriminate the printed codes and to characterize the printing process regarding the substrate.

Besides, the same analysis made on the code printed at a 42.4 μm dot size showed that the size distribution was close to the digital file for both prints, on coated and uncoated papers. It is due to the fact that the printing resolution is four times lower than the hardware resolution. It is therefore easier to print dots or groups of dots that suffer little from dot gain and deterioration.

4.2 Case of the second print

Figure 16 shows that the size distribution of the true code is very different from the two attempts of coun-

Table 3: Number of elements in the class area 0

Process	Paper	Resolution			
		2400 dpi (10.6 μm)	1200 dpi (21.2 μm)	800 dpi (31.8 μm)	600 dpi (42.4 μm)
Waterless offset	Coated	108	183	214	252
	Uncoated	808	1261	536	1069
Conventional offset	Coated	866	-	-	-
	Uncoated	1615	-	-	-

terfeiting. The high number of small elements (class 0), higher than 3333 for both true and counterfeit code with the direct method, is due to the printing process. Indeed, in dry electrophotography, there are a lot of satellite particles all around the initial dot (Nguyen et al.,

2013). Whatever the counterfeiting method, more elements are recorded in the classes 1 to 15 for the true code than for the counterfeit ones. The small elements have been gathered in bigger elements in the counterfeiting process.

5. Conclusions

The analysis method of the codes developed in this study allows pointing out the two main phenomena generated by the printing and then the counterfeiting:

- the appearance of very small elements – class 0 (not existing in the digital file),
- the agglomeration of the small elements to form elements of bigger size (not represented on the graphics for readability considerations).

From this study, carried out for waterless and conventional offset on coated and uncoated papers, the main conclusions can be drawn:

- for a 10.6 μm dot, printed on a coated paper, there are less elements in the class 0 for waterless offset (108) than for conventional offset (866),
- a ratio 1/2 is observed in the class 0, for a code printed on uncoated paper, for waterless offset (808) compared to conventional offset (1615).

Regarding the attempts of counterfeiting, a method was developed to re-build the code and the results showed that the size distribution analysis developed in this

project is relevant to distinguish the true from the false codes for electrophotography process.

Therefore, the suitability of the method to characterize 2D codes – original and counterfeit – regarding the printing process and the kind of substrate used was demonstrated. The next step to these promising results will be to characterize groups of dots arranged according to particular configurations and also to apply the counterfeiting method to offset-printed 2D codes. The final objective consists in plotting dot profiles for different printing processes and different printed substrate and also to establish recommendations for digital model development.

In this study, we focused attention on the development of image analysis tools to be able to process pictures with automatic procedures. The next step of our study is to develop models based on physical law, on wettability of substrates and spreading of liquids in order to characterize the deposition behavior of a particular ink regarding the substrate.

Acknowledgments

This research was supported by grants from the Agence Nationale pour la Recherche (A.N.R., France – ANR-10-CORD-019).

“LGP2 is part of the LabEx Tec 21 (Investissements d’Avenir - grant agreement N° ANR-11-LABX-0030) and of the Énergies du Futur and PolyNat Carnot Institutes (Investissements d’Avenir - grant agreements N° ANR-11-CARN-007-01 and ANR-11-CARN-030-01).”

“This research was made possible thanks to the facilities of the TekLiCell platform funded by the Région Rhône-Alpes (ERDF: European regional development fund).”

References

- VISILOG. [online] Available at <<http://www.tnpc.fr/en/visilog.html>> [Accessed 13 September 2015].
- Chagas, L., Reverdy-Bruas, N., Pflimlin, M. and Passas, R., 2013. Characterization of a printed 2D code by image analysis. In: Enlund, N. and Lovreček, M., eds., *Advances in Printing and Media Technology*, Chemnitz: IARIGAI, Darmstadt, Germany, 40, pp. 161–168.
- Chu, C.-H., Yang, D.-N., Pan, Y.-L. and Chen, M.-S., 2011. Stabilization and extraction of 2D bar codes for camera phones, *ACM Multimedia Systems Journal*, 17(2), pp. 113–133.
- DENSO WAVE, *Answers to your questions about the QR code*. [online] Available at <<http://www.qrcode.com/en/>> [Accessed 28 March 2013].
- Halvorson, M., 2008. *Visual Basic® 2008 Etape par etape*. Microsoft® Press, 548 p.
- Jotcham, R., 2005. Overview of anti-counterfeiting technologies. In: *The International Anti-counterfeiting Directory*, ICC Counterfeiting Intelligence Bureau, Barking, Essex, United Kingdom, pp. 29–32.
- Lemaire, F., 2011. Data matrix adopted by French pharmaceutical industry, *European Industrial Pharmacy*, 8, pp. 14–15. [online] Available at <<http://www.industrialpharmacy.eipg.eu/records/EIP8/EIP8%20Feb11%20P14.pdf>> [Accessed 28 March 2013].
- Nguyen, Q.T., Delignon, Y., Chagas, L. and Septier, F., 2014. Printer identification from micro-metric scale printing. In: *IEEE International Conference on Acoustic, Speech and Signal Processes*, Florence, Italy, pp. 6277–6280.
- Stevenson, R., 2005. Laser marking matrix codes on PCBs. *Printed Circuit Design & Fab*, UP Media Group, 22(12) pp. 32–36. [online] Available at <<http://pcdandf.com/cms/images/stories/mag/0512/0512stevenson.pdf>> [Accessed 28 March 2013].
- Swetake, Y., 2007. *How to create QR code*. [online] Available at <http://www.swetake.com/qr/qr1_en.html> [Accessed 28 March 2013].
- Ulichney R., Gaubatz M. and Simske S., 2010. Encoding information in clustered-dot halftones. In: *The 26th International Conference on Digital Printing Technologies*, HP Laboratories, 5 p.
- UNITAG, *Générateur de QR codes*. [online] Available at <<http://www.unitag.fr/qrcode>> [Accessed 07 February 2013].
- Wang, H. and Zou, Y., 2006. 2D bar codes reading: solutions for camera phones., *International Journal of Signal Processing*, 3(3), pp. 164–170.

JPMTR 068 | 1431
DOI 10.14622/JPMTR-1431
UDC 001.92 : 659.3

Research paper
Received: 2014-07-30
Accepted: 2015-08-18

Investigating the effects of publishing approaches using print, electronic and augmented reality media on user experience

Elena Fedorovskaya, Lufei Yu

Rochester Institute of Technology, Rochester, NY 14623, USA E-mail: eafppr@rit.edu
lxy4140@rit.edu

Abstract

To evaluate the potential role of modern augmented reality (AR) technology in publishing and its usefulness for interactive print, we conducted a study where we investigated the influence of different methods of presenting content on the users' story reading experience. The stories were produced in print and electronic media, with and without augmented reality component, using a multi-media setup consisting of a computer with the monitor display, a smartphone, and a printed material. A 2×2 within-subjects experimental design was implemented (2 levels of medium: print and electronic; and 2 levels of augmentation with video clips: yes or no), wherein 32 participants aged 18–29 years old were asked to read short stories produced with different publishing methods and evaluate their preferences for the presentation of the content, as well as interestingness, comprehension and overall experience with the stories on a 7 point scale using a questionnaire. AR and the medium–AR interaction were found to be significant in determining the preference for the publishing method. The paper–AR combination had the highest score among all the methods and was rated statistically different from the paper only version, which, in turn, had the lowest score. For the overall experience ratings a significant medium–AR interaction was observed, with the trend, similar to the publishing preference ratings. Overall experience was linked to the users' preference ratings for the publishing methods, interestingness and enjoyment of the stories, and the ease of understanding the story line. The results indicate that AR enhances user experience, particularly with print media, making it on par or even higher valued than commonly used electronic media. In contrast, the traditional print version without augmentation was least preferred.

Keywords: publishing, augmented reality, print, digital media, storytelling

1. Introduction

With the rapid development of digital technology, the emergence of cross-media publishing provides more opportunities for publishers to enrich content and broaden the audience. Recently, the concept of augmented reality (AR) emerged as an innovative approach to enhance print-based graphic communication and publishing (Perey, 2011). According to Vehmas et al. (2011), a significant rise of innovative interactive print products by 2020 is projected, with AR as one of the enabling technological platforms.

Furht (2011, p. 3) in the “Handbook of Augmented Reality” defines AR as “a real-time direct or indirect view of a physical real-world environment that has been enhanced/augmented by adding virtual computer-generated information to it”. Augmented reality can be considered a combination of virtual and real environments, and also a new medium, which aims at providing relevant and useful digital (e.g. web-based) information to the user that can be linked and blended with any tangible medium including print.

AR attracts significant attention due to its interactive nature, multimodality (sound, video and 3D graphics), and ability to bring web information to a point of a user's physical interaction with the environment mediated by personal computing devices. Put differently, AR turns smartphones or tablets into a viewing pane that opens up an interactive 3D world around a physical object to people. These characteristics of AR have been recognized as particularly appealing in marketing, with the goal to cause consumers remember an experience or action related to a product, rather than a static image or text common to traditional print based advertising methods (Connolly et al., 2010).

While many professionals are excited by the prospects of AR applications in publishing, marketing, and advertising, some scholars and analysts think that it is the novelty factor that drives interest toward AR. As Craig (2013, p. 151) suggests, “augmented reality is new enough that people are interested in it just because it is augmented reality. This will wear off very quickly”.

Additionally, Grushka (2013) points out some existing challenges with AR including cumbersome user experience, fragmented ownership of AR platforms, and a lack of value-added content.

Despite a recent heightened interest toward the AR technology and the existence of several popular products and open source tools, such as Aurasma, Layar, and Wikitude, commercial AR applications are still in their infancy.

It is not yet well understood how to make the most of this new medium for graphic communications, and even more so, how it can be used in the future. While AR technology is considered an enabler for the recently emerged concept of interactive print, research on the applicability and effectiveness of AR in publishing has been limited.

2. Related work

The first AR systems appeared in 90-s, with early papers describing head mounted display prototypes for air force and military applications (see, for example, Rosenberg, 1993). Currently, studies involving AR technology focus primarily on its use for advertising, tourism and education and deal with either technology improvements or the evaluation of the technology benefits. Several recent research papers are described below. We categorized them as those related to advertising and those related to education.

2.1 AR in advertising

Connolly et al. (2010) examined effectiveness of AR use in advertising by evaluating observers' information retention from AR advertisements in comparison to standard paper-base media. Computer generated 3D representations of vehicle models were used as AR; 2D images with the same product information were used to simulate traditional print advertising. The stimuli were displayed on a computer screen. As a result, both traditional two-dimensional image and three-dimensional AR advertisements were shown as equally effective in presenting visual components of a product, or in generating product interest. The data also indicated that traditional 2D images were more effective in delivering factual text-based information. However, this latter result could have been caused by limitations of 3D visualization software to clearly show textual information.

Chehimi, Coulton and Edwards (2007) described a concept of a unique system that allowed complex and highly interactive visual 3D advertisements to be viewed on mobile phones equipped with a camera. One of the key features of the proposed system is its capability to provide a location-based service. According to Chehimi, Coulton and Edwards (2007, p. 7), "interactive and

To assess the role and usefulness of AR in publishing, we ask the following questions: How do users evaluate their experience with different publishing methods, including AR? Is publishing with AR truly more attractive to people than the traditional publishing approach? How does it affect understanding and retention of communicated information? What is the role of print in novel publishing platforms?

In order to answer these questions, we compared several methods for publishing short stories from a user experience point of view. We implemented printed and electronic versions of the stories with and without the AR component. In the experiment, video clips on a mobile phone triggered by the story content served as AR, thus utilizing a basic definition of AR as "virtual computer-generated information".

entertaining location-based services systems will have the greatest impact of all mobile marketing on customers' experiences and businesses' logistic marketing mixes."

Shiva, Raajan and Jayabhavani (2013) implemented and tested an AR system prototype for virtual tourism and advertisement using computer vision algorithms. Their system augments physical objects in the real world environment with 3D video to increase persons' conceptual understanding of the surrounding objects.

While researchers recognize potential benefits of the AR systems for marketing and advertising, none of the papers described above have provided significant measurable empirical evidence for AR advantages nor used the technology to augment printed material for publishing. Connolly et al. (2010) attempted to simulate traditional print advertising in their study but they did not use actual printed material, and instead, showed the images on the computer screen.

2.2 AR in education

Several studies demonstrated the effects of AR on learning, engagement and enjoyment in the context of education. According to Di Serio, Ibáñez and Kloos (2013), motivational factors of attention and satisfaction in an AR-based learning environment were rated higher than those obtained in a traditional, slidesbased presentation of teaching material in a visual art course. Participants in the experiments reported higher levels of engagement and enjoyment when using AR, and appreciated its multimedia nature. In other studies, AR was shown to influence learning outcomes. Using Augmented Books (purposefully created educational AR books that overlay 3D virtual content over real book pages with the help

of an AR system) for teaching electro-magnetism at the highschool level tended to improve test performance and retention of the material compared to traditional textbooks (Dünser et al., 2012). Similar positive results were obtained in Gutiérrez et al. (2010), where an AR book has been designed to provide 3D virtual models to help engineering students perform visualization tasks. The study concluded that the training had a measurable and positive impact on students' spatial ability.

Although the above-mentioned studies show the positive effects of AR on learning and students' experience, their primary goal was to demonstrate the role of AR in education, underscoring its interactivity and 3D visualization. There was no attempt to address the role of print or any type of tangibility factor in such systems. Di Serio et al. (2013) did not use printed material at all, and for Gutiérrez et al. (2010) and Dünser et al. (2012) the experimental variable under investigation was the presence or absence of AR, which, in principle, does not require print.

Yet, many scholars and industry leaders acknowledged specific advantages of the print medium: physicality/tangibility, portability, unique sensory qualities, its asso-

ciation with more effective reading comprehension, and information retention; emphasizing therefore, its significance in the media communication realm (Mangen, Walgermo and Brønnick, 2013). These observations suggested that not only augmentation and interaction with the virtual data, but presence of a tangible carrier of the original information to which AR is linked, and with which the user could interact, might be important factors to influence effectiveness and user experience with the AR systems, including AR-enhanced publications.

Consequently, we hypothesized that users would prefer printed stories with AR than any other production methods, whether or not they included the same virtual material.

The objective of our study was, therefore, to evaluate the influence of two factors, AR and publishing medium, on participants' reading effectiveness, preference and experience by comparing different methods of content production: using print or electronic display with or without augmented reality. To our knowledge this is the first attempt to perform such an assessment.

3. Study methodology

3.1 Experimental set up

In the present study we used a multi-media setup, consisting of an iMac computer with the 27-inch monitor display, a Google Nexus 5 smartphone, and printed material produced on the 8.5" × 11" Mohawk 215 g/m² (80 lb) Color Cover paper with a Canon imagePress C1 printer according to SWOP standards. A free version of the Aurasma Android application was installed on the smartphone and was used to create AR content. The monitor was calibrated with a white point of 5000 K, gamma 2.2 and the 80 cd/m² maximum luminance level.

The experiment took place in the lab that approximated a typical office environment with the artificial "Cool white" fluorescent illumination (5000 K) and the illuminance level around 320 lux.

3.2 Study design

In order to investigate the influence of AR and the publishing medium on the user preferences and experience when reading short (two-page) cartoon stories, we used a 2 × 2 within-subjects experimental design with two independent variables and two levels for each variable: (1) medium: print versus electronic medium, and (2) augmentation with the smartphone using video clips: the presence versus absence of AR.

The following conditions were compared: 1) a print version that contained text and illustrations; 2) a print version with text, illustrations and an AR component in the form of video clips; 3) a webpage with text and illustrations; 4) a webpage with text, illustrations and an AR component. To represent a typical modern interactive electronic publication we also included 5) a webpage with text and video clips, which could be played by clicking. Thus, we have used two versions for the electronic medium without the AR condition.

Each participant viewed five different stories produced using five different methods, 1) through 5), to eliminate familiarity with the story content. The story and publication method pairings were pseudo-randomized across participants making sure each combination had the same number of occurrences across the participants. The webpages were displayed on the monitor screen, while AR video clips were accessible by positioning a smartphone over images that served as triggers for an AR application installed on the smartphone.

The participants filled paper-based questionnaires after reviewing each story and also at the end of the experiment, after experiencing all five stories. Study questionnaires consisted of seven-point Likert-type scales to rate several attributes of the story reading experience, including understanding, ease of reading, interestingness, liking of story content and the method of publishing, and

overall experience. Additional questions to recall specific information about the stories and indicate preferred features from the list were also included. In comparison with the questionnaires after each story, the final questionnaire contained both rating and ranking items. The scales were represented graphically as lines with the seven equal intervals numbered from 1 to 7, where 1 corresponded to the lowest value for the rated attribute, 4 – the neutral value, and 7 – to the highest value for the attribute to help participants visualize the scale.

The goal was to obtain an interval-level measurement, whereas a category based Likert-type scale typically provides an ordinal-level measurement. The questionnaire example is provided in Appendix. Additionally, post-study follow-up phone interviews were conducted to collect recall data.

3.3 Stimulus material

Five different cartoon stories of similar genre and comparable interest level adapted from Oliver Jeffers' picture books for children ("Lost and Found", "How to Catch a Star", "The Way Back Home", "The Incredible Book Eating Boy", and "The Heart and the Bottle") were chosen for the experiment. For every story five versions were prepared using different publishing methods described above. Each story had two pages that included text and two illustrations per page. The pages were designed using Adobe InDesign. The page layout was similar for all the stories and is illustrated in Figure 1. For the text we used American Typewriter 15 pt (body) and 35 pt (title). The story pages were saved as PDF files.

For the print-based publishing, the files were printed as such. For the print-AR publishing method, slight modifications of the PDF files were prepared and printed. Those copies had play button tags near the illustrations to inform the participants about the AR availability as illustrated in Figure 1.

The webpages for all five stories were created separately using HTML, CSS, and JavaScript languages in Adobe Dreamweaver. Compared with the printed versions, the webpages used the same PDF files, which were designed in Adobe InDesign. For the webpage with the video clips conditions – the appropriate video clips were embedded in the HTML files.

Video clips for the stories, four clips for each story, were created from animations found on YouTube and Vimeo. The video clips started with the same frames as the corresponding illustrations and lasted about 20 s in duration.

To enable AR, the video clips were uploaded onto the smartphone, together with the trigger images (the same images that were used for the illustrations), and processed by Aurasma software installed on a Google Nexus 5 smartphone to create AR projects for each story.

The appearance of stories on print and on the screen was equalized in terms of the page size, font size and color reproduction.

3.4 Participants

Student participants were recruited via email and flyers posted throughout the RIT campus. A simple survey to collect information about the name, gender, college, and available time was emailed to people who volunteered to take part in the experiment. Based on the survey, prospective participants were screened prior to the experiment to select equal number of female and male students from different colleges. This was done in order to avoid potential gender and education biases. As a result, sixteen male and sixteen female RIT students in the 18–29 years old age group participated in the experiment with the average age of 23 years old. They had normal or corrected to normal vision and no reading difficulties. As an added incentive, every participant was rewarded with a \$20 gift card to Java's, a local Rochester coffee shop.

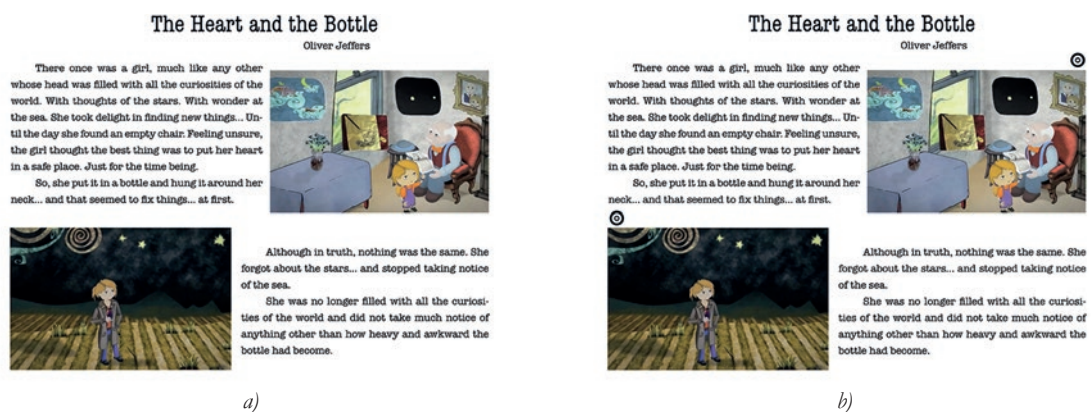


Figure 1: An example of a story layout: a) print version, b) print with AR version

3.5 Procedure

All participants were informed, prior to their participation, about the commitment involved in the experiment. Upon arrival, the participants read the introduction sheet, signed the consent form and filled in the pre-test questionnaire with some basic information including their reading habits and familiarity with AR. Next, they were asked to read and interact with the content (when appropriate) of five two-page cartoon stories published using five different methods described above. For every subject the order of the stories was randomized before the experiment. Table 1 shows the stimulus presentation sequence for two experimental participants, as an example. Both participants saw all five stories and were exposed to all five methods, however the story-publishing method combinations and the presentation order were different.

We allowed a maximum reading time of 10 minutes per story, and recorded the actual time participants spent with the material. After reading each story, every participant filled the story questionnaire (see Appendix) and rated his or her understanding of the content; readability; interestingness; overall story liking; publishing method liking; and provided their assessment of interactivity, and other features. At the end of the experiment, the participants were asked to compare (rank) all five stories on the same attributes and overall experience, as well as rate these attributes for the second time using the post-test questionnaire. The average duration of the experiment was approximately 30 minutes per participant. There were a few subjects who completed the experiment in more than 30 minutes, but no one exceeded one hour time period. Participants' responses were submitted via paper-based questionnaires and organized in 32 separate folders to preserve all data.

One month after the completion of the experiment, we approached the participants with the request for a short phone interview regarding the study. Ten subjects, who agreed to participate, were asked to recall information about the stories.

3.6 Data analysis

Data from the study were obtained from printed questionnaires and transferred to an Excel spreadsheet. The data analysis was done with the Excel and the JMP 11 statistical software.

We analyzed scaling data in several ways. Firstly, we considered rating responses as ordered categories and used generalized linear model implemented in JMP to test the significance of the independent variables and their interaction.

Secondly, we applied Thurstone's law of categorical judgment (condition D) described in Torgerson (1958) to rescale our data from ordinal scale to interval scale. To this end, we calculated frequencies and cumulative frequencies of rating categories for every question across all participants, then cumulative proportions and corresponding the z scores. Subsequently, we computed scale values and category boundaries for every attribute.

Based on this analysis we were able to conclude that the "raw" data approximates interval scale very well. Figure 2 shows the linear relationship between scaled category boundaries and seven categories for overall experience attribute. Rescaled data for other attributes followed similar relationship. Our findings are in agreement with existing publications (e.g. T aylor, 1983) pointing out that Likert-type items perform closely to scales that are perceived as equal intervals, and can satisfy the equal distance assumption required for parametric statistical analysis.

Finally, following confirmation that the original rating categories are largely perceived as equal intervals, we applied ANOVA and multiple linear regression analysis to our data and compared the results of both approaches. There was a good agreement between two types of analyses. Since no discrepancy was found regarding the effects, we report the results obtained with parametric statistical analysis techniques.

Table 1: Comparison of stimulus presentation sequence for two experimental participants

Order	Participant #2		Participant #7	
	Story	Publishing Method	Story	Publishing Method
1	Lost and Found	Web/AR	The Way Back Home	Paper
2	The Incredible Boy Eating Books	Paper/AR	The Incredible Boy Eating Books	Web
3	Heart and Bottle	Paper	Lost and Found	Paper/AR
4	The Way Back Home	Web/Video	Heart and Bottle	Web/AR
5	How to Catch a Star	Web	How to Catch a Star	Web/Video

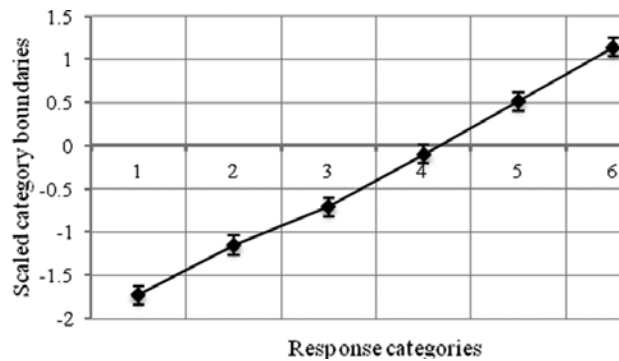


Figure 2: The relationship between response categories and scaled category boundaries using Overall Experience attribute data as an example

4. Results

We examined the main effects of the independent study variables, *Medium* and *AR*, and their interaction on all rated attributes using the two way ANOVA. There were no significant effects on understanding, readability, interestingness ratings, and on information retention score, calculated as a number of elements the subjects were able to correctly remember at the end of the experiment. The attributes, for which the significant effects were obtained, are described below.

4.1 Analysis of preferences for publishing methods

There was a statistically significant main effect of *AR* ($F = 13.15, p < 0.000$) and also a significant interaction effect of *Medium* versus *AR* ($F = 4.41, p = 0.037$) for the publishing platform liking question from the story questionnaire. The same significant effects were found for the post-test questionnaire, when the users had completed viewing all five stories: *AR* ($F = 9.98, p = 0.046$); *Medium* versus *AR* ($F = 5.06, p = 0.026$). The stories presented with *AR* were rated significantly higher than without *AR*. The interaction effect is demonstrated in Figure 3.

The fact that the analysis results were similar for the two instances of using the questionnaire, after each story, and after viewing all five stories, adds validity to

the data. The significant interaction effect shows that the paper-based method gains the most from adding *AR* to the story content and is rated the highest. To directly compare all five versions of publishing, we ran the one way ANOVA, using the *Publishing Method* as an independent variable with five levels: *Paper*; *Paper/AR*; *Web*; *Web/AR*; *Web/Video*. The effect was significant ($F = 5.42, p < 0.000$). The *Paper/AR* condition had the highest score among all methods, significantly different from the *Web* ($p < 0.001$) and *Paper* ($p < 0.000$) conditions, with the latter having the lowest score (Figure 4). Other differences were insignificant, although preference for the *Paper/AR* condition in comparison with the *Web/Video* condition was close to the 5 % significance level ($p = 0.061$).

4.2 Analysis of overall experience ratings

None of the main effects, neither *Medium* nor *AR*, were statistically significant for the overall experience ratings. There was, however, a statistically significant interaction effect of *Medium* versus *AR* ($F = 6.93, p < 0.009$), demonstrating the same behavior as was found for the platform liking data. Namely, adding *AR* changed the paper-based version from the least preferred to one the most preferred making it equal with electronic publishing methods in terms of overall experience. The one way

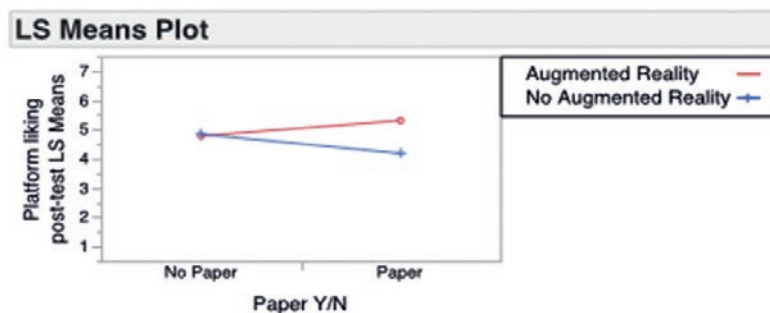


Figure 3: Interaction effect of Medium versus AR on publishing platform liking

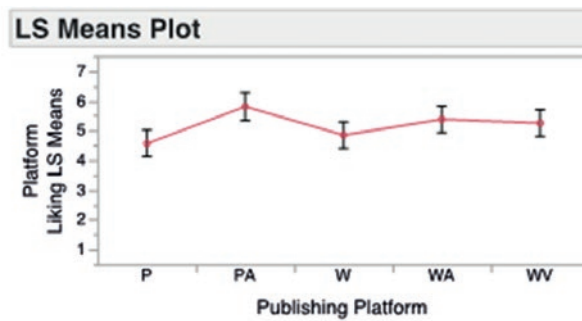


Figure 4: The effect of publishing method on platform liking (P – Paper, PA – Paper/AR, W – Web, WA – Web/AR, WV – Web/Video)

ANOVA showed a significant effect for the *Publishing Method* variable ($F = 2.68, p = 0.034$), with the *Paper* condition being substantially lower rated (Figure 5).

The absence of the main effects led us to test the influence of the story-related attributes, including interestingness, understanding, readability, story liking, as

well as platform liking, using multiple regression analysis. The effects for all these variables were significant ($p = 0.04, R^2 = 0.62$) showing the importance of other attributes on the overall experience, particularly associated with the story content. We did not find any gender differences, or significant differences between the participants.

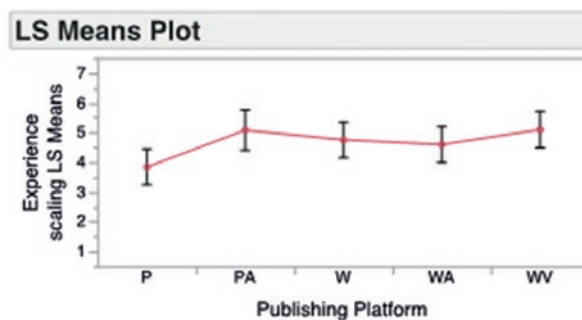


Figure 5: The effect of publishing method on the overall experience rating

5. Discussion

Our data demonstrate the statistically significant influence of AR on the users' preferences for different publishing methods. Specifically, adding AR enhanced users' experience with printed publications and made this method of publishing as one of the most preferred ways to read the content. Moreover, without AR, print publications were evaluated as the least preferred by the group of young college students, which are reading electronic media on a regular basis. This result is novel and points toward advantages that can be gained by incorporating AR to interactive print publications. The consistent substantial interaction effect of combining the publication

medium and AR on the users' preferences and experience speaks about qualitative change of media integration and potential direction that can be explored for various applications in graphic communications and publishing.

We did not identify any significant effects of AR and or medium on the reading performance, possibly because of the story types we have chosen for the experiment. Our stories were short and easy to read and remember without any difficulty. It would be interesting to conduct a study with more challenging content, such as for example scientific publications.

6. Conclusions

Our study demonstrates that augmented reality significantly affects preferences for the publishing format of short stories, providing a particularly strong influence for the stories printed on paper. Overall experience rat-

ings reveal a similar trend, where we found a significant medium–AR interaction effect. The study results are consistent with the findings from research in advertising and education that show positive effects of AR on

the user experience with the material at hand. However, our study has a relatively small sample of participants and is confined to the lab settings. In order to prove the real-life utility of AR in publishing, a larger study, beyond the lab experiment, is necessary. This will help

to address concerns about novelty factor playing a major role in AR preferences, as well as to understand how to properly design interaction experience to justify additional efforts on the consumers' side associated with using AR.

Acknowledgements

The authors would like to express their appreciation to the following individuals and organizations: Junpeng Chang, a graduate student in the school of Media Sciences at Rochester Institute of Technology, for his help support during media creation and data collection; Lauren Purvis, a senior project assistant in the school of Media Sciences at Rochester Institute of Technology, for her administrative assistance with the project; all RIT students who participated in the experiment. We are also grateful to Aurasma, who made a free version of their AR application available, Oliver Jeffers, an illustrator and writer from Australia, for his wonderful and popular storybooks, and to all people and companies, who create and upload their videos on YouTube and Vimeo based on Oliver Jeffers' stories.

References

- Chehimi, F., Coulton, P. and Edwards, R., 2007. Augmented reality 3D interactive advertisements on smartphones. In: Archer, N., Hassanein, K. and Yuan, Y., eds. *IEEE International Conference on the Management of Mobile Business*. Toronto, Ont., p. 21.
- Connolly, P., Champers, C., Eagleson, E., Matthews, D. and Rogers, T., 2010. Augmented reality effectiveness in advertising. In: *65th Midyear Conference on Engineering Design Graphics Division of ASEE*. 3–6 October 2010. Houghton, Michigan, pp. 109–115.
- Craig, A. B., 2013. *Understanding augmented reality: Concepts and applications*. Burlington: Morgan Kaufmann.
- Di Serio, Á., Ibáñez, M.B. and Kloos, C.D., 2013. Impact of an augmented reality system on students' motivation for a visual art course. *Computers & Education*, 68, pp. 586–596.
- Dünser, A., Walker, L., Horner, H. and Bentall, D., 2012. Creating Interactive Physics Education Books with Augmented Reality. In: *Proceedings of the 24th Australian Computer–Human Interaction Conference*, Melbourne, Victoria, Australia, pp. 107–114.
- Furht, B., ed., 2011. *Handbook of Augmented Reality*. New York: Springer-Verlag New York Inc.
- Grushka, K., 2013. The trendiest trends in package design: AR [AUGMENTED REALITY]. *Brand Packaging*, 17(7), p. 29.
- Gutiérrez, M.J., Saorín, J.L., Contero, M., Alcañiz, M., López, P.D.C. and Ortega, M., 2010. Design and validation of an augmented book for spatial abilities development in engineering students. *Computers & Graphics*, 34(1), pp. 77–91.
- Mangen, A., Walgermo, B.R. and Brønnick, K., 2013. Reading linear texts on paper versus computer screen: Effects on reading comprehension. *International Journal of Educational Research*, 58, pp. 61–68.
- Perey, C., 2011. *Print and publishing and the future of Augmented Reality*. [online] Available at: <http://www.perey.com/White_Paper_for_ARCH-P&P_January_12.pdf> [Accessed 28 July 2014].
- Rosenberg, L., 1993. Virtual fixtures as tools to enhance operator performance in telepresence environments. In: Kim, W.S., ed. *SPIE 2057, Telemanipulator Technology and Space Telesrobotics*. Boston, MA, pp. 10–21.
- Shiva, G., Raajan, N.R. and Jayabhavani, G.N., 2013. Augmented Reality based 3D commercial advertisements. In: *IEEE International Conference on Emerging Trends in VL, SI, Embedded System, Nano Electronics and Telecommunication System (ICEVENT)*. Tiruvannamalai, India, pp. 1–4.
- Torgerson, W.S., 1958. *Theory and methods of scaling*. New York: Wiley.
- Traylor, M., 1983. Ordinal and interval scaling. *Journal of the Market Research Society*, 25(4), pp. 297–303.
- Vehmas, K., Kariniemi, M., Linna, H., Jokiahho, K. and Torniainen, E., 2011. *Future of European Printing Industry*. [online] Available at: <[http://www.printpower.eu/download/Report_Future-of-European-Printing-Industry\(1\).pdf](http://www.printpower.eu/download/Report_Future-of-European-Printing-Industry(1).pdf)> [Accessed 28 July 2014].

Appendix

Questionnaire (For each story)

What is the topic of this story?

What is the main character in this story?

How easy was for you to understand the story?

Extremely easy		Neutral			Extremely difficult	
1	2	3	4	5	6	7

How easy was for you to read the story?

Extremely easy		Neutral			Extremely difficult	
1	2	3	4	5	6	7

How interesting do you find the story you just viewed?

Not at all		Neutral			Extremely	
1	2	3	4	5	6	7

How much do you like the story?

Not at all		Neutral			Extremely	
1	2	3	4	5	6	7

How much do you like the way the story was published/presented?

Not at all		Neutral			Extremely	
1	2	3	4	5	6	7

If the story includes an interactive publishing part, how do you like the interactive part?

(If no, please skip this question)

Not at all		Neutral			Extremely	
1	2	3	4	5	6	7

Please circle three most important features in this story

- Layout Design
- Content
- Readability
- Interactivity
- Color
- Video clips
- Illustrations
- Other _____

Please circle three most enjoyable features in this story

- Layout Design
- Content
- Readability
- Interactivity
- Color
- Video clips
- Illustrations
- Other _____

Please write down any comments and observations you may have.

Topicalities

Edited by Markéta Držková

Contents

News & more	229
Bookshelf	231
Events	237

News & more

Graphic technology ISO standards news

While at the beginning of this year the upcoming ISO 32000-2 Document management – Portable document format – Part 2: PDF 2.0 standard was under DIS (draft International Standard) ballot and publishing was expected for 2016, its second DIS ballot was necessary in the end. According to the international standardization body for the printing industry, finalisation is expected for 2016, with publication in late 2016 or in 2017.

Few weeks ago, guidelines for the use of standards for print media production were published as a technical report (ISO/TR 19300:2015). During 2015, a number of ISO standards under the responsibility of ISO technical committee TC 130 Graphic technology have been confirmed (12643-1:2009, 12643-2:2010, 12643-3:2010, 12643-4:2010) or reconfirmed (2834-1:2006, 2846-1:2006, 11084-2:2006, 12642-2:2006, 15930-4:2003, 15930-6:2003). New and revised ISO standards are introduced in following text.

ISO 2834-2:2015

Graphic technology – Laboratory preparation test prints Part 2: Liquid printing inks

This second edition published in May 2015 cancels and replaces the first edition (ISO 2834-2:2007). The standard specifies a test method for preparation of test prints produced with liquid water- or solvent-based printing inks as used in flexography and gravure printing. These test prints are intended primarily for optical tests, such as gloss, colorimetry, transparency and reflection density. They can also be used for testing light fastness and the chemical, physical and mechanical resistance regarding either printing ink and/or substrate. Flexographic inks with higher viscosity, such as those cured by radiation, are also covered. This part of ISO 2834 is not applicable to inks for ink jet printing.

ISO 12647-5:2015

Graphic technology – Process control for the manufacture of half-tone colour separations, proof and production prints Part 5: Screen printing

Fifth part of ISO 12647 standard was published in January 2015 and specifies the requirements for the screen printing of four-colour process-colour material used for display, signage, and graphics using flat bed or cylinder printing equipment. Both the size and resolution of the finished product are unrestricted. Data preparation and delivery, proof production, printing forme preparation, and production printing process stages are covered.

ISO 12646:2015

Graphic technology – Displays for colour proofing – Characteristics

This third edition published in July 2015 cancels and replaces the second edition (ISO 12646:2008), which has been technically revised to improve the compatibility with the requirements of soft proofing defined in ISO 14861. Requirements for two conformance levels for the characteristics of displays to be used for soft proofing of colour images are specified, including requirements for uniformity and variations of electro-optical properties with viewing direction for different driving signals.

PrintTalk 1.5 released by CIP4 New version of specification for print industry web automation



PrintTalk is a specification for the exchange of business information between customer systems, Web-to-print eCommerce systems, and print estimating, scheduling and MIS, extending the process automation to both the customer and to the supply chain of printer. The data gathered in the print buying process, such as requests for estimates, estimates or approvals, could be directly moved forward into production via JDF.

CIP4 organization announced in July 2015 the release of the PrintTalk 1.5 Schema and Reference Implementation, tightly integrated

with the current 1.5 version of JDF (PrintTalk 1.4 was skipped). Accordingly, PrintTalk 2.0 is under development to complement JDF 2.0; it will be very similar to PrintTalk 1.5 with the exception that the transport element will be XJDF rather than JDF. PrintTalk 1.5 adds requested capabilities to subscribe to order-status updates, request stock levels, support for multiple JDF items on the same order, and manage percentage calculations on invoices.

Test paper for printing ink tests



The APCO II/II test paper, used for many years to test the colour coordinates, transparency and film thickness ranges of process inks, is no longer manufactured and only a limited stock remains. Therefore, IGT ensured the production of a successor paper. All colour aims for process inks in ISO 2846-1 standard developed for APCO II/II are still valid for the new substrate. IGT will prepare a draft for the revision of the standard as well.

Toshiba TEC inkjet head with large drop-volume



TOSHIBA

The commercial availability of CF1XL large drop-volume inkjet head was announced by Toshiba TEC Inkjet Business Group. Extending the CF1 family to better suit different application areas, the CF1XL head has a native drop size of 36 pl, and jets drop volumes up to 180 pl, thus complementing the CF1L head (64–90 pl) and the CF1 head (6–42 pl). All CF1 family heads are based on an efficient through-channel fluid recirculation system combined with side-shooter architecture. Due to the capability to jet particle sizes up to 2.2 µm, the need for highly-refined particle processing is reduced and a wider range of materials can be applied (e.g. for 3D-embossing and texturing). Toshiba TEC claims that viscosities up to 43 mPa·s can be achieved to carry greater pigment loads, increasing print opacity, colour saturation and vibrancy.

Plate for UV and aqueous coating from Trelleborg



Vulcan X-Coat is the new fabric-less coating plate with a rubber-based top compound and thickness of 1,15/1,35 mm, designed to be used with both UV and aqueous coatings. This solution provides features such as cleaner plate preparation, easier strip with visible cut lines, reduced ink back-trapping, simpler handling and runs up to 100,000 copies.

Wide Format Laser Photo Printer and XY-Cutter for XXL Formats

Imaging Solutions AG launched the laserprinter proPrint 30SHS with integrated photo paper development and the photoCut XY flatbed cutter with automatic nesting software for the finishing of wide format posters, images or book covers in photo quality.



ISO 14861:2015

Graphic technology – Requirements for colour soft proofing systems

This document published in August 2015 specifies requirements for systems that are used to produce, from digital data, images on electronic displays that are intended to simulate a characterized printing condition defined by a set of characterization data and spot colours defined by a physical reference. Recommendations are provided with regard to equipment selection, setup, operating, and environmental conditions. Appropriate test methods associated with these requirements are specified.

ISO 17972-1:2015 and ISO 17972-4:2015

Graphic technology – Colour data exchange format

Part 1: Relationship to CxF3 (CxF/X)

Part 4: Spot colour characterisation data (CxF/X-4)

The base document of the standard dealing with the future colour data exchange using Extensible Markup Language (XML), ISO17972-1:2015, was finished in April and published in May 2015. It defines an exchange format for colour and process control data (and metadata necessary for its proper interpretation) in electronic form, identifying the use of the publicly available Color Exchange Format version 3 (CxF3) for prepress data exchange and verification. Where required, this part of ISO 17972 also defines additional requirements for a valid CxF/X file. Using XML, all CxF3 and CxF/X documents also support the exchange of data outside of the graphic arts workflow and can support future standards. Additional parts of ISO 17972 will use custom resources in conjunction with CxF3 to define the required and optional data for a particular workflow. Part 2: Scanner target data (CxF/X-2), and Part 3: Printer target data (CxF/X-3) are under development. ISO 17972-4:2015 was already published in July 2015 and defines an exchange format for spectral measurement data of inks to provide a means to characterise spot colour inks to allow reliable printing and proofing of products designed using these inks. This part of ISO 17972 is limited to isotropic (paper-like) substrates and application areas where the same ink and paper combination that has been characterised is used when printing.

ISO 18619:2015

Image technology colour management – Black point compensation

This standard published in July 2015 specifies a procedure, including computation, by which a transform between ICC profiles can be adjusted (compensated) to take into account differences between the dark end of the source colour space and the dark end of the destination colour space. This is referred to as black point compensation (BPC). The relative colorimetric encoding of ICC profile transforms already provides a mechanism for such adjustment of the light (white) end of the tone scale.

ISO/PAS 15339-1:2015 and ISO/PAS 15339-2:2015

Graphic technology – Printing from digital data across multiple technologies – Part 1: Principles

Part 2: Characterized reference printing conditions, CRPC1–CRPC7

Publicly available specification ISO/PAS 15339-1:2015 establishes principles for the use of colour characterization data as the definition of the intended relationship between input data and printed colour for copy preparation, job assembly, proofing, and graphic arts production printing. The specification ISO/PAS 15339-2 defines a limited number of characterized reference printing conditions that span the expected range of colour gamuts used for the production of printed materials from digital data, regardless of the printing process used. Both parts were published in August 2015.

Bookshelf

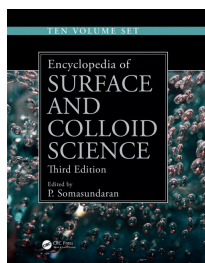
Encyclopedia of Surface and Colloid Science

The third edition of Encyclopedia of Surface and Colloid Science, which is dedicated to the interface-related aspects of chemistry, materials sciences and engineering, biology, physics, computer sciences, and applied mathematics, has grown into a ten volume set. This edition includes 70 new entries discussing important advancements made since 2nd edition published in 2006. Primarily, the understanding of the fundamental theories in colloid and surface science, the development of new and improved methods, and the design of particles–nanoparticles are stressed. Among topical subjects, many fundamental aspects and applications related to drug design and delivery can be found, as well as the development of highly efficient catalysts including novel ways to generate renewable energy.

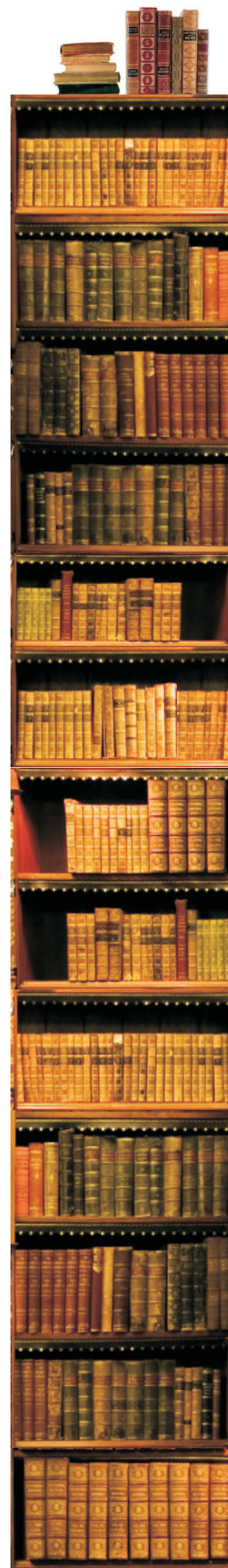
The aim is to provide current state of knowledge on utilization of surfactants, colloids, emulsions, foams, gels, and nanoparticles, with updated coverage of mechanisms of catalysis, transport, and adsorption. Further, the chemical behaviour at electrochemical, fluid–fluid, polymer, soil, mineral, and atmospheric boundaries is addressed. The content is alphabetically organized into volumes as follows: I: Absorption–Bubbles; II: Calcite–Crude Oil; III: Crystal Dissolution–Electrokinetics; IV: Electromagnetic–Hysteresis; V: Ice–Liquid; VI: Magnetic–Microporous; VII: Mineral–Phospholipid; VIII: Photocatalytic–Protein; IX: Proteins: Adsorption–Supercritical; X: Supported Metal–Zeta–Potential.

Like in previous editions, several tens of pages deal with papermaking and printing, where papermaking is divided into two parts being the first one surface and colloid chemistry of pulping processes and the second one of papermaking processes. For printing, all major printing techniques are introduced: letterpress, lithography, flexography, gravure printing, screen printing, toner printing (especially electrophotography), and inkjet printing. For further description of printing processes, featuring printing units, printing plates, printing inks, fountain solutions, etc., two groups of printing processes are distinguished according ink viscosity (paste and liquid inks). Within interfacial aspects of printing, surface tension of printing inks is explored, comprising among others dynamic surface tension measurement by maximum bubble pressure and differential maximum bubble pressure methods. Similarly, surface free energy of printing substrates is explained along with critical surface tension, two-liquid method with geometric mean and harmonic mean approaches, and acid–base approach. Finally, the ink–plate–substrate interactions are discussed, including wetting, leveling and penetration, where Lucas–Washburn theory and Kubelka–Munk model are applied, adhesion, and adsorption, covering also the stability of pigment dispersions and inks and adsorption of surfactants at the solid/liquid interface. New entries more or less related to the field include e.g. Water-in-oil microemulsions: preparation of nanoparticles or Nanoparticles for the conservation of cultural heritage: paper and wood.

This Taylor & Francis Group encyclopedia is also available through online subscription, offering corresponding benefits such as citation tracking or active reference linking.



Encyclopedia of Surface and Colloid Science
 Editor: Ponisseril Somasundaran
 Publisher: CRC Press
 3rd ed., August 2015
 ISBN: 978-1-4665-9045-8
 8480 pages
 Hardcover, Ten Volume Set



Fundamentals of Patenting and Licensing for Scientists and Engineers

Author: *Matthew Y. Ma*

Publisher: World Scientific Publishing Co.
2nd ed., April 2015
ISBN: 978-9814452533
364 pages, Hardcover
Also as an eBook



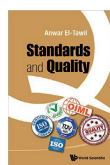
This book ties the many technical, legal and business aspects of patent enforcement to the innovation and patenting stage in the patent value chain, with the objective of helping inventors to create valuable patents that can be capitalized. Written in easy-to-understand language by the author with extensive technical background and experience in intellectual property licensing, the book covers basic concepts of patent laws and rules, innovation protection, patenting, patents post-granting and patent licensing, supported by numerous tables, figures, cases and examples, and a comprehensive index.

The second edition incorporates the latest changes in the America Invents Act (AIA), with additional case studies and illustrations, and provides guidelines and step-by-step instructions on preparing and filing a US provisional patent application.

Standards and Quality

Author: *Anwar El-Tawil*

Publisher: World Scientific Publishing Co.
1st ed., February 2015
ISBN: 978-9814623575
196 pages, Hardcover
Also as an eBook



The book aimed at practicing engineers, students of engineering and managers in industry deals with both voluntary and mandatory standards and explains their benefits and relationship with trade.

The readers will be introduced to standardization process and certification and accreditation steps validating a conformity to standards. The national standards body as well as international standardization are described. Quality and quality management systems, environmental management systems and some

Label Design and Origination: Repro and prepress processes

As is stated in the introduction of this book, "An appreciation of the design to print processes and related terminology is the key to ensuring that each print job meets expectations and that any problems and inconsistencies are anticipated and eliminated from the value chain." This is true for any print production and label printing is not an exception. Therefore, the aim is to provide a complete overview of the progress of a typical label or packaging job from design rough through to its arrival on the printing press and thus contribute to an enhanced communication and co-operation between the designer, printer and brand owner. Both authors are experienced in the field and have been involved in various activities related to training and education in the label and packaging sector.

Developments in the design to print process, which is still very complex and must always fit the printing process involved, are examined. Prepress stages of design and origination, preparation for printing, proofing, and prepress output are described. Among other creative, graphic, technical and technological aspects, book covers e.g. barcodes, various file formats, management information systems and Job Definition Format or common quality issues. Supply chain issues are discussed in the last chapter.



Label Design and Origination:
Repro and prepress processes
Authors: *John Morton, Robert Shimmin*
Publisher: Tarsus Exhibitions & Publishing
1st ed., February 2015
ISBN: 978-1-910507-03-2
80 pages
Softcover
Available also as an eBook

Conventional Label Printing Processes: Letterpress, lithography, flexography, screen, gravure and combination printing

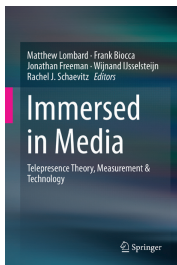
The book written by the same author team as the above-mentioned title explains the principles of each of the main conventional printing processes used in the production of labels as well as the types of printing equipment used. Although the popularity of digital processes is growing, the authors are convinced that it still remains important to have a fundamental understanding of conventional printing processes, the mechanics behind them and how they are evolving and changing, which this book aims to provide in a clear and concise way. After the discussion of key developments changing the landscape of label printing, label press configurations and ancillary equipment are described. Following chapters deal with the letterpress, lithographic, flexographic, screen printing, and gravure printing processes. At the end, the press combining different printing and converting processes using a system of interchangeable cassettes is detailed.

Conventional Label Printing Processes:
Letterpress, lithography, flexography,
screen, gravure and combination printing
Authors: *John Morton, Robert Shimmin*
Publisher: Tarsus Exhibitions & Publishing
1st ed., August 2014
ISBN: 978-0-9547518-9-0
96 pages
Softcover
Available also as an eBook



Immersed in Media: Telepresence Theory, Measurement & Technology

This collection has been put together by leading international scholars to highlight key research currently being undertaken within the field of telepresence, thus helping designers to optimize presence for users of advanced media technologies such as virtual and augmented reality, collaborative social media, robotics, and artificial intelligence. Topics, otherwise covered mainly in narrowly-focussed journal articles and conference proceedings, deal with the state-of-the-art in presence theory, research and technology design for an advanced academic audience, providing better understanding of human cognition, emotion and behaviour. The book defines presence and explains basic concepts, an evolutionary model and action-based approach to presence, spatial presence theory and ways to measure it, an integrative approach to presence and self-motion perception research, patterns of place, collaboration in immersive and non-immersive virtual environments, and presence-inducing media for mental health applications.

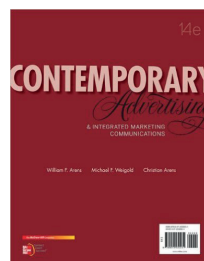


Immersed in Media: Telepresence Theory, Measurement & Technology
Editors: Matthew Lombard, Frank Biocca, Jonathan Freeman, Wijnand IJsselstein, Rachel J. Schaevitz
 Publisher: Springer
 1st ed., June 2015
 ISBN: 978-3-319-10189-7
 332 pages, 18 images
 Hardcover
 Available also as an eBook

Contemporary Advertising and Integrated Marketing Communications

This popular title is now available with an access to a Connect learning platform. Part one on advertising perspectives introduces advertising and IMC (Integrated Marketing Communications) today, the evolution of IMC, economic and regulatory aspects, and the scope of advertising. Second part concerns with crafting marketing and advertising strategies, marketing and consumer behaviour, market segmentation and the marketing mix, gathering information for IMC planning, marketing and IMC planning as such, and planning media strategy to disseminate the message. Creating advertisements and commercials, creative strategy, process, and execution are described in the third part along with print, electronic, and digital media production. Part four then covers the use of advertising, print, electronic and digital interactive media, as well as out-of-home, exhibitive, and supplementary media. The book concludes by fifth part on integrating advertising with other elements of IMC, introducing social media, relationship building through direct marketing, personal selling, and sales promotion, and also through public relations, sponsorship, and corporate advertising. In addition, an epilogue on repositioning a brand and appendix with marketing plan outline and advertising plan outline are presented.

Contemporary Advertising and Integrated
Marketing Communications
Authors: William Arens, Michael Weigold, Christian Arens
 Publisher: McGraw-Hill
 14th ed., December 2012 (with Connect March 2015)
 ISBN: 978-1-259-67612-3
 722 pages
 Loose Leaf



other like social responsibility and food safety management systems are detailed. Last but not least, the role of metrology as the quality infrastructure is explored.

Letter Fountain

Author: Joep Pohlen



Publisher: Taschen
 2nd ed., May 2015
 ISBN: 978-3836554534
 640 pages
 Softcover

This ultimate typeface handbook is widely appreciated and often described as amazing; its hardcover edition received a Certificate for Typographic Excellence from Type Directors Club New York in 2010. The form and anatomy of every letter in the alphabet, punctuation marks, and special characters are explored in depth. In addition, the book examines over 150 typefaces, their origins and font characteristics, with full page tables including scale, weight, and useful alternatives. A manual for developing digital fonts, advice on typographic rules, a thorough comparison between sans-serif and serif typefaces, and an essay about measuring systems and indications are also included, with special attention to finding the right typeface for a given job. The extensive appendix contains four indexes, a graphical dictionary, and a bibliography for further reading.

Logo Design

Editor: Julius Wiedemann



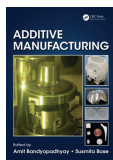
Publisher: Taschen
 1st ed., June 2015
 ISBN: 978-3836556347
 664 pages
 Hardcover

This reference book for students and professionals in design and marketing or for anyone else interested in graphic representation of brand identity gathers diverse brand markers from around the world. Organized into chapters by theme, it explores how text, image, and ideas evolve into a logo across events, fashion, media, music, and retailers.

Additive Manufacturing

Author: Amit Bandyopadhyay,
Susmita Bose

Publisher: CRC Press
1st ed., September 2015
ISBN: 978-1482223590
389 pages, 254 images
Hardcover
Also as an eBook

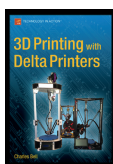


This title is an alternative choice to “Additive Manufacturing Technologies: 3D Printing, Rapid Prototyping, and Direct Digital Manufacturing” introduced in the Bookshelf earlier this year. With an comprehensively interdisciplinary approach, Additive Manufacturing introduces various additive manufacturing technologies based on their utilization in different classes of materials and discusses important application areas of additive manufacturing such as bioprinting and multifunctional printing for incorporating electronics into 3D parts. Latest advancements in 3D printing and additive manufacturing technologies are highlighted, including material innovations. Furthermore, regulatory challenges associated with the emergence of additive manufacturing as a mature technological platform are explored.

3D Printing with Delta Printers

Author: Charles Bell

Publisher: Apress
1st ed., July 2015
ISBN: 978-1484211748
368 pages, 184 images
Softcover
Also as an eBook



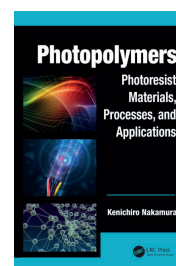
Delta 3D printers have very different needs for setup, configuration, calibration, and maintenance than Cartesian printers. This book brings detailed descriptions of the innovative delta design including its unique requirements and nuances. After an introduction to delta 3D printers, delta printer hardware and software is explained, followed by tips for building a delta printer. In next chapters, calibrating the printer, delta printer troubleshooting, maintenance and enhancements are described, concluded by an overview of common problems and their solutions.

Photopolymers: Photoresist Materials, Processes, and Applications

Advancements in photopolymers have led to groundbreaking achievements in a number of diverse fields, not excluding print, where UV curable inks and varnishes, printing plates, or 3D printing can be listed as examples. With the aim to provide valuable insight into current and future opportunities for photopolymer use, the book reviews progress in the development of photopolymers spanning from core concepts, providing the chemical formulae and structures of the materials discussed, to industrial applications with practical case studies from some of the largest corporations.

First part introduces basics of photopolymerization – radical and cationic polymerization, monomers and initiators, polymerization inhibition, photocrosslinking and scission of polymers. Next, chemically amplified resists are explored together with progress of resolution limit, immersion lithography, double patterning, extreme ultraviolet lithography, and direct self-assembly. In relation to nanoimprinting, thermal and UV nanoimprinting are explained, including cationic and ene-thiol polymerization of UV nanoimprinting and soft lithography. Finally, industrial applications of photopolymers cover electronics, optical adhesive polymers, holographic photopolymers, medical materials and microelectromechanical systems.

Photopolymers: Photoresist Materials,
Processes, and Applications
Author: Kenichiro Nakamura
Publisher: CRC Press
1st ed., August 2014
ISBN: 978-1-4665-1728-8
189 pages, 151 images
Hardcover
Available also as an eBook



New Horizons in Nanoscience and Engineering

This book represents a selection of contributions from some of innovators closely involved since the launch of Nanoscience and Engineering Symposium organized by SPIE. Key advances, which are believed to indicate the breadth and scale of recent progress, are divided into nine chapters: Increasing the density and functionality of photonic integration with nanowaveguides and nanostructures; Silicon microresonators: how to give a new twist to silicon photonics; Two-photon 3D microfabrication of organic, inorganic, and hybrid materials; Noncovalent interactions in polymer nanocomposites; Molecular engineering for solar energy conversion and lighting materials; The material genome for organic electro-optics and silicon/plasmonic-organic hybrid technology; Bio-based nanomaterials for photonic applications including the application of DNA biopolymers in printed photodetectors; Bio-based nanomaterials for electronic applications; and Organic materials – silk fibroin synergies: a chemical point of view.

New Horizons in Nanoscience and Engineering
Editors: David L. Andrews, James G. Grote
Publisher: SPIE Publications
1st ed., July 2015
ISBN: 978-1-62841-795-1
472 pages
Hardcover
Available also as an eBook



Bookshelf

Academic dissertations

Multispectral imaging: Fast acquisition, capability extension, and quality evaluation

Multispectral imaging has proved to be beneficial for a wide range of applications, but its use was limited in part due to slow speed, high complexity and cost. The most common imaging technology, employed in majority of current digital cameras and smart devices, is digital color imaging. It acquires an color image of a scene as a 3-band image – usually with red, green, and blue imaging channels. Digital color imaging has several drawbacks such as metamerism, environment dependency, and sensitivity only in the visible spectral range. Multispectral imaging effectively overcomes these limitations by increasing the number of imaging channels. This enables to capture physical properties of objects in the form of their spectral reflectances, including the information from ultraviolet and infrared regions.

The research was aimed on new multispectral imaging solutions fulfilling the requirements on fast, practical, and inexpensive system. Three different multispectral imaging systems and technologies have been proposed. The multi-camera system joins n (two or more) digital cameras with optimally chosen optical filters, enabling acquisition of a $3n$ -band image in a single exposure. Second, filter array system is based on using n -color filter mosaic pattern; n filters enable acquisition of an n -band image in a single exposure. Third system uses an RGB camera with a combination of three optimally selected non-overlapping narrow band LED (Light Emitting Diode) lights in each of the n exposures, thus enabling to capture $3n$ -band image very fast. Each of these three multispectral imaging systems has been evaluated in detail through simulations and experiments. In addition, a novel framework and methodology based on first two mentioned technologies have been suggested, enabling multispectral imaging in an arbitrary illumination condition, while avoiding complicated and constraining calibration methods. Two new applications, spectral film scanner and density measurements in photographic paper manufacturing process, have been shown as well.

Towards a sustainable media system: Explorative studies of emerging media consumption trends and media processes for content production

The starting point of the thesis was a need to deepen a knowledge within the research area of media and sustainability and to explore the future media landscape together with its environmental impact, which is seen as an urgent challenge for people working in the industry as well as for media consumers and other stakeholders. A number of methods has been used, such as qualitative interviews, workshops, scenarios, case studies, process studies, and life cycle assessment. The characteristics of the media consumption trends are presented in four scenarios based on an assumption that the strength of influence from the government in combination with the strength of commercial powers will strongly affect the future of media. When discussing the environmental aspects of media consumption, eleven central parameters related to electronic devices, travel, transportation, energy use and waste are defined. The research results confirm an increasingly important role of mobile devices and show an increased focus on individualized news, with more co-creation and sharing of media content. The amount of non-text formats for news is growing, as is the need for

Doctoral thesis – Summary

Author:
Raju Shrestha

Speciality field:
Computer Science

Supervisors:
Jon Yngve Hardeberg
Fritz Albrechtsen

Defended:
9 December 2014 at University of Oslo
/ Department of Informatics
Oslo, Norway

Contact:
jon.hardeberg@hig.no

Doctoral thesis – Summary

Author:
Malin Picha Edwardsson

Speciality field:
Media technology

Supervisors:
Johan Stenberg
Nils Enlund
Åsa Moberg

Defended:
8 May 2015 at KTH
Royal Institute of Technology
Stockholm, Sweden

Contact:
picha@kth.se

instant media content accessibility. Finally, more data is collected by media companies about the consumption habits, and more surveillance is carried out by governments and corporations. According to the interviewed experts, the scenario of strong governmental control and strong commercial powers is regarded as the most probable and also as the most desirable of the four scenarios. However, this scenario is mixed, or even negative, from an environmental perspective, because the total volume of consumption in society has increased a great deal. Moreover, the interviewed consumers were not aware of environmental effects of media consumption. In current media development, media companies are rapidly becoming more commercialized and focused on entertainment instead of on producing serious journalism concerned with social, political and cultural matters, including global challenge of climate change. Considering an environmental impact of the major editorial processes, business travel, trips to work and back, use of electronic devices, and energy use were identified as the key factors. In the area of media and sustainability in a broader sense, it is vital that media industry managers take on a perspective of the entire life cycle of a product or a service. In conclusion, the author believes that it is possible to create a sustainable media system, but it will require some conscious effort of people working in the media industry, of consumers, and ultimately at the level of regulatory authorities.

Doctoral thesis – Summary

Author:
Ying Ying Lim

Speciality field:
Wearable electronics

Supervisors:
Yee Mey Goh
Changqing Liu

Defended:
1 June 2015 at
Loughborough University
Loughborough, United Kingdom

Contact:
y.y.lim@lboro.ac.uk
limyingying80@gmail.com

Printing conductive traces to enable high frequency wearable electronics applications

With the emergence of the Internet of Things, wireless body area networks are becoming increasingly pervasive in everyday life and there are growing interests to investigate the performance of body area networks operating at higher frequencies (e.g. millimetre-wave band). Therefore, this thesis aimed to realise printed conductive traces on flexible substrates, targeted for high frequency wearable electronics applications. Specifically, investigations were performed in the areas pertaining to the surface modification of substrates and the electrical performance of printed interconnects.

A novel methodology was proposed to characterise the dielectric properties of a non-woven fabric (Tyvek) up to 20 GHz. Electromagnetic simulation was utilised to improve the analytical equations based on transmission line structures. To reduce the substrate roughness, an UV-curable insulator was used to form a planarization layer on a non-porous substrate via inkjet printing. The results obtained demonstrated the importance of matching the surface free energy of the substrate to the ink to minimise the ink de-wetting phenomenon, which was possible within the parameters of heating the platen. Furthermore, the fact that the substrate surface roughness affects the printed line width significantly was taken into account. Silver ink de-wetting was observed when overprinting silver onto the UV-cured insulator, and studies were performed to investigate the conditions for achieving electrically conductive traces using commercial ink formulations, where the curing equipment may be non-optimal. Various techniques were used to characterise the samples at different stages in order to evaluate the surface properties and printability, and to ascertain if measurable resistances could be predicted. It was demonstrated that measurable resistance could be obtained for samples cured under an ambient atmosphere, which was verified on Tyvek samples. Lastly, a methodology was proposed to model for the non-ideal characteristics of printed transmission lines, to predict the high frequency electrical performance of those structures. The methodology was validated on transmission line structures of different lengths up to 30 GHz. The results obtained demonstrate the significance of the paste levelling effect on the extracted DC conductivity values, and the need for accurate DC conductivity values in the modelling of printed interconnects.

Events

11th Plastic Electronics Conference Enabling the Internet of Everything

 Dresden, Germany
6–8 October 2015

Plastic Electronics conference and exhibition is a place where the conventional electronics industry can meet with flexible and large-area electronics one. This year's conference theme reflects the beliefs that plastic electronics and related technologies including flexible, printed, organic and large-area electronics allows to effectively integrate smart systems into everyday objects, utilizing a wide variety of substrates from low temperature plastic foils to curved glass, textiles, and even pharmaceutical and food packages. Keynote speakers include Chuck Milligan, Ilkka Kaisto, Christopher Bower, Octavio Trovarelli, John de Mello and Mark James.

2nd Annual InkJet Conference 2015

Düsseldorf, Germany
7–8 October 2015

The Inkjet Conference
Inkjet Engineering & Inkjet Chemistry

 **TheIJC.com**

This event is organized by ESMA, European association for printing manufacturers in screen, digital and flexo technology. The aim is to bring together industry and universities as well as research institutes to speak about

the latest advances and future developments driving digital print, with a focus on inkjet engineering and a review on fluid and ink components. Two tracks of the programme for this year offers e.g. lectures on a way towards an agreed standard method for inkjet drop measurements, machine vision used to accelerate inkjet development, atomic force microscopy and conductivity analysis of inkjet printed electrode structures or high-resolution inkjet printing for touch panel applications.

Regarding the technology, various new printheads, sol-gel PZT for inkjet printhead actuators, silicon MEMS, printhead calibration, a role of electrical charge in system reliability, electrostatic jetting, ink-jet dryer wetting, setting and fixation mechanisms and UV LED systems will be introduced. Further, ink formulations optimization, inkjet ink filtration, controlling pigment properties, particle size characterising and optimization, complete polymerization of UV inks, hybrid UV inks, ceramic inks, aqueous inkjet printing, reactive dispersant technology, next generation of the colorant, low cost copper-based conductive ink, functionalised magnetite nanoparticles as platform for magnetic inks, inkjet LED masterbatches for industrial ink manufacturing are covered. Understanding colour, colour process control, achieving maximum inkjet quality with screening, new approaches to manage colours in industrial printing applications, fabric preparation and its effects on colours and fastness, real-time process monitoring by overlaid imaging, embedded software for imaging, efficient software workflow will be also discussed. The application examples include digital textile printing, direct product decoration, digital coating-finishing technologies, UV curing of inkjet printed packaging containers, high speed and high volume materials deposition and the challenges in industrial inkjet printing applications.

WAN-IFRA Events

 World Association of Newspapers and News Publishers

World Publishing Expo 2015

Hamburg, Germany
5–7 October 2015

The featured side events comprise 14th International Newsroom Summit, Mobile News Summit and World Printers Forum Conference 2015.

Digital Media LATAM 15

Mexico City, Mexico
23–24 October 2015

DIGITAL MEDIA | LATAM 2015

For Latin American event, these five themes were identified: boosting mobile strategy, developing audience intelligence, the quest for digital revenue, media for and by millennials and new video formats and web-TV development.

Digital Media Asia 2015

Hong Kong, Hong Kong
17–19 November 2015

DIGITAL MEDIA | Asia 2015

The themes for Asia edition are even more similar to those of Digital Media Europe held earlier this year.

6th ICFPE 2015 International Conference on Flexible and Printed Electronics

Taipei, Taiwan
21–23 October 2015

 The International Conference on Flexible and Printed Electronics

The three-day conference, co-located with 2015 TPCA Show, offers

a number of keynotes and lectures e.g. on Internet of things, wearable electronics, OLEDs, TFTs, flexible displays, sensors and photovoltaics.

The 2015 SGIA Expo

Atlanta, Georgia, USA
4–6 November 2015



This event is organized to showcase specialty imaging products, innovative applications, methodologies and services. The Expo also offers more than a hundred of educational sessions to learn about new opportunities and new markets.

In conjunction, SGIA Industrial Printing Symposium is organized for the first time, starting on November 3rd. Topic areas include printing on difficult surfaces, UV-LED curing technologies, 3D printing technologies, digitally-printed thermoformed parts, production automation strategies, future technologies for industrial process measurement, and lean manufacturing. Concurrently, 2015 SGIA Printed Electronics Symposium is scheduled, with sessions on new materials for printed electronics, conductive ink developments, advanced screen printing meshes, organic printed electronics, advances in capacitive-touch switches, modular digital manufacturing solutions, printed electronics expanding to meet shrinking technology and managing teams to build a lean organization.

InPrint

Munich, Germany
10–12 November 2015

InPrint is the exhibition for industrial print technology, exclusively designed for this emerging sector of the print industry, showcasing solutions for both functional and decorative printing in industrial production, including specialty, screen, digital, inkjet and 3D technologies.



Visitors come from ceramics, textile, packaging, aeronautical, automotive, electronics, engineering, sportswear, pharmaceutical and printing industries, as well as IT, R&D, technical consultancy and publishing sectors.

CIC23 – 23rd Color Imaging Conference



Darmstadt, Germany
19–23 October 2015

This annual conference on colour science and engineering systems, technologies, and applications is sponsored by the Society for Imaging Science and Technology. In 2015 it is held in Europe for the first time and focuses on material appearance and colour. The event offers numerous workshops and a full technical papers program.

Three keynotes are scheduled. The opening one, 'Possibilities and limitations of the bidirectional texture function as appearance representation' given by Reinhard Klein, is related to digital reproduction of the characteristic appearance of materials, which is of considerable importance for the creation of photorealistic images. Acquisition devices as well as data compression and rendering techniques will be reported, with possible application areas ranging from virtual prototyping to cultural heritage. Paul O'Brien in his talk on 'Quantum dots: new and exciting coloured materials – their properties and structures' addresses an origin of colour in quantum dots in simple as well as more complicated systems; their history and potential for technological application also will be briefly surveyed. In the closing keynote of Scott White, '3D printing: building rich and seamless workflows for advanced fabrication', challenges associated with matching designers' intent to fabricated objects, especially for advanced visual and mechanical properties, will be discussed. Meeting these challenges will in some cases require entirely new ways to specify and encode printing data.

Among technical papers can be highlighted contributions on 'Hierarchical integrated color matching in a stereoscopic image based on image decomposition', 'Spatio-spectral gamut mapping and separation', 'Measuring relative image contrast of projection displays', 'A computer aided color appearance design system for metallic car paint', and 'Yarn colour measurement and reproduction by multispectral imaging system'.

CIC23 short course program offers several courses divided into five tracks: Color, vision, and basic colorimetry (8 hours), Color and design (two 4-hour courses), and Physics and HDR, Appearance and 3D, and Color and images (each comprising four 2-hour courses).

9th International Paper and Coating Chemistry Symposium International Paper Physics Conference



Tokyo, Japan
29 October to 1 November 2015

Following the previous event held in Sweden 2012, the joint conferences will bring together paper scientists from all over the world once again this year at the University of Tokyo. The busy program will start with a special lecture on Current situation of the Japanese pulp and paper industry.

The 9th International Paper and Coating Chemistry Symposium will feature a keynote by Tom Lindström named 'From microfibrillar cellulose to nanocellulose applications – an account of the evolutionary developments. A hype or a revolution for the Forest Products Industry?' Invited lectures include 'Fundamentals of superhydrophobicity, growth of non-wetting cavities and wetting transitions probed by AFM colloidal probe microscopy', 'Nanoparticle stabilized ASA emulsions', 'Physicochemical dynamics and fractal analysis of GCC preflocculation', 'Preparation, characterisation and functionalisation

of ultraporous materials made from cellulose nanofibrils', 'Nanocellulose architectures and hybrid nanomaterials', 'Paper electronics – Paper as substrate for printed electronics and sensors', 'Bioactive paper fabrication, printing and coating filter paper', 'Use of nanocellulose in paper coating', and 'Nanocrystalline cellulose particles with chains protruding from both ends'.

The keynote of International Paper Physics Conference, 'Complex matters: things that matter' will be given by Tetsu Uesaka. The list of invited lectures consists of 'Paper physics as an important contribution to nanoscience', 'Grammage-dependence of effectiveness of dry-strength chemicals on tensile properties', 'Applicability of acoustic emission monitoring for the evaluation of naturally aged papers', 'Novel paper applications to water quality sensing, bacterial culture and power generator systems', 'Determining pulp heat of sorption from isotherm models and calorimeter measurements', 'Nanostructure and nanomechanics of NFC-reinforced nanocomposites', and 'Strength enhancement in high-bulk, tissue-grade handsheets with use of novel modified pulps'.

FTA's Fall Conference 2015

Columbus, Ohio, USA
2–4 November 2015



Flexographic Technical Association's Fall Conference communicates the technical content complemented by practical examples.

The innovation, being the creative utilization of an existing invention, is considered as a key factor differentiating the company and its products from the rest. Digital Flexo Excellence technology, granted of the 2015 FTA Technical Innovation Award, is a system of technologies to digitize and automate the workflow, set-up and run of a flexographic press for labels and packaging. The magazine cover printed using this technology will serve as a step-by-step guide to printing high quality expanded gamut flexography. The methods of optimization, fingerprinting, process control, characterization, as well as the methods of continuous improvement, will be explored, concluded by visual evaluation and measuring of the samples.

WCPC Annual Technical Conference



Swansea, UK
9–10 November 2015

This conference is an opportunity to get introduced to the latest research of WCPC (Welsh Centre for Printing and Coating) aimed at functional materials, plastic electronics and bio printing and to discuss the findings with researchers. The conference will be opened by Stan Farnsworth, arguing if there is a role for aesthetics in printed electronics applications.

Besides the talks on printing of conductive features, large area electronics, printed RF energy harvesting system, solar cells, and OLED lighting, the program offers lectures dealing with the formulation of advanced materials and various aspects of rheological processes and surface chemistry. Further, 'Investigation of effect of plasticizers on nanocellulose constructs for wound dressing applications', 'The effects of mesh ruling and particle size for EL phosphors', 'Fabrication of electronic contacts using aerosol jet', and 'Novel pressure sensor utilising direct contact between two piezoresistive layers' will be presented.

Evolutions in Food Packaging Printing

Brussels, Belgium
18 November 2015



An international network meeting, organised jointly by iarigai and vige, is an opportunity to meet with researchers and industrials in the field. Discussions on printing with low-migration UV-curable inkjet inks directly on food packaging, legislation issues, Flemish project exploring optimum inking levels for offset packaging, and odour characteristics of packaging materials are scheduled.

Color 2015

Phoenix, Arizona, USA
5–8 December 2015

Formerly the Color Management Conference, Color 2015 will encompass new colour-related standards, expanded-gamut colour, managing colour across media, real world packaging design, and essentials for digital media content design.

Digital Print for Packaging Europe

Berlin, Germany
8–9 December 2015

This European counterpart of the US conference that was held in June will address the challenges at different levels of the supply chain and for different substrates. Among other topics, success stories, colour management, digital direct

printing for glass container or closures decoration, and metallized surfaces to refine digitally printed products

can be found in the program. The 2015 conference introduces pre-event workshop on 3D printing for fast consumer goods packaging and 'Thought Leader Tables', a selection of roundtable discussions to provide interactive, subject-specific learning.



Call for papers

The Journal of Print and Media Technology Research is a peer-reviewed periodical, published quarterly by **iarigai**, the International Association of Research Organizations for the Information, Media and Graphic Arts Industries

JPMTR is listed in Index Copernicus, PiraBase and PaperBase (by Smithers Pira) and NSD – Norwegian Register of Scientific Journals, Series.

Authors are invited to prepare and submit complete, previously unpublished and original works, which are not under review in any other journals and/or conferences.

The journal will consider for publication papers on fundamental and applied aspects of at least, but not limited to, the following topics:

- ⊕ Printing technology and related processes
Conventional and special printing; Packaging; Fuel cells and other printed functionality; Printing on biomaterials; Textile and fabric printing; Printed decorations; Materials science; Process control
- ⊕ Premedia technology and processes
Color reproduction and color management; Image and reproduction quality; Image carriers (physical and virtual); Workflow and management
- ⊕ Emerging media and future trends
Media industry developments; Developing media communications value systems; Online and mobile media development; Cross-media publishing
- ⊕ Social impact
Environmental issues and sustainability; Consumer perception and media use; Social trends and their impact on media

Submissions for the journal are accepted at any time. If meeting the general criteria and ethic standards of scientific publishing, they will be rapidly forwarded to peer-review by experts of high scientific competence, carefully evaluated, selected and edited. Once accepted and edited, the papers will be printed and published as soon as possible.

There is no entry or publishing fee for authors. Authors of accepted contributions will be asked to sign a copyright transfer agreement.

Authors are asked to strictly follow the guidelines for preparation of a paper (see the abbreviated version on inside back cover of the journal). Complete guidelines can be downloaded from:

<http://www.iarigai.org/publications/>

Papers not complying with the guidelines will be returned to authors for revision.

Submissions and queries should be directed to:

journal@iarigai.org

Guidelines for authors

Authors are encouraged to submit complete, original and previously unpublished scientific or technical research works, which are not under review in any other journals and/or conferences. Significantly expanded and updated versions of conference presentations may also be considered for publication. In addition, the journal will publish reviews as well as opinions and reflections in a special section.

Submissions for the journal are accepted at any time. Papers will be considered for publishing if meeting the general criteria and ethic standards of the scientific publication. When preparing a manuscript for JPMRT, please strictly comply with the journal guidelines, as well as with the ethic aspects. The Editorial Board retains the right to reject without comment or explanation manuscripts that are not prepared in accordance with these guidelines and/or if the appropriate level required for scientific publishing cannot be attained.

A - General

The text should be cohesive, logically organized, and thus easy to follow by someone with common knowledge in the field. Do not include information that is not relevant to your research question(s) stated in the introduction.

Only contributions submitted in English will be considered for publication. If English is not your native language, please arrange for the text to be reviewed by a technical editor with skills in English and scientific communication. Maintain a consistent style with regard to spelling (either UK or US English, but never both), punctuation, nomenclature, symbols etc. Make sure that you are using proper English scientific terms.

Do not copy substantial parts of your previous publications and do not submit the same manuscript to more than one journal at a time. Clearly distinguish your original results and ideas from those of other authors and from your earlier publications - provide citations whenever relevant. For more details on ethics in scientific publication, please consult:

<http://www.elsevier.com/ethicguidelines>.

If it is necessary to use an illustration, diagram, table, etc. from an earlier publication, it is the author's responsibility to ensure that permission to reproduce such an illustration, diagram etc. is obtained from the copyright holder. If a figure is copied, adapted or redrawn, the original source must be acknowledged.

Submitting the contribution to JPMTR, the author(s) confirm that it has not been published previously, that it is not under consideration for publication elsewhere and - once accepted and published - it will not be published under the same title and in the same form, in English or in any other language. The published paper may, however, be republished as part of an academic thesis to be defended by the author. The publisher retains the right to publish the printed paper online in the electronic form and to distribute and market the Journal (including the respective paper) without any limitations.

B - Structure of the manuscript

Title: Should be concise and unambiguous, and must reflect the contents of the article. Information given in the title does not need to be repeated in the abstract (as they are always published jointly).

List of authors: i.e. all persons who contributed substantially to study planning, experimental work, data collection or interpretation of results and wrote or critically revised the manuscript and approved its final version. Enter full names (first and last), followed by the present address, as well as the e-mail addresses.

Separately enter complete details of the corresponding author - full mailing address, telephone and fax numbers, and e-mail. Editors will communicate only with the corresponding author.

The title of the paper and the list of authors should be entered on a separate cover page (numbered as 0). Neither the title nor the names of authors can be mentioned on the first or any other following page.

Abstract: Should not exceed 500 words. Briefly explain why you conducted the research (background), what question(s) you answer (objectives), how you performed the research (methods), what you found (results: major data attained, relationships), and your interpretation and main consequences of your findings (discussion, conclusions). The abstract must reflect the content of the article, including all the keywords, as for most readers it will be the major source of information about your research. Make sure that all the information given in the abstract also appears in the main body of the article.

Keywords: Include three to seven relevant scientific terms that are not mentioned in the title. Keep the keywords specific. Avoid more general and/or descriptive terms, unless your research has strong interdisciplinary significance.

Abstract and keywords should be entered on a separate page, numbered as page 1. Do not continue with the main body of the text, regardless of the possible empty space left on this page.

D - Submission of the paper and further procedure

Before sending your paper, check once again that it corresponds to the requirements explicated above, with special regard to the ethic issues, structure of the paper as well as formatting. Once completed, send your paper as an attachment to: journal@iarigai.org. You will be acknowledged on the receipt within 48 hours, along with the code under which your submission will be processed. The editors will check the manuscript and inform you whether it has to be updated regarding the structure and formatting. The corrected manuscript is expected within 15 days. At the same time the first (or the corresponding) author will be asked to sign and send the Copyright Transfer Agreement.

Your paper will be forwarded for anonymous evaluation by two experts of international reputation in your specific field. Their comments and remarks will be in due time disclosed to the author(s), with the request for changes, explanations or corrections (if any) as demanded by the referees. After the updated version is approved by the reviewers, the Editorial Board will consider the paper for publishing. However, the Board retains the right to ask for a third independent opinion, or to definitely reject the contribution. Printing and publishing of papers once accepted by the Editorial Board will be carried out at the earliest possible convenience.

Introduction and background: Explain why it was necessary to carry out the research and the specific research question(s) you will answer. Start from more general issues and gradually focus on your research question(s). Describe relevant earlier research in the area and how your work is related to this.

Methods: Describe in detail how the research was carried out (e. g. study area, data collection, criteria, origin of analyzed material, sample size, number of measurements, equipment, data analysis, statistical methods and software used). All factors that could have affected the results need to be considered. Make sure that you comply with the ethical standards, with respect to the environmental protection, other authors and their published works, etc.

Results: Present the new results of your research (previously published data should not be included). All tables and figures must be mentioned in the main body of the article, in the order in which they appear. Do not fabricate or distort any data, and do not exclude any important data; similarly, do not manipulate images to make a false impression on readers.

Discussion: Answer your research questions (stated at the end of the introduction) and compare your new results with the published data, as objectively as possible. Discuss their limitations and highlight your main findings. At the end of Discussion or in a separate section, emphasize your major conclusions, specifically pointing out scientific contribution and the practical significance of your study.

Conclusions: The main conclusions emerging from the study should be briefly presented or listed, with the reference to the aims of the research and/or questions mentioned in the Introduction and elaborated in the Discussion.

Introduction, Methods, Results, Discussion and Conclusions - as the scientific content of the paper - represent the main body of the text. Start numbering of these sections with page 2 and continue without interruption until the end of Conclusions. Number the sections titles consecutively as 1, 2, 3 ..., while subsections should be hierarchically numbered as 2.1, 2.3, 3.4 etc. Use Arabic numerals only.

Note: Some papers might require different structure of the scientific content. In such cases, however, it is necessary to clearly name and mark the appropriate sections.

Acknowledgments: Place any acknowledgments at the end of your manuscript, after conclusions and before the list of literature references.

References: The list of sources referred to in the text should be collected in alphabetical order on a separate page at the end of the paper. Make sure that you have provided sources for all important information extracted from other publications. References should be given only to documents which any reader can reasonably be expected to be able to find in the open literature or on the web. The number of cited works should not be excessive - do not give many similar examples. Responsibility for the accuracy of bibliographic citations lies entirely with the authors.

Please use only the Harvard Referencing System. For more information consult, e. g., the referencing guide at:

<http://libweb.anglia.ac.uk/referencing/harvard.htm>.

List of symbols and/or abbreviations: If non-common symbols or abbreviations are used in the text, you can add a list with explanations. In the running text, each abbreviation should be explained the first time it occurs.

Appendix: If an additional material is required for better understanding of the text, it can be presented in the form of one or more appendices. They should be identified as A, B, ... etc., instead of Arabic numerals.

Above sections are supplementary, though integral parts of the Scientific content of the paper. Each of them should be entered on a separate page. Continue page numbering after Conclusions.

C - Technical requirements for text processing

For technical requirement related to your submission, i.e. page layout, formatting of the text, as well of graphic objects (images, charts, tables etc.) please see detailed instructions at <http://www.iarigai.org/publications/journal>.

Journal of Print and Media Technology Research

Scientific contents

Lubrication theory of ink hydrodynamics in the flexographic printing nip

Hans Martin Sauer, Dominik Daume, Edgar Dörsam

163

Effect of coating pigment, binder type and binder amount on planar liquid wicking on coated substrates

Eveliina Jutila, Risto Koivunen, Patrick A. C. Gane

173

Formation and photoluminescent properties of nanophotonic elements with nanosized ZnO for smart packaging, deposited by screen printing

Olha Sarapulova, Valentyn Sherstiuk

187

Formulation of drop on demand soy inkjet inks

Alexandra Pekarovicova, Zahra Mashbadi Khodabakhsh, Paul D. Fleming III

195

Image analysis as a tool to discriminate counterfeit from true 2D printed codes

Nadège Reverdy-Bruas, Lionel Chagas, Jean-Pascal Poletti, Raphaël Passas

205

Investigating the effects of publishing approaches using print, electronic and augmented reality media on user experience

Elena Fedorovskaya, Lufei Yu

217



9 772223 890003

Editor-in-Chief

Gorazd Golob (Ljubljana)

Published by **iarigai**

The International Association of Research Organizations for the Information, Media and Graphic Arts Industries

www.iarigai.org